Production of hiPSC-derived atrial cardiomyocytes to study the contribution of the *KCNN3* variants to lone atrial fibrillation

by

Sarabjit Singh Sangha

B.Sc. (Hons.), Simon Fraser University, 2016

Thesis Submitted in Partial Fulfillment of the
Requirements for the Degree of
Master of Science

in the
Department of Biomedical Physiology and Kinesiology
Faculty of Science

SIMON FRASER UNIVERSITY
Summer 2019

Approval

Name:	**Sarabijt Singh Sangha**
Degree:	**Master of Science**
Title:	**Production of hiPSC-derived atrial cardiomyocytes to study the contribution of the *KCNN3* variants to lone atrial fibrillation**
Examining Committee:	**Chair:** Damon Poburko Associate Professor

Glen Tibbits
Senior Supervisor
Professor

Thomas Claydon
Supervisor
Associate Professor

Zachary Laksman
Supervisor
Adjunct Professor

Peter Ruben External
Examiner Professor
Department of Biomedical
Physiology and Kinesiology

Simon Fraser University

Date Defended/Approved: May 28, 2019

Abstract

Atrial fibrillation (AF), is the most common cardiac arrhythmia worldwide. AF increases the risk of stroke five-fold and heart failure three-fold. Over a quarter of AF patients suffer from lone AF which has been found to have a significant genetic component. Recently, a number of GWAS studies have found *KCNN3,* the gene expressing a Ca^{2+}-activated K^{+} channel SK3, to be associated with lone AF.

AF is a complex disease that is difficult to study with current experimental models. The advent of pluripotent stem cell (PSC) derived cardiomyocytes (hPSC-CMs) has revolutionized the field of cardiac research. For the first time, we are able to study human disease in human models while avoiding the challenges of obtaining biopsy tissue. Additionally, we are able to study a patient's disease in a personalized manner by the use the patient-derived induced pluripotent stem cells (hiPSCs).

Current differentiation protocols result in a mixed cardiac population that consists of nodal, atrial, and ventricular cells. This makes the study of chamber-specific diseases, like atrial fibrillation (AF), difficult. As such, the development of atrial-specific differentiation protocols is vital.

Using retinoic acid, we optimized a protocol to selectively differentiate hiPSC-derived atrial cardiomyocytes (hiPSC-aCMs). We found that the addition of retinoic acid from days 4 – 6 at a concentration of 0.75 μM resulted in a predominantly atrial phenotype at a transcript, protein, and functional level.

We then used CRISPR-Cas9 genome editing technology to insert an early stop codon into exon 7 of the *KCNN3* gene to knockout its expression. In the future, we hope to differentiate these cells into hiPSC-aCMs to determine the contribution of SK3 to cardiac function and potentially AF.

Keywords: Atrial Fibrillation; human pluripotent stem cell derived atrial cardiomyocytes; *KCNN3*

I’d like to dedicate this thesis to my family, who have always supported me in any and all my endeavours.

Acknowledgements

First, I would like to give thanks to Dr. Sanam Shafaattalab for her friendship and guidance throughout the years. Sanam worked tirelessly to build the iPSC group from the ground up. I was fortunate to learn the basic techniques from her directly and I consider myself lucky to have the privilege of expanding her work. Sanam is someone I see as both a friend and mentor for years to come.

I'd like to thank my good friend Valentine Sergeev. We sat beside each other for a year and through thick and thin you supported (and weren't shy to criticize) every one of my so-called epiphanies. Next, I'd like to thank Dr. Samrat Thouta. I was lucky enough to work under Sam in my directed studies course. Sam was both helpful and kind and taught me invaluable lessons that I have kept with me today.

I'd like to thank Drake Comber for his friendship for the last 2 years. Drake sat beside me for the majority of my graduate studies. His work ethic and talent for science have been apparent since the beginning. Drake has grown to be a great scientist and will be an even better doctor during his medical studies. I'd like to thank Dr. Alison Li for her friendship. Dr. Li is a superwoman and supermom rolled into once package. She has always been willing to listen openly and give advice whenever I needed it. She is both talented and extremely humble. Thanks for everything mama Alison!

I'd like to give a special thanks Barun (Lydia) Kim. Barun is one of my closest friends and confidants. She has been my supporter through every challenge no matter what. She is one of the best human beings I know and wish her nothing but success and good fortune in the future.

I'd like to give a special shout out to my colleague and one of my closest friends, Marvin Gunawan. Marvin and I both undertook an extremely challenging project in expanding the labs capabilities to address atrial arrhythmia. He has been both an invaluable friend and collaborator during my master's thesis. These achievements would not have been possible without him. Getttin er done bro!

Thank you to the rest of MCPG for your support, this experience has helped me grow in so many ways and it would not have happened without all of you!

I'd like to thank Dr. Zachary Laksman, for his guidance over the last three years. Although I have only known him for a short time, He has taught me a great deal. Dr. Laksman helped me with initial experiment design and his wealth of knowledge in this field has been invaluable in my growth.

Next, I'd like to thank Dr. Thomas Claydon for his guidance and support. I first started as a volunteer with MCPG in Dr. Claydon's lab filling pipette tips and performing mini preps. Eventually, I was lucky enough to complete a directed-studies course and a USRA in his lab. Throughout my undergraduate and graduate studies Dr. Claydon has gone above and beyond his responsibilities to ensure my success. He taught me a great deal about thoughtful experimentation and study design. Dr. Claydon invests a great deal in his students and exemplifies good character. I'd consider myself lucky to become a half of the person he is.

Last but definitely not least, I'd like to thank my senior supervisor Dr. Glen Tibbits. I first met Dr. Tibbits as an undergraduate student in BPK 412. I will never forget the day I first learned about human pluripotent stem cells, and my intrigue with the potential this model provided. Dr. Tibbits' passion and drive to make a difference in people's lives was apparent and drove me to also want to help make a difference as well. I was fortunate enough to complete my Honour's project with under his guidance and continued with him as a MSc student. Dr. Tibbits provided an immense amount of support through struggles in both my personal and professional life. Even when others had given up on me, Dr. Tibbits was present and never lost faith in my abilities. Thank you Dr. Tibbits because without you, I would not be here today. I will be forever grateful for this experience.

Table of Contents

List of Tables

List of Figures

List of Acronyms

aCMs	Atrial Cardiomyocytes
AF	Atrial Fibrillation
CMs	Cardiomyocytes
cTnT	Cardiac troponin T
ESC	Embryonic stem cells
hPSCs	Human pluripotent stem cells
hiPSCs	Human induced pluripotent stem cells
MLC-2A	Myosin light chain 2A
MLC-2V	Myosin light chain 2V
PCR	Polymerase chain reaction
qPCR	Quantitative polymerase chain reaction
RT-qPCR	Real time quantitative polymerase chain reaction
RT-PCR	Reverse transcriptase polymerase chain reaction
vCMs	Ventricular Cardiomyocytes

Chapter 1.

Background

1.1. Cardiac development

1.1.1. Heart development

The heart is critical for delivering oxygenated blood and nutrients throughout the body. The heart is a complex structure made up of a number of different cell types. These include but are not limited to myocardial cells, and pace-making cells (which include the sinoatrial and atrioventricular nodes). The myocardial cells are excitable and contract in a coordinated fashion to pump blood.

The heart is made up of 4 chambers; the upper chambers are called the atria and the lower, larger, chambers are called the ventricles. Although both are comprised of myocardial cells, there are noticeable differences between these cardiomyocytes at a structural and functional level. The heart is the first functional organ in the fetus, its development is an eloquent interplay of multiple transcription factors that direct structural development and functional specification.[1]

The zygote, formed following fertilization, is a single cell surrounded by a thick membrane called the zona pellucida.[2] The cells inside continually divide to form a structure called the morula, which will divide further to form two distinct cell layers, called the trophoblast and the embryoblast. Over time, the zona pellucida disappears, and the inner cell mass migrates to one pole. This process is known as blastulation, and the structure is referred to as a blastocyst; the remaining cavity is called the blastocoel. Over time, another cavity will form within the inner cell mass called the amniotic cavity. The inner cell mass will subdivide into two distinct cell layers, called the epiblast (which will eventually make up the mature human being) and the hypoblast. Together these are called the bilaminar disc. The epiblast begins to invaginate starting at the caudal-end along the rostro-caudal plane to form what is called the primitive streak. The primitive streak folds in on itself creating the endoderm and the mesoderm. The epiblast layer is now referred to as the ectoderm. This process of forming three cell layers is called gastrulation.[1,3]

Cardiogenic precursors begin to form before gastrulation.[4] They flank the primitive streak and migrate through to become part of the lateral anterior splanchnic mesoderm. Here they begin to migrate cranially and meet, forming the cardiac crescent (or anterior heart field). The pharyngeal mesoderm forms late-differentiating progenitors in an area which sits posterior to the cardiac crescent, called the second heart field.[1,5]

The cardiac crescent will go on to form endocardial tubes which are anterior to the developing gut and lead posteriorly into the left and right dorsal aortae. The dorsal aortae then join caudally. The endocardial tubes eventually fuse completely to form the primitive heart tube which is connected to the foregut by dorsal mesocardium. The second heart field will contribute at both the arterial and venous poles of the elongating heart tube after its formation.[5,6]

The heart tube is recognized by its peristaltic beating pattern.[7] It is spatially organized in a manner that corresponds to various future structures in the heart. Most inferiorly, the left and right sinus venosus carry blood into the primordial atrium. These are subsequently followed by the primordial ventricle, bulbus cordis, and finally to the truncus arteriosus, from which the blood will leave through the aortic arches. The heart tube begins to stretch outward whereas the sinus venosus and primordial atria move posteriorly then cephalically. The heart then loops, clockwise creating the orientation that will eventually be defined by separate structures.

The primordial ventricle contributes to the left ventricle and the truncus arteriosus will form the aorta and pulmonary artery. The bulbus cordis will form the pulmonary trunk and other structures including the outflow tracts and the right ventricles. Many portions of heart tube will form the final atrial structure. The sinus venosus forms the right atrium (as well as the vena cava and the coronary sinus). The primordial atrium forms the left and right atrial appendages as well as the left atrium.

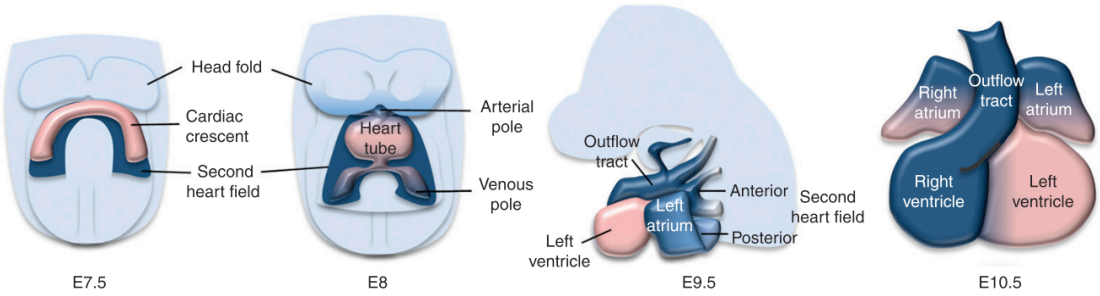

Figure 1. Schematic representing the first and second heart field derivatives in the cardiac crescent, as well as heart folding.
Original figure from Kelly, 2012.[5]

Transcriptionally, gradients of Wingless-related integration site (WNT), and nodal growth differentiation factor (NODAL) (secreted from Hansen's node) is required for primitive streak formation in the embryo, and eventually mesoderm induction.

NODAL functions to induce WNT signalling by driving Bone morphogenic protein 4 (BMP4) expression. This signalling is restricted to the posterior portion of the epiblast through various antagonists. WNT signals the expression of T (Brachyury) which activates mesoderm posterior bHLH transcription factor 1 (MESP1).[8,9] Work by Saga et al.[10] found that MESP1 is an early signature for cardiac development, marking the cardiac mesoderm stage.[10] It is involved in morphogenesis and expressed highly during gastrulation then, downregulated quickly afterwards.[10,11] MESP1 is essential in the formation of the heart tube.[12] Saga et al.[12] found that murine models lacking MESP1 had clear heart defect stemming from a delayed migration from the primitive streak. As cells migrate cranially and laterally, Dickkopf-related protein (DKK1) signalling from the lateral visceral endoderm acts to inhibit WNT signalling which allows MESP1 to direct cardiac differentiation.[13] This activation and subsequent inhibition of WNT signalling plays an important role in cardiac differentiation, especially when applying these principles to human pluripotent stem cells (hPSCs).[14] MESP1 goes on to turn on a number of pathways in both heart fields. MESP1 activates T-box transcription factor 5 (TBX5) in the first heart fields, and, Insulin gene enhancer protein ISL-1 (ISL-1) in the second heart field.[15]

ISL-1^{+} is a marker of second heart field lineage.[1,5] The caudal portion of the second heart field, in addition to ISL-1, is further denoted by WNT2 expression and contributes to both atria.[16] The cranial portion of the secondary heart field is marked by the expression

of Fibroblast Growth Factor 10 (FGF10), and gives rise to the arterial pole as well as the right ventricle.[17]

MESP1 also activates Homeobox protein NKX-2.5 and transcription factor GATA4 which are expressed in both heart fields.[18] NKX 2.5 expression is maintained by the polycomb-group protein RAE 28.[19] These genes signify the formation of cardiac progenitors.[20,21] NKX 2.5 has been associated with patterning of the heart tube. NKX 2.5 and, TBX5 associate with one another to promote further differentiation, specifically during atrial and left ventricular formation.[22] This includes co-binding to the atrial gene promoters for *GJA5* (the gene expressing connexin 40) and *NPPA* (the gene expressing atrial natriuretic peptide) to activate expression.[22,23] The posterior portion of the second heart field is made up of a $TBX18^{+}/NKX2.5^{-}$ population which will eventually contribute to the sinus venosus, and eventually the SA node in the mature heart.[24]

In later development, TBX5 expression becomes localized to the posterior sinoatrial segments and promotes atrial specification. TBX5 expression in the heart globally results in arrested development and abolition of ventricular myosin light chain (MLC-2V) expression.[15] TBX5 and NKX2.5 also bind with retinoic acid inducible, GATA4. A study by Sepulveda et al.[25] showed that GATA4 induces a conformational change in NKX 2.5 that moves the inhibitory domain, which allows it to bind targets with specific promoters.[25] GATA4 promotes the expression of myosin heavy chain- α (MHC-α), cardiac troponin T (cTnT), and ß-Actin, these sarcomeric proteins are expressed in stem cell derived as well as mature cardiomyocytes.[26,27]

It should be noted that although the model discussed above (based on potentiated first and second heart field) represent the current paradigm, more recent studies have called into question the validity of such a simplistic model. The first study, conducted by Lescoart et al.[28] found that two distinct $MESP1^{+}$ progenitor populations exist before the formation of the heart fields. A later study, conducted by Bardot et al.[29] in 2017, found that forkhead box protein A2 (FOXA2) progenitors, at gastrulation, give rise to ventricular myocytes, yet did not give rise to atrial myocytes. Together, both studies found that lineage specification is quite complex and occurs before the formation of distinct heart fields.

Additional signalling pathways are involved in atrial specification, including the retinoid pathway, the specifics of which will be discussed below.

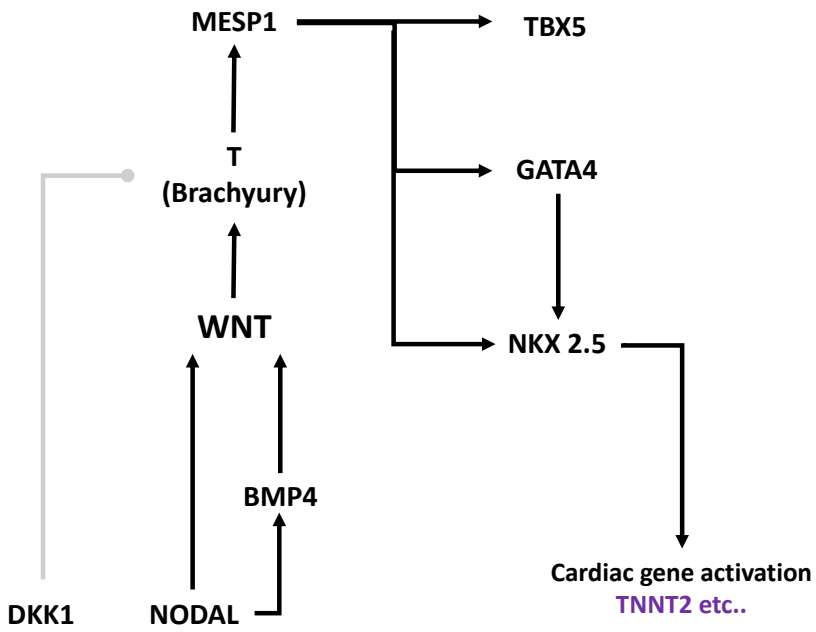

Figure 2. WNT effector pathway summary in relation to cardiac development.

1.1.2. Retinoic acid signalling determines atrial fate

Retinoic acid (RA) was first discovered as the metabolically active derivative of vitamin A (or retinol) in the kidneys.[30] Since then, retinoid pathways have been found to play an important role in fetal organ and limb development.[31,32]

Retinoic acid is derived through the modification of its inactive form, retinol through various redox reactions (Figure 3). In the first step, retinol binds to retinol binding protein 4 (R-BP4) which in turn binds to the retinoic acid 6 receptor/transporter (STRA6) which shuttles it into the cytoplasm.[33] From here, retinol dehydrogenases convert retinol to retinaldehyde.[34] Retinaldehyde is then converted to RA by three different retinaldehyde dehydrogenases named RALDH1, RALDH2 and RALDH3.[35,36] Of these retinaldehyde dehydrogenases, RALDH2 is the most important in heart development.[37] RA will then go on to bind retinoic acid receptors (RAR-α, RAR-ß, and RAR-γ) and retinoid X receptors, in areas within the nuclease called RA response elements. Once bound, there is either an activation or repression of gene expression.[38,39] A spatio-temporal balance of RA is needed for proper cellular development and function.[40,41] As such, there is also an active RA degradation pathway. Retinoic acid is degraded by a family of cytochrome P450 enzymes. These enzymes, CYP21A1, CYP21B1, and CYP26C1 hydroxylate RA, and render it metabolically inactive.[42] These CYP enzymes play an important role in containing

RA signalling to specific areas.[43–46] For example, knockout of the *CYP26B1* gene knockout in mice led to significant limb truncations.[43]

RA is thought to influence the expression of over 500 different genes either directly or through intermediate transcription factors.[47] It plays both a direct and indirect role in cardiac development. RA from the liver is shown to increase Insulin-like growth factor 2 (IGF2) expression in the heart which helps ventricular development.[42] In the atria, RA has a more direct developmental role. A study by Moss et al.[48] used a RARE-LacZ reporter to determine colocalization of both RA and RALDH2. In early development, the reporters were found to be localized to the sinus venosus in the heart tube, but as the heart develops, they spread to the primordial atria. This implies that the mesoderm can respond to RA, and has the potential to convert retinaldehyde to RA.

A study by Kostetskii et al.[49] found that deprivation of retinol in quails led to mass malformations in the heart, highlighted by shrunken atria and abnormally large ventricles. Xavier-Neto et al.[50] determined that the addition of RA to gestating mice resulted in enlarged atria and a severe reduction in ventricular size as well as abolition of the outflow tract. Stopping RA synthesis resulted in loss of the atrial chambers. These findings were confirmed by Niederreither et al.[37] who showed that loss of *RALDH2* gene impaired development of the sinus venosus and primordial atria in mice. Interestingly, these outcomes could be reversed by the addition of exogenous RA

Collectively, RA determines anteroposterior patterning, provides positional information to caudal progenitors, and determines sinoatrial identity.[37,51] This response to RA is limited to the late gastrulation stage which coincides with cardiac mesoderm induction.[50,52–54]

These results were recapitulated in stem cell models in a study by Lee & Protze (co-first authors) et al.[55] They determined that atrial cardiomyocytes originate from a unique mesoderm characterized by RALDH2^{+} expression. This mesoderm has the potential to convert retinol to retinoic acid confirming that this mesoderm is responsive to retinol, whereas mesoderm with ventricular cardiogenic potential does not. This mesoderm is marked by increased CD235A^{+} and CYP26 expression.

Although the function of RA is not fully understood, it has been implicated in atrial development mechanisms. TBX5 expression is highest in the caudal sections of the heart

tube and declines cephalically.[56] Retinoid patterning is along a similar plane.[48] Liberatore et al.[15] found that in chicken embryos, there was a significant increase in TBX5 expression in response to global RA treatment. In addition, TBX5 protein expression was no longer restricted to the posterior poles but spread cephalically. This suggests that RA is involved in the control of TBX5 patterning and expression (refer to previous section for details on TBX5 downstream effectors). More recently, Wu et al.[57] found that the Chicken Ovalbumin Upstream Promoter Transcription Factor 2 (COUP-TFII) protein (expressed by the *NR2F2* gene) in determining atrial identity. COUP-TFII was found to regulate *TBX5*, the hairy/enhancer-of-split related with YRPW motif protein 2 expressing gene *HEY2,* and Iroquois homeobox protein 4 expressing gene *IRX4*. mRNA expression results showed that after a COUP-TFII knockout, there was a decrease in TBX5 expression but an increase in HEY2 and IRX4 protein expression. This suggests that COUP-TFII promotes atrial programming whilst downregulating ventricular programming. Work by Devalla et al.[58] in stem cell-derived atrial cardiomyocytes, showed that RA addition led to an upregulation of both *NR2F2* and *NR2F1*.

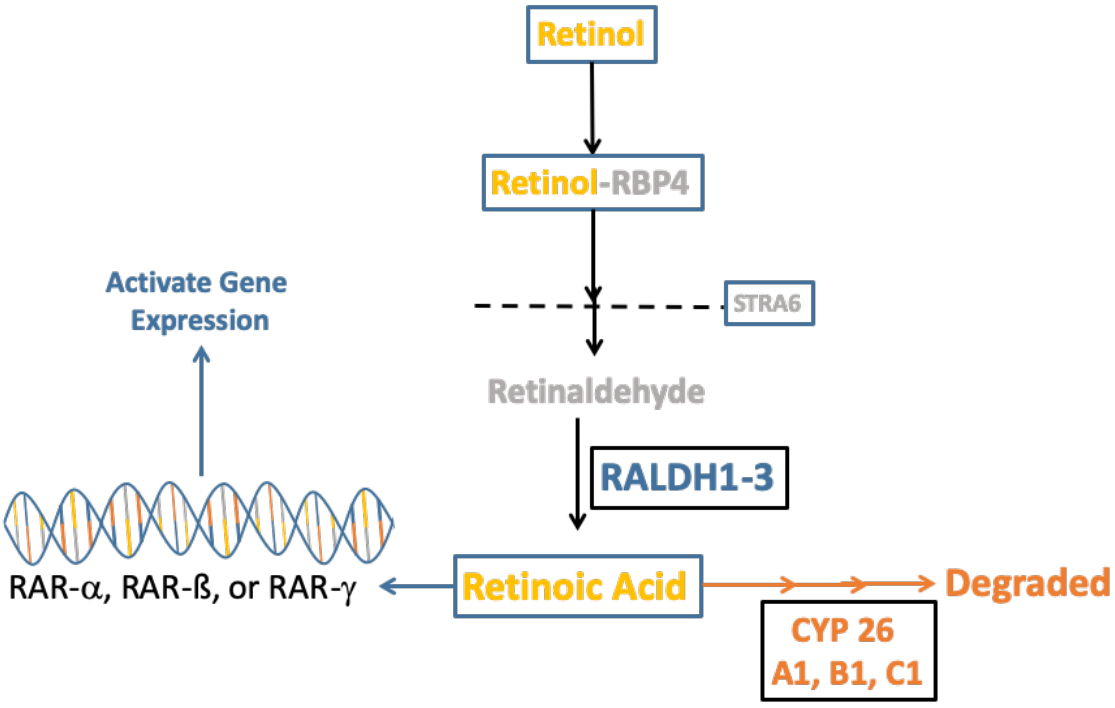

Figure 3. The retinol pathway from the conversion of retinol to retinoic acid, then its subsequent binding or degradation.

RA has also been associated with promoting the SA nodal programming through *TBX5* gene activation in TBX18^{+} progenitors. TBX5 activates the Short Stature Homeobox

2 gene (*SHOX2*, expressing the SHOX2 protein), which then activates T-box transcription factor 3 gene *TBX3* and inhibits *NKX 2.5*.[59] Subsequently, *TBX3* (which is inhibited by NKX 2.5) turns on nodal programming. NKX 2.5 plays an important role in determining differentiation borders. NKX 2.5 is absent in TBX18^{+} progenitors, through downregulation by SHOX2, and therefore the SA nodal program is generally dis-inhibited.[60–62] This is confirmed in *NKX2.5* null embryos, which showed a global expression of TBX3 and HCN4, as well as SAN conduction in the primordial ventricles.[63,64]

Together, these data suggest that RA is involved in promoting both atrial and nodal programming while downregulating ventricular programming through the COUP-TF network and TBX5.

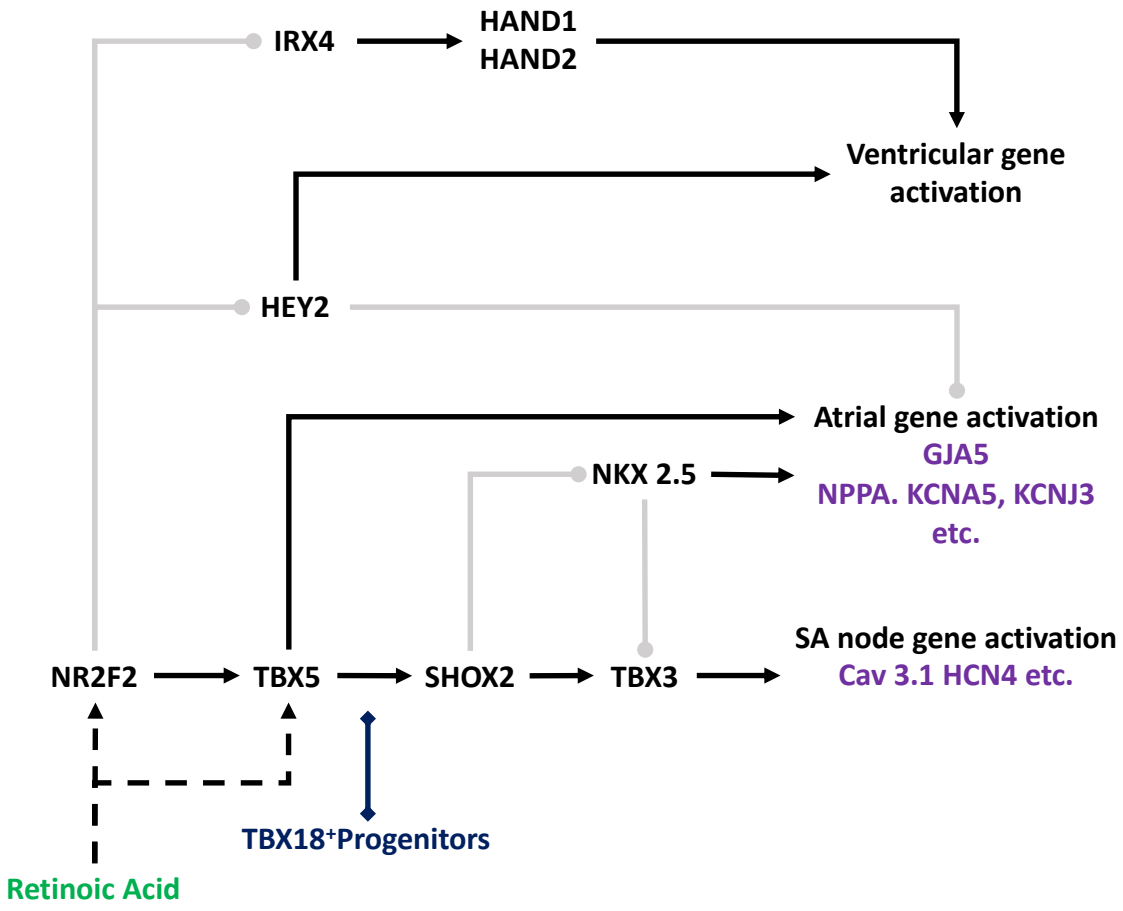

Figure 4. Retinoic acid pathway summary.
Contributions to atrial and SA nodal programming. Effector genes are denoted in purple. The *NR2F2* gene expresses the COUP-TFII protein

1.2. Models of disease

1.2.1. hiPSC models

Human pluripotent stem cells (hPSCs) are a powerful tool to study disease; they can be differentiated down cardiac lineages to study disease and function. Traditionally human ES embryonic stem cells (ES cells), which are derived from fetal tissue, have been used but faced ethical hurdles that limited their applications. Additionally, with ES cells, it is not possible to study disease or drug interactions in a patient-specific manner. In 2006, a seminal paper by Takahashi and Yamanaka et al.[65,66] found that the infection of dermal fibroblasts by four factors, Oct 3/4, Sox-2, c-MYC, and Klf4 was able to revert them into a naïve pluripotent state. These cells were named as human induced pluripotent stem cells (hiPSCs), and the factors were collectively named the "Yamanaka factors". hiPSCs use does not have the same ethical dilemma as ESCs. Furthermore, with the advent of CRISPR-Cas9 genome editing technology, researchers are able to insert or remove disease-causing mutations in cells with patient-specific genomes.

1.3. Cardiac differentiation

1.3.1. Application to hiPSC differentiation

As mentioned earlier, activation and subsequent inhibition of canonical WNT signalling is important for cardiac differentiation. WNT transcription factors are activated through palmitoylation and released from the cell. WNT then binds to G-protein coupled receptors which begin a cascade of downstream signalling.

There are two main WNT pathways, canonical and non-canonical. The canonical WNT pathway, which is more relevant to cardiac differentiation, regulates transcription through the phosphorylation of ß-catenin. WNT binds a cell surface frizzled receptor which destabilizes the ß-catenin destruction complex in the cytoplasm, following recruitment of lipoprotein receptors-related proteins (LRP).[67] Serine/threonine kinase glycogen synthase kinase 3 (GSK3) (along with casein kinase 1a, protein phosphatase 2A, and the scaffolding protein Axin) is a key protein in the complex. Destabilization of the destruction complex prevents degradation and allows ß-catenin to bind target genes. If the frizzled receptor is unbound, the GSK-3 in the destruction complex phosphorylates ß-catenin and

the transcription factor is degraded.[68–70] DKK1, a WNT antagonist, binds LRPs and prevents them from being recruited by the frizzled receptors, resulting in ß-catenin degradation.[13] DKK1 is patterned in a high-cephalic, low-caudal concentration. As cells begin to migrate, the increased DKK1 concentration switches off WNT signalling which allows MESP1 to direct differentiation.

In vitro cardiac differentiation protocol development have applied the principles learned in embryonic development and WNT signalling plays an important role in differentiation. Historically, protocols have been variable with low cardiac differentiation efficiency, showing a low expression of the pan cardiac marker cTnT (or the gene *TNNT2)*. Over the past 15 years substantial improvements have been made in these protocols.[71–73] There are currently two main methods of cardiac differentiation.

The first, an "ActivinA/BMP" protocol, that was pioneered by the Gordon Keller lab.[74,75] As mentioned in previous sections, BMP signalling plays an important role in mesoderm induction during gastrulation through WNT activation, and NODAL signalling acts to drive BMP expression. NODAL is not stable for in vitro culture, therefore Activin A, which also binds the same signal transducers as NODAL, is used as a replacement.[76]

This protocol differentiates cardiomyocytes (CMs) in the form of embryoid bodies through treatment with Activin A, fibroblast growth factor 2 (FGF2), and BMP4 from day 1 (the start of differentiation) until day 4. This step turns on WNT signalling. Then from days 4 – 8, cells are incubated with vascular endothelial growth factor A and DKK1. Later, work by Willems et al.[77] using a small molecule, WNT inhibitor that blocks palmitoylation of WNT, further improved this protocol.[78] These methods were further simplified into an easier monolayer-based protocol, but suffered from low differentiation efficiencies.[79–82]

Furthermore these protocols are expensive, requiring extensive monitoring, and a line-by-line optimization of the various transcription factor concentrations.[83] Line by line optimization is required because each line has different intrinsic levels of NODAL/BMP. As such, this protocol would not be favourable for studying patient-derived hiPSC lines.

In 2012, Lian et al.[14,83] outlined a novel approach to cardiac differentiation. Instead of directly activating WNT signalling, they used CHIR 99021, a small molecule that inhibits GSK3, preventing ß-catenin degradation. This protocol produced 80-98% pure populations of cardiomyocytes in a relatively inexpensive and easy to optimize manner.

Burridge et al.[84] also further modified this approach in 2014. Collectively, these "CHIR" protocols are better suited to patient-specific arrhythmia studies.

It should be noted that the above protocols result in mixed cardiac populations, with 50-63% being positive for the ventricular myosin light chain, MLC-2V.[83–85] To create hiPSC-CMs that are predominantly atrial, a modified protocol is required.

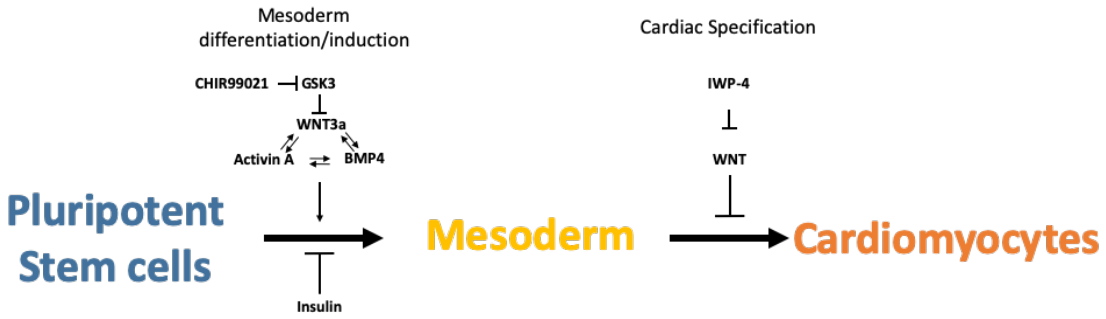

Figure 5. Cardiac differentiation schematic
Various approaches to WNT modulation are described above.

1.3.2. Atrial differentiation protocols

As mentioned earlier, the Lian et al.[14] differentiation protocol uses intrinsic levels of WNT to initiate differentiation. As such, this protocol does not allow for modification of specific mesoderm populations. During gastrulation, mid to late migrating mesoderm (which eventually becomes the atria) passes through a RA expressing region, implying that cells can both produce and be receptive to RA.[52] This assertion is significant when creating a CHIR based atrial differentiation protocol as it further implies that implies that RALDH2^{-} populations can be receptive to RA. These assertions proved true in various CHIR based differentiation protocols.

Zhang et al.[86] published the first study demonstrating a hPSC-derived atrial differentiation protocol. Using an ActivinA/BMP4 based protocol, RA was added at a concentration of 1 μM, from days 5-8 after initiation of differentiation. IRX4 transcript expression was significantly lower in RA-treated cells compared to controls. Western blots showed that MLC-2V expression was severely reduced in RA cells. Cardiac differentiation efficiency, however, was reduced in the RA cells, with cTnT protein expression reduced by 14% compared to the control protocol. Interestingly, the group observed an increase in beating frequency in the RA compared to controls, 150 vs. 50 bpm, respectively.

Devalla et al.[58] used MESP1 as a marker of cardiac mesoderm expression. Using a cocktail of activin A/BMP4 as well as CHIR 99021 to initiate differentiation, they found that MESP1 expression peaked at day 3. They then optimized a protocol in which 1 μM of retinoic acid was added from days 4 - 7 post initiation. The group observed no change in fold expression of *TNNT2* and *NKX 2.5* between the atrial and control protocols while observing an increase in expression of the atrial markers *NPPA* and *PITX2*. A decrease in the ventricular markers *HEY2* and *IRX4* was also observed. NKX 2.5 protein expression in these atrial cardiomyocytes was 56% compared to 65% in the controls and the beating frequency was higher in RA cells compared to control cells, with rates of 60 bpm and 45 bpm, respectively.

Lee & Protze et al.[55] published a seminal paper in 2017, describing not only an atrial differentiation protocol but also investigating differences in atrial- and ventricular-potentiated mesoderm. They modified the Activin A/BMP4 protocol with a 2:3 ratio instead of a 6:10 ratio to promote the development of $RALDH^+$ mesoderm. Retinoic acid was added either 2, 4, 6, or 11 days after initiating differentiation. When 0.5 μM RA was added 2 days post initiation, there was an increase in fold expression of genes thought to be atrial-specific: *NR2F2, TBX5, NPPA, CACNA1D, KCNJ3, KCNA5*, and *GJA5*. However, *MYL7*, the gene expressing what is thought to be an atrial myosin light chain, MLC-2A, did not increase. This may be because MLC-2A is expressed in immature ventricular CMs as well. There was a decrease in fold expression of *IRX4,* the gene expressing ventricular specific myosin heavy chain MHC-ß, *MYH7*; and *MYL2* (gene expressing MLC-2V). There was no difference in the fold expression of *TNNT2*. Protein expression assays recapitulated the transcript observations, where there was no difference in cTnT, and there was a significant decrease in MLC-2V expression. Beating frequency was on average around 70 bpm for 3B/2A cells and 30 bpm in the control cells, notably lower than their counterparts.

Argenziano et al.[84] used a commercially available differentiation medium based on the Burridge “CHIR” protocol.[84] Cells were treated with 1 μM RA on day 5 post initiation until day 10. This window of RA addition is longer than the previous methods that had been described to date. Similar changes to atrial, ventricular, and cardiac transcripts were also observed. Unlike earlier studies however, this group did a more extensive protein expression analysis. They observed an increase in $K_V1.5$ protein expression with flow cytometry. They also found an increase in COUP-TFII and $C_{av}3.1$ protein expression in

their western blots. Beating frequency was monitored from days 15 to 30, and the RA cardiomyocytes had a consistently higher rate than the controls. The beating frequency was maintained at around 100 bpm in the RA cells compared to the control cells which maintained a rate around 50 bpm.

A recent study, by Cyganek et al.[87] completed the most thorough investigation of marker phenotype of an atrial-specific differentiation protocol. This group modified the Burridge based "CHIR" protocol in which RA was added at a concentration of 1 μM from days 3 - 6 post initiation (one day after WNT inhibition).[84] Cardiac differentiation efficiency was unchanged, with cTnT expression being consistently above 90%. Immunocytochemistry data showed a decrease in MLC-2V in RA cells. RT-qPCR analyses found significant increases in atrial markers *HEY1, TBX5, ATP2A2, MYH6, NR2F2, NR2F1, KCNA5, KCNJ3*, and *KCNK3* and a reduction in the expression of ventricular markers *MYL2, MYH7, GJA1, KCNJ2, HAND1, HEY2*, and *IRX4*. Most notably, this group completed both a full transcriptome and proteomic analysis. Both of these analyses showed that atrial and ventricular CMs formed differing clusters in component analyses.

1.4. Electrophysiological and contractile characteristics of cardiomyocytes

One of the unique properties of cardiomyocytes is their ability to conduct electrical signals and translate them into a contractile force. The following two sections will summarize the basic electrophysiological and excitation-contraction coupling properties of cardiomyocytes as well as mention the differences in gene expression between the atria and ventricles.

1.4.1. Electrophysiological properties

The action potential is a temporary change in membrane voltage mediated by the movement of various ions across the plasma membrane. The cardiac action potential consists of five phases. The resting phase (4), the rapid upstroke phase (0), The early repolarization phase (1), and the plateau (2) and rapid repolarization phase (3). There are noticeable differences between the action potential morphology between the atria and ventricles. Namely the atria have a shorter action potential duration (APD) with a more negative and abbreviated plateau phase compared to the ventricles.[88]

Phase 4 is the resting phase of the action potential, which is maintained at approximately -80 mV. The inward rectifier potassium current I_{K1} is the main contributor in maintaining the resting membrane potential, allowing for the efflux of potassium ions. As the membrane becomes more positive, the pore is blocked by polyamines decreasing the conductance of this channel. This is especially important for the maintenance of the plateau phase of the action potential. In the atria, an additional inward rectifier current $I_{K,ACh}$ is present. This current is correlated to $K_{ir}3.1/K_{ir}3.4$ channels associated with the *KCNJ3/KCNJ5* genes.

Sodium channels open in response to changes in membrane potential at a threshold crossing -55 mV, allowing for activation of the inward sodium current I_{Na}. This depolarizing current is represented in phase 0 of the action potential. $Nav_{1.5}$, the ion channel correlate to I_{Na} is expressed in both the atria and ventricles. Although there is little difference in expression of the α-subunit, the ß-subunit is expressed at higher levels in the atria.[89]

Approaching peak potentials, sodium channels inactivate. Around the same time, a transient outward current I_{kto} rapidly but only partially repolarizes the cell. This is phase 1 of the action potential, I_{kto} is related to the $K_V4.3$ potassium channel. In the atria, there is a greater $I_{K,to}$ current amplitude, which is thought to have some contribution to the abbreviated plateau phase.[90]

The plateau phase, phase 2, of the action potential is unique and important to cardiac muscle. The longer contraction facilitates ventricular emptying as well as prevents the transmission of erroneous impulses. The currents that make up this phase are inward L-type calcium currents ($I_{Ca,L}$) and sodium calcium exchanger currents (I_{NCX}), as well as outward delayed rectifier potassium currents ($I_{K,DR}$).[91,92] In the ventricles, I_{ca} is mainly correlated to the $C_{av}1.2$ calcium channel (expressed by the *CACNA1C* gene) whereas the atria, along with $C_{av}1.2$, there is expression of two additional calcium channels. The L-type $C_{av}1.3$ (expressed by the *CACNA1D* gene) and interestingly, the T-type $C_{av}3.1$ (expressed by the *CACNA1G* gene).[89]

$I_{K,DR}$ currents play an important role in phase 2 and phase 3 of the action potential. There are 3 main delayed rectifier currents: I_{Ks} correlated to $K_v7.1$, I_{Kr} correlated to HERG, and I_{Kur} correlated to $K_v1.5$. Both I_{Kr} and I_{Ks} are present in the atria but their current

densities are larger in the ventricles.[93,94] In the atria, I_{Kur} is the predominant delayed rectifier current that is absent in the ventricles.[95] It activates during the early repolarization phase, and is sustained through the rapid repolarization phase.[91] This results in the abbreviated plateau phase relative to that in ventricular cardiomyocytes mentioned above.

$I_{SK,\ Ca}$, the current associated with the small conductance channel SK2, has recently emerged as an important atrial current.[96] It is expressed exclusively in the atria, and gated by calcium independent of voltage.[97]

The resting membrane potential (E_m) is determined primarily by the high I_{K1} conductance which drives E_m towards E_K. The correlated channel $K_{ir}2.1$, has a higher expression in ventricular CMs compared to atrial CMs.[89] This contributed to the less negative resting membrane potential (-65 mV) and to the slower late repolarization.[98]

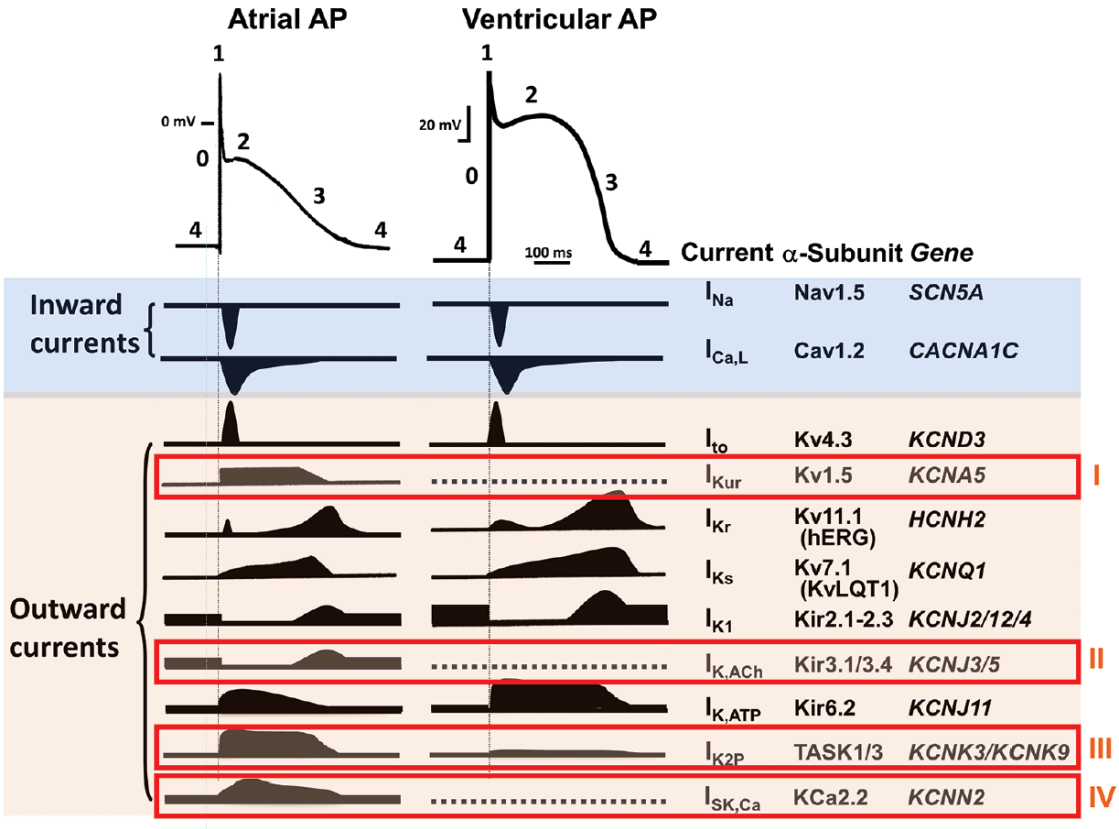

Figure 6. Schematic representation of the various ion channels that make up atrial and ventricular action potentials.
Original figure by Ravens, 2017.[99]

1.4.2. Cardiac excitation-contraction coupling

Excitation-contraction (EC) coupling refers to the process by which the electrical signaling in the heart results in contraction of the myocyte.[100] These two processes are bridged by an increase in cytosolic Ca^{2+}. During phase 2 of the action potential, L-type calcium channels ($C_{av}1.2$) which are localized primarily in the t-tubules open, allowing entry of extracellular calcium. L-type calcium channels are located at proximity to ryanodine receptors as dyads.[101] As Ca^{2+} enters the cytosol it binds and activates the ryanodine receptor which allows some of the Ca^{2+} stored in the sarcoplasmic reticulum (SR) to also enter the cytosol. This phenomenon is referred to as calcium induced calcium release. T-tubules are largely absent in atrial cardiomyocytes and dyads are confined to the edge of the cell, resulting in a less homogenous Ca^{2+} response.[88]

As Ca^{2+} leaves the SR, it binds to a structure called the myofilament. The myofilament is made up a number of proteins, divided into thick and thin filaments. The thick filament is primarily made up of a structure called myosin which is in turn made up of a regulatory light chain (MLC) and a heavy chain (MYH). These myosin chains differ in expression between the atria and the ventricles. MHC-α (*MYH6)* is expressed primarily in the atria whereas MHC-ß (*MYH7*) is expressed in the ventricles.[102] Similarly, MLC-2A (*MYL7*) and MLC-2V (*MYL2)* are expressed in the same respective chambers.[102] The thin filament is made of actin, tropomyosin, and the troponin complex. The troponin complex has three proteins: the first troponin C (TnC) which binds cellular Ca^{2+}, Troponin I (TnI) which binds to actin, and Troponin T or cTnT (expressed by the *TNNT2* gene) which connects to tropomyosin.[103] *TNNT2* and cTnT are pan cardiac markers and are often used to determine cardiac differentiation efficiency.[102]

Once Ca^{2+} binds to site II on TnC, the TnI binding site on the regulatory domain on TnC is exposed. TnI binds TnC at the regulatory domain and tropomyosin shifts to expose the myosin binding pocket, myosin can now bind actin to allow for crossbridge cycling. Myosin can then form cross-bridges, resulting in muscle contraction. Eventually, Ca^{2+} is re-sequestered back into the SR by SERCA2a and pumped out of the cell through the sodium calcium exchanger (NCX1.1). This rise and fall of cytosolic Ca^{2+} is referred to as the calcium transient.

Cardiac muscle beats as a functional syncytium, meaning that electrotonic signals can be conducted from one myocyte to another through intercalated discs. The intercalated disks include structures called gap junctions that connect the cytoplasms of each cell. Over twenty different gap junction proteins are expressed in the heart, connexin 40 (cx40) expressed by the *GJA5* gene and connexin 43 (cx43) expressed by the *GJA1* gene are the most well known in the heart. Cx43 is expressed throughout the heart whereas Cx40 is expressed exclusively in the atria. Porcine studies have shown *GJA5* is the main contributor to atrial conduction, and mutations in *GJA5* gene have been associated with AF.[104,105]

Taken together one can see that cardiac function is a tightly regulated series of events. Changes in these properties can result in altered function and disease. With respect to the atria, atrial fibrillation is a growing health concern.

1.5. Atrial Fibrillation

1.5.1. General background

Atrial fibrillation (AF) is a disorder of the upper cardiac chambers that is characterized by an irregular rhythm, leading to a decline in mechanical function.[106] A heart in AF exhibits very rapid and irregular electrical activity, a stark difference from sinus rhythm which originates from the sinus node and results in coordinated electrical and mechanical function of the atria and ventricles. On an electrocardiogram, AF is characterized by an irregularly irregular QRS complexes and the absence of coordinated atrial activity.[107] The disease manifests at different stages. The earliest, paroxysmal AF is defined as recurrent episodes that stop in less than 7 days, usually stopping within twenty-four hours.[108] Persistent AF is recurrent episodes lasting longer than seven days that can stop on their own or with treatment.[108] Lastly, permanent AF is recurrent episodes that will not stop without treatment.[108]

Although it is not directly a fatal disease, bouts of AF can be debilitating and result in decreased quality of life.[109] The disordered and ineffective mechanical and pump function that results, increases the likelihood of forming a thrombus, which may result in thrombo-embolic events including stroke.[109] AF increases the risk of stroke five times, more than doubles the odds of developing dementia, and triples the risk of congestive

heart failure.[110,111] AF is thought to affect 33 million people world-wide.[112] The lifetime risk of developing AF is 26% for men and 23% for women; when accounting for previous myocardial infarction and congestive heart failure, the lifetime risk still remains high at 17%.[113]

Additionally, atrial remodeling resulting from AF can beget further AF, making its treatment progressively more difficult. Remodeling can be both structural and electrical. Structurally, an increase in tissue fibrosis may cause changes conduction velocity as well as altering local conduction pathways.[114] Electrically, there are a multitude of changes that can occur. First, there is an increased I_{K1} current, which has been shown to increase cardiac excitability, as well as shorten the action potential duration.[115,116] In addition, an increased I_{K1} current has been shown to stabilize fibrillatory rotors.[116] More prominent are changes in calcium handling. Because of the high atrial rate there is a resultant increase in basal cytosolic calcium levels. As a result, $C_{av}1.2$ expression is reduced via the Nuclear factor of activated T-cells (NFAT) pathway to decrease I_{CaL}.[117] The resultant decrease in current can shorten the ADP and cause further re-entry. Other changes include enhanced calcium/calmodulin-dependent protein kinase II (CamKII) activity resulting in an increased CaMKII dependent SR calcium release.[118] Also, Small conductance calcium activated potassium (SK) channels have been shown to have an increased expression during the development of AF, possibly contributing to a shortening of the APD.[119]

As a consequence, AF poses a substantial monetary strain on public and private healthcare systems. The estimated incremental cost of AF in the US is estimated at $26 billion a year.[120] In Canada, the total yearly hospitalization costs are over $800 million without accounting for outpatient and in-home care.[121] Information on the effect of AF on populations in Africa, Eastern Europe, and South America is limited.[122] Thus, the total global cost of AF is unknown, and current information is likely an underestimate. There are nearly 5 million new cases of AF annually, and individuals with the disease prevalence is expected to double over the next two decades.[123] Some estimates predict that the age-adjusted prevalence of AF in the US will be 15.9 million by 2050.[124]

1.5.2. Pathogenesis and treatments

AF can manifest from two functional changes in the atria. The first is a rapid ectopic beat that arises from a group of fibers outside the normal conduction system.[125] These are

typically caused by changes in calcium handling, which can lead to either, delayed or early after depolarizations (DADs and EADs).[126] DADs result from inappropriate calcium release in diastole that can be related to either overload or dysfunction of the sarcoplasmic reticulum (SR).[127] EADs are related to lengthening of the action potential duration resulting in depolarization, via calcium related mechanisms.[126] The second is a sustained re-entrant waveform, which requires both a trigger and a substrate for the reentry.[126] These can both result from remodeling of the atrial action potential. Triggers result from either EADs or DADs and are often ectopic in nature. Evidence has shown the tissue around the pulmonary veins to be heavily involved in triggering AF, but its mechanisms are yet to be elucidated. [128] Substrates for reentry are typically related to changes in structure or ion channel function that alter the refractoriness of the tissue i.e., change the tissue's ability to respond normally to further stimulation

Currently there are main two schools of thought relating to mechanisms of reentry. The first, and more widely accepted, is the spiral wave notion.[129] This theory models reentry as a rotor rapidly circulating around a central core. Increased excitability of the tissue as well as shortened action potential duration (APD) seem to make the rotor rotate more rapidly, stabilizing it. The second theory is the leading circle concept.[130] This theory models reentry as a circus movement of depolarizing waveforms. The mechanisms have been related to the slowing of conduction velocity and the shortening of the APD. In both cases, lengthening of the APD can restore normal sinus rhythm.[126] Interestingly, it seems that mutations relating to remodeling of APs result from either gain of function mutations in potassium channels or loss of function mutations in sodium channels, both of which result in a shortened APD.[131]

Before a course of therapy is taken, other possible co-morbidities (both cardiovascular and non-cardiovascular diseases) associated with AF such as hypertension, valvular disease, family history, and alcoholism should be taken into consideration. Rate control drugs are typically the first to be prescribed to patients in an attempt to maintain a constant ventricular rate.[132] These include ß-blockers, non-dihydropyridine (DHP) calcium channel blockers like verapamil, and digitalis glycosides like Digoxin.[109] If a patient is still symptomatic, then rhythm control therapies, either by themselves or in concert with rate control, are recommended.[106] Rhythm control aims to maintain sinus rhythm in patients by modifying AP duration, morphology, and conduction velocity among others. These drugs include a blocker of predominantly sodium channels

like flecainide, and mixed ion channel blockers like amiodarone. Although it should be noted that these classifications are simplified explanations of targets, whereas in fact all antiarrhythmics target multiple ion channels. Rhythm therapies can be recommended as a first attempt if the patient is highly symptomatic.[109] In general, (I say in general because ablation can be recommended as an alternative to amiodarone or another failed antiarrhythmic in some cases) if none of the above pharmacological therapies show useful change in symptoms then catheter ablation is recommended.[109]

Catheter ablation is a surgical technique derived from observations that ectopic foci seem to frequently originate around the pulmonary vein.[128,133] In this procedure termed a pulmonary vein isolation of PVI, a catheter is inserted (typically through the femoral vein) and brought to the left atrium. Then, using point-by-point radiofrequency, laser light, or cryoenergy lesions, the areas of interest are electrically isolated.[134]

Surgical interventions do not come without their share of problems with major complications occurring in 6% of ablation procedures.[135] Catheter ablation procedures have also been found to have low success rates. A five-year follow up study found that only 20.1% of patients who received a single ablation treatment were successful, and only 55.6% were successful despite multiple procedures.[136]

From a drug development perspective, there is an absence of new antiarrhythmics being released on the market. The first problem relates to cost. Bringing a drug into market typically costs around $2.9 billion.[137] As such, companies are not permitted to proceed to clinical trials if it does not show efficacy pre-clinically. Many of the drugs that have been successful pre-clinically in animal models do not show similar outcomes during clinical trials in humans.[138] And those that are eventually released are also recalled due to adverse side effects.[139] The use of hiPSC-derived cardiomyocytes (hiPSC-CMs) would allow for testing novel antiarrhythmics in atrial fibrillation in a human model. This will likely mitigate the lack of effectiveness observed during clinical trials as well as be invaluable for toxicology screening.

1.5.3. AF affects the young

Although AF is traditionally thought to be a disease of the elderly and related to structural changes in the heart, nearly a quarter of AF patients suffer from this disease in

the absence of any overt structural changes.[140,141] This form, known as lone AF, is prevalent in young to middle-aged adults and is thought to be hereditary, with nearly 30% of first degree relatives also having lone AF.[122,140–144] Recent genome-wide association studies (GWAS) found a multitude of genes associated with AF.[96,119,145,146] Recently, data from the GWAS studies was used to discover a transcriptional connection between TBX5 and PITX2 in regulating expression of certain cardiac channels.[147] Another target, *KCNN3*, the gene encoding for the small conductance Ca^{2+}-activated K^+ channel SK3 has been of particular interest.

The first study found a SNP with an odds ratio (OR) of 1.56 (1.38-1.77) at rs13376333, located in an intron between the first and second exon of *KCNN3*.[119] Studies in two other cohorts also found a significant association between this SNP and AF (OR= 1.45 (1.26-1.66) and 1.55 (1.19-2.03)).[119] The SNPs rs11264280 and rs34245846 were also associated with lone AF but with lower odds ratios (1.12 [1.09-1.15] and 1.14 [1.09-1.19], respectively).[145,146]

1.6. KCNN3

1.6.1. Channel structure and gating

SK channel paralogs SK1 (expressed by the *KCNN1* gene), SK2 (*KCNN2*) and SK3 (*KCNN3*) were first discovered in the central nervous system and were originally characterized by their varying sensitivities to the bee venom apamin.[148,149]

Despite the differences in amino acid sequences, SK channels have a similar architecture to that seen in voltage-gated (K_v) ion channels. Notably, regions around the pore share considerable homology.[150] In SK channels, both the C- and N-terminal regions have unique domains and motifs that contribute to their function. The C-terminus contains an occupied calmodulin-binding domain (CaMBD) as well as a protein phosphatase, PP2A.[151,152] Distal to this, there are coiled-coil domains through which SK subunits can form homo-tetramers or hetero-tetramers (with the other SK paralogs).[153] The N-terminus contains a phosphorylating kinase CK2 and, unique to SK3 channels, there is also a N-terminal coiled-coil.[151] SK channels are gated by Ca^{2+} and independently from voltage.[150] In a Ca^{2+} unbound (apo) state, the N-lobe of each calmodulin remains free. In this state, the S6 gate domains are tilted inwards and the pore is blocked. Upon binding of Ca^{2+} to

the N-lobes of each respective calmodulin (CaM) complex, hydrophobic moieties are exposed, and adjacent CaMs aggregate through their respective N-lobes. As a result, the S6 domains are pulled apart and the pore opens.[97] The CK2 and PP2A domains function to phosphorylate and dephosphorylate SK bound CaM, respectively, and modulate its activity. Phosphorylation of calmodulin blunts calcium sensitivity and results in accelerated channel deactivation.[151]

The role of SK channels in the heart is poorly understood. $I_{SK,Ca}$, the current associated with SK (specifically SK2) channels, is typically observed at 50% and 90% of the action potential duration (APD_{50} and APD_{90}) in both murine and human atrial cardiomyocytes.[154,155] In contrast, the current produced through SK3 channels in mouse models is predominantly active at APD_{90} and not APD_{50}.[148]

Experiments performed on rabbit and murine cardiomyocytes showed SK1 and SK2 to be preferentially expressed in atrial tissue compared to ventricular tissue while SK3 did not show any differences in expression between atrial and ventricular tissue.[156] Similarly, SK2 channels are expressed preferentially in adult human atria compared to ventricular tissue.[154] In humans, atrial SK1 and SK3 expression relative to ventricular expression has not yet been studied.

1.6.2. SK Channels in AF

The possible contribution of SK channels to AF remains undetermined. A burst pacing model of AF in rabbits showed a decrease in APD secondary to increased membrane expression of SK channels.[157] As a shortened atrial APD decreases refractoriness, thereby creating a substrate for arrhythmia and therefore, increased expression of SK channels is consistent with the pathogenesis of AF. In contrast, in a single study using human tissue, SK2 and SK3 expression were significantly decreased in patients with chronic AF compared to healthy controls.[155] Furthermore, the contribution of SK3 specifically to the human atrial action potential is unknown, and there are no data that elucidate a clear SK3 contribution to AF.

Therefore, it would be rational to first create a human model to test the contribution of SK3 channels to the human atrial action potential by creating a knockout (KO) of the *KCNN*3 gene in human induced pluripotent stem cell-derived atrial cardiomyocytes

(hiPSC-aCMs). This approach will help to elucidate the function of SK3 in human cardiomyocytes and allow one to test hypothesized mechanisms by which the rs13376333 SNP may be arrhythmogenic. For example, if a KO of *KCNN3* results in a significant lengthening of the APD, then the significant contribution of the SK3 channel to atrial function may directly be associated with AF. If no significant difference is seen, then it suggests that the impact of the rs13376333 SNP could be associated with some distal regulatory element.

1.6.3. SK3 knockout (KO) using nonsense mediated decay

Typical channel KO strategies remove the pore domain of the channel by creating insertion/deletion (indels) mediated by non-homologous end joining (NHEJ). This intended strategy is to produce a protein that either does not pass quality checkpoints at the endoplasmic reticulum and is tagged for degradation or is expressed on the surface but is not able to pass current. With SK3, however, simply deleting the pore may not be sufficient to knockout the channel. For example, SK3-1/285, a N-terminal truncated variant of SK3, expresses and is localized to the nucleus. More importantly, it abolishes all endogenous SK2 current, in a dominant negative fashion.[158] Therefore, deletion of only the SK3 pore domain would leave an intact N-terminus and risk inhibiting SK2, possibly confounding the analysis of the functional impact of a SK3 KO.

Another method is to knock out multiple regions of interest in the gene. These would include targeting the pore domain, C- and N-terminal coiled coil domains, and any nuclear localization domains. The approach, however, would require multiplexing CRISPR which is not only technically challenging, but expensive. Firstly, the number of possible outcomes is proportional to the deletion targets, making the approach cumbersome. Additionally, using non-homologous end joining (NHEJ), due to its unprecise nature, will result in heterogeneous genetic profiles within the selected colonies containing the knockouts leading to further confounding factors. Finally, there would be a requirement to run a number of assays to prove that the gene is in fact knocked out. These would include protein level expression analysis using western blots, a timely and challenging technique to optimize as their success or failure relies on the quality of the antibody.

A better method of knocking out SK3 would be to take advantage of the native surveillance pathway, nonsense-mediated mRNA decay (NMD).[159] NMD is a quality

control mechanism that degrades mRNA that have premature stop codons greater than 55 nucleotides (nt) from the exon-exon junction, thereby preventing the translation of aberrant proteins.[160] An additional advantage of leveraging NMD is that, because it results in abolishment at the mRNA level, a single qRT-PCR assay is sufficient in determining whether the gene has been knocked out.

A CRISPR-Cas9 mediated knockout leveraging NMD can be made in two ways. The first is to only make a cut using CRISPR-Cas9 and rely on non-homologous end joining (NHEJ) to introduce a premature stop codon. Although NHEJ occurs much more readily than homology directed repair (HDR), the genetic variance between colonies, as mentioned earlier, is undesirable. The second approach takes advantage of HDR, a more precise DNA repair mechanism. In this approach, adding an asymmetric single stranded donor oligonucleotide (ssODN) containing an early stop codon[160,161] would create a precise knockout of the *KCNN3* gene with a true isogenic control.

Chapter 2.

Hypotheses and aims

I hypothesize that the addition of retinoic acid at an optimized concentration, over an optimized window of application will create functional hiPSC-derived cardiomyocytes which exhibit an atrial phenotype (hiPSC-aCMs).

- These atrial cardiomyocytes will express an increase in atrial markers and a reduction in ventricular markers with no change to cardiac differentiation efficiency. They will display a fetal-like atrial action potential morphology and calcium handling properties.
- Furthermore, I will be able to use these atrial cardiomyocytes to study genetic variants thought to be associated with lone AF.

In order to achieve these outcomes, there are three aims:

1. The first aim is to create an assay infrastructure for the phenotyping of hiPSC-aCMs. This would allow for batch-to-batch comparisons and help determine causes of variability in the cardiomyocytes. I will optimize a flow cytometry assay which will determine the expression of certain cardiac- and chamber-specific proteins. I will also optimize markers to assess transcript level expression through RT-qPCR.

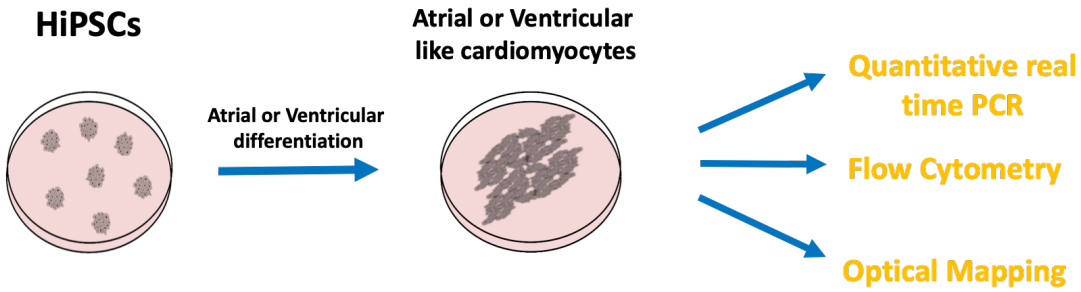

Figure 7. Schematic depicting the workflow to differentiate and analyze cardiomyocytes

2. Using the aforementioned assays as tools, I will create a usable atrial differentiation protocol. This protocol will modify the existing CHIR-based Lian et al.[14] protocol, that is routinely used by the Tibbits group, by the addition of retinoic acid to differentiate cells down an atrial lineage. Along with the above assays, the

hiPSC-aCMs will also be characterized using optical mapping. Then, they will be further tested for a differential response by the addition vernakalant, which is FDA-approved drug for AF cardioversion by IV injection.

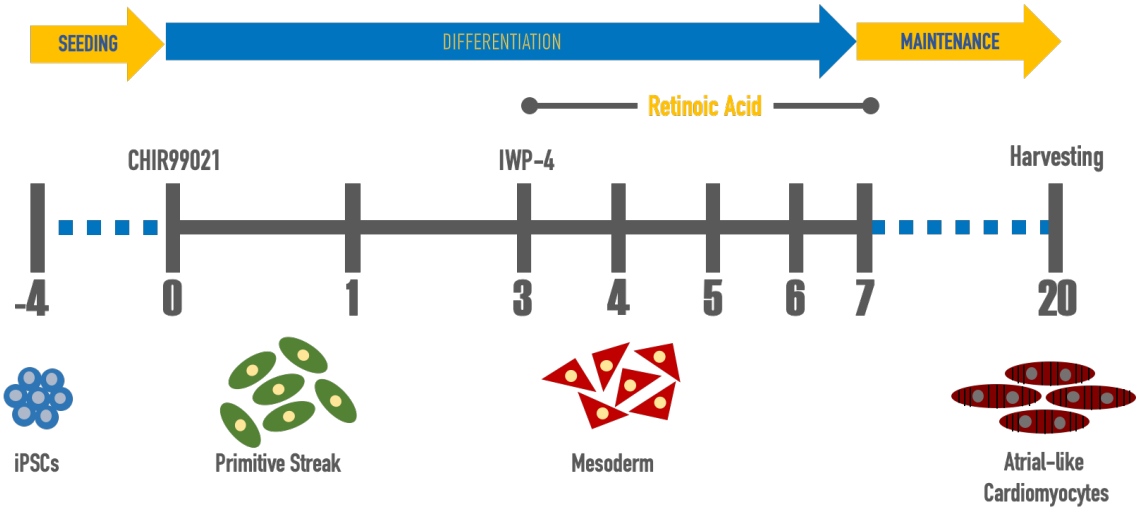

Figure 8. Cardiac differentiation protocol with the addition of retinoic acid

3. Once the necessary infrastructure is in place, I will use CRISPR-Cas9 genome editing technology to insert an early stop codon into exon 7 of the *KCNN3* gene in an HiPSC line to create a functional knockout.

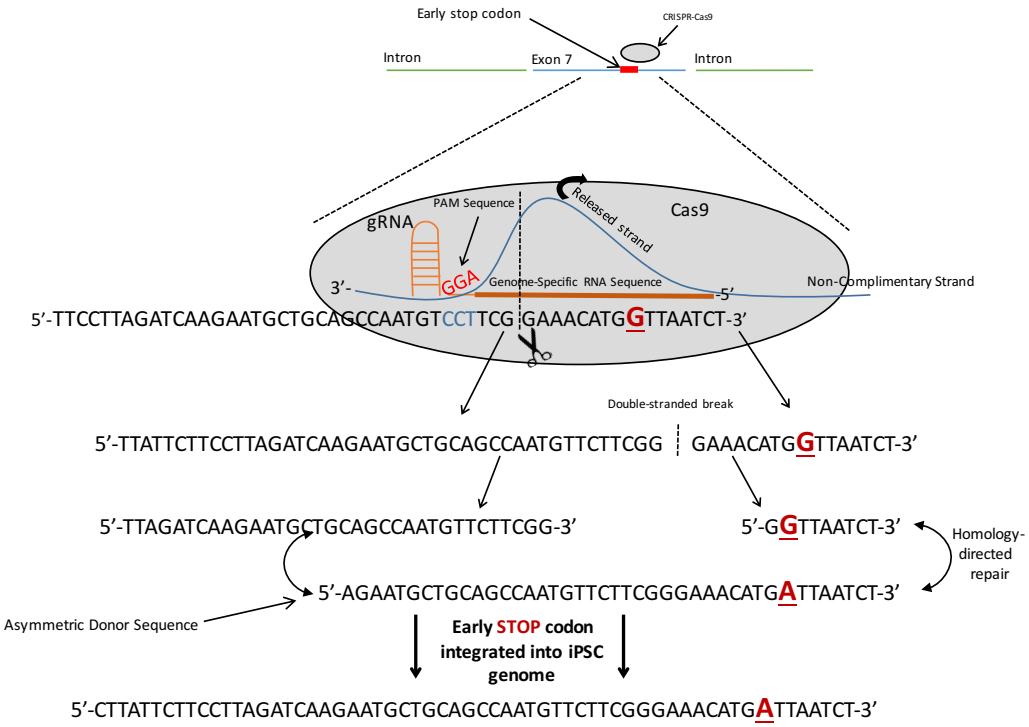

Figure 9. Graphic depicting the use of CRISPR-Cas9
The use of homology-directed repair to insert an early stop codon into exon 7 of the KCNN3 gene.

Chapter 3.

Materials and Methods

3.1. Cell culture

3.1.1. Coating plates

Corning® Matrigel (catalog #: 356231) was aliquoted into microcentrifuge tubes in 1 mg aliquots for single use. Just prior to use, the Matrigel aliquot was thawed at room temperature and immediately added to 12 ml of DMEM/F12 (Gibco, catalog #: 11330-032). The contents were mixed and then distributed into 2 x 6 well plates at 1 ml/ well. The Matrigel was left to set for 1 hour, after which 1 ml of DMEM/F12 was added to each well as a top up. Plates were stored in an incubator at 37 °C, at 5% CO_2 for storage for up to a week before use.

3.1.2. Thawing hiPSCs

Frozen hiPSCs were stored in cryovials in liquid nitrogen. Upon removal, they were gently thawed in warm water until small ice crystals were visible. The tube was disinfected and placed in a biosafety cabinet. The contents were then transferred to a 15 ml Falcon tube, after which 10 mL of mTeSR1 medium (STEMCELL Technologies, catalog #: 85850) was added dropwise to the tube. Subsequently, the cells were centrifuged for 5 min at 200 RCF. After spinning, the supernatant was aspirated. Then, 4 mL of mTeSR1 medium (STEMCELL Technologies, catalog #: 85850) supplemented with 1 µM of the ROCK inhibitor Y-27632 (Biogems, catalog #: 1293823) was gently added to the tube. Cells were resuspended by gently pipetting up and down, being careful to maintain cell clump size. Finally, 2 ml of cell suspension was added per 9.6 cm^2 well.

3.1.3. hiPSC maintenance and passaging

hiPSCs were acquired commercially from WiCell (WiCell, Madison, WI – line IRM-90). Cells were maintained in 6 well plates (VWR catalog #: 10062-892) in mTeSR1 medium (STEMCELL Technologies, catalog #: 85850) on a 1:12 dilution factor of 1 mg Corning® Matrigel (catalog #: 356231). For passaging, cells at 80% confluence were

treated with Versene (Gibco™, catalog #: 15040066) for 8-9 min at room temperature. The cells were manually detached using a 5 ml serological pipette and then added to a 6-well plate containing mTeSR supplemented with 1 μM of Y-27632 (Biogems, catalog #: 1293823) at a 1:15 split ratio.

3.1.4. hiPSC seeding and differentiation into CMs

hiPSCs at 80% confluence were incubated in Accutase® (Innovative Cell Technologies catalog #: AT104) for 8 mins at 37°C. Cells were spun at 200 RCF for 5 min, then resuspended in 2 mL mTeSR + 1 μM ROCK inhibitor and re-plated at 87 500 cells/cm^2. Once the cells reached >95% confluence, differentiation was initiated (day 0) according to the GiWi[14] protocol using CHIR99021 (Biogems, catalog #: 2520691) in RPMI-1640 (Gibco™ catalog #: 11875-085) medium supplemented by B27 minus insulin (Thermo Scientific, catalog #: A1895601).[14] At day 2, medium was replaced with RPMI-1640 with B27 minus insulin. At day 3 cells were incubated with inclusion of the WNT inhibitor IWP-4 (Biogems, catalog #:6861787). At day 5 the medium was replaced with RPMI-1640 with B27 minus insulin. Then finally at day 7, the medium was replaced with maintenance media (RPMI-1640 with B27 with insulin). Thereafter, maintenance medium was replaced every 4 days. For determining an optimal atrial differentiation protocol, retinoic acid (Sigma-Aldrich, catalog #: R2625) was added at various concentrations and days.

3.2. Quantitative real time PCR

HiPSC-CMs were removed from -80^o C after which total RNA was extracted using RNeasy Mini Kit (Qiagen, catalog #: 74104). cDNA was then reverse transcribed using the QuantiTect Reverse Transcription Kit (Qiagen, catalog #: 205311). The assay was performed on a Bio-Rad CFX96 Touch™ instrument with SsoFast™ EvaGreen Supermix (Bio-Rad, catalog #: 1725202). All reactions were done in triplicate with *GAPDH* and *ACTB* functioning as housekeeping genes (see Table 1). These housekeeping genes were validated for use in cardiac differentiation in our lab by Dr. Sanam Shafaattalab. RT-qPCR oligo efficiency was calculated by plotting the $\log_{10}$(DNA concentration) against the C_t value, then taking the slope of the regression equation $y = mx + b$ and inserting into the equation where efficiency: $E = 10^{(-1/slope)}$. The C_t, the value which represents the cycle in

which the fluorescence crosses a set threshold, is expected to increase with each dilution. Data were analyzed using the $\Delta\Delta C_t$ method. *n* was defined as number of individually thawed vials of the WiCell cell line. This was decided because on average the greatest possible variability would originate from this point.

3.3. Flow cytometry

3.3.1. CM phenotyping assay

Beating CMs were washed 1x in $PBS^{-/-}$ then incubated in 0.025% trypsin EDTA (General electric catalog #: SH30042.01) for 6-8 minutes at 37°C or until cells were visibly beginning to lift. The trypsin was inactivated with a 6x (relative to trypsin) volume of DMEM/F12 (Gibco, catalog #: 11330-032) and 10% fetal bovine serum and filtered through a 70 µm filter (Miltenyi, catalog #: 130-110-916). The filtered cells were centrifuged at 200 RCF and aspirated, then fixed in 4.1% PFA solution (BD catalog #: 554655) for 25 min. The cells were then washed and permeabilized in Saponin/FBS (BD, catalog #: 554723). Cells were then incubated in primary mouse-cTnT (Thermo catalog #: MA5-12960, 1:2000) and rabbit-MLC2V (Abcam, catalog #: ab79935, 1:1000) antibodies overnight. The next day, cells were washed 3x and incubated in secondary goat anti mouse Alexa-488 (Thermo, catalog #: A-21121, 1:500) and goat anti rabbit Alexa-647 (Thermo Scientific, catalog #: A-21245, 1:2000) antibodies for 1 hour, respectively. Cells were then washed 3x and resuspended in $PBS^{-/-}$ for analysis. All analyses are performed on the BD JAZZ Fluorescence Activated Cell Sorter. n was defined as number of individually thawed vials of the WiCell cell line.

3.4. Optical mapping assay

The optical mapping methods and paradigms were designed, built, and coded by Dr. Eric Lin and then optimized by Dr. Sanam Shafaattalab, and Marvin Gunawan. At days 20 - 30, differentiated cells were re-plated onto and maintained in a 24-well plate (VWR catalog #: 10062-896). For analysis, the medium was replaced by Ca^{2+} Tyrode's solution (117 mM NaCl, 5.7 KCl, 4.4 mM $NaHCO_3$, 1.5 mM NaH_2PO_4-H_2O, 1.7 mM $MgCl_2$, 10 mM Na-HEPES($C_8H_{18}N_2O_4S$), 5 mM glucose, 5 mM creatine, 5 mM Na-Pyruvic acid, 1.8 mM $CaCl_2$) and incubated at 37°C with 5% CO_2 for 20-30 min. The monolayers were transferred to the temperature-controlled multi-well instrument and loaded with 5 µM of

the potentiometric dye RH-237 (Thermo Scientific, catalog #: S1109) for 50 minutes. After this, cells were incubated in 15 μM of the myosin ATPase inhibitor blebbistatin (Toronto Research Chemical, catalog #: B592500) and 5 μM of the Ca^{2+} reporter Rhod-2AM (Thermo Scientific, catalog #: R1244) for 40 minutes. Data were collected and analyzed using custom software designed by Dr. Eric Lin using Interactive Data Language (IDL). Other statistical analyses were completed on Microsoft Excel as mentioned the figure captions where appropriate.

3.5. CRISPR-mediated Genome Editing

3.5.1. sgRNA preparation

To anneal the sgRNA, 1 μL of each of the forward and reverse pre-phosphorylated sgRNA (100 μM) and 8 μL of ddH_2O were added to a PCR tube and cycled at 95ºC for 5 min after which the temperature ramped down to 25ºC at a rate of 5ºC/min. The annealed sgRNA was then cloned into the pCCC vector.

3.5.2. Cell transfection

hiPSCs were transfected in a 24-well plate with 500 ng of pCCC-KCNN3KO and 10 pmol of ssODN using lipofectamine 3000 (Thermo, catalog#: L3000015) according to the outlined protocol. Two days post transfection, cells were re-suspended using EDTA and sorted into 6 well plates containing 2 ml mTeSR, 1x CloneR (STEMCELL, catalog #: 05888), and 1% pen strep antibiotic (Thermo, catalog #: 15070063). The medium was changed two days after sorting. Approximately 10 days after sorting, colonies were manually picked and placed into a 96-well plate containing mTeSR and ROCK inhibitor.

3.5.3. Direct lysis

Sorted hiPSC colonies were aspirated and washed 1x with $PBS^{-/-}$. The Direct lysis media containing 50% direct lysis buffer (Viagen, catalog #: 302-C), 50% ddH_2O and 50 μL/ml of 1mg/ml proteinase K (Viagen, catalog#: 501-PK) was added to the wells. The 96-well plate is then wrapped in foil, placed in a Tupperware container with a moist cloth, and placed in a shaker at 200 RPM at 55ºC for 4 hours. The contents were cooled for 1 hour at 4ºC and then placed in a thermocycler at 85ºC to deactivate the proteinase K.

3.5.4. Nested PCR

Two sets of flanking primer pairs were designed with the first, an outer pair, for initial amplification and a second, inner pair, to further amplify the product. In a 96-well PCR plate 2.5 µL of each of forward and reverse primer at 2.5 µM, 12.5 of 2x ABM taq polymerase mastermix (ABM, catalog#: G013-dye) and 7.5 µL of cell lysate were added to each well. After completion of the first PCR reaction, the second PCR was prepared and conducted the same way using the inner primer pairs and 7.5 µL of the first initial PCR product instead of the cell lysate. All reactions were conducted using Biorad C100 thermal cycler.

All Direct lysis and nested PCR techniques were developed and optimized by Valentine Sergeev.

3.5.5. Magnetic PCR purification

To each well in a 96-well PCR plate, 1.8x volume (relative to PCR product volume) of Magnetic PCR reagent (Magbio, catalog #: AC-60050) was added, mixed thoroughly and allowed to incubate at room temperature for 5 min. The PCR plate was then placed on a magnetic tray for 3 minutes to segregate the DNA-bound magnetic beads. The remaining media was aspirated. Next, 500 µL of 70% ethanol was added and incubated at room temperature, then aspirated. This step was repeated before letting the beads dry for 3-5 min. Once dry, the plate was removed from the magnet and 40 µL of warm sterile ddH_2O was added and mixed. After incubation for another 2 min at room temperature, the plate was again placed on the magnet for another two minutes. The DNA contained in the supernatant was then pipetted out.

3.5.6. Magnetic activated cell sorting

Differentiated cells were dissociated into single cells using 0.25% Trypsin-EDTA solution (Thermo Scientific, catalog #: 25200072) at 37°C for 8-10 minutes and inactivated with 6x (relative to the trypsin-EDTA solution) volumes of DMEM/F12 (Gibco, catalog #: 11330-032) and 10% Fetal bovine serum. The cells were then filtered through a 70 µm filter (Miltenyi, catalog #: 130-110-916). Following this, the cells were enriched using a MidiMACS LS Magnet column setup (Miltenyi, catalog #: 130-042-301) and the PSC-

derived CM Isolation Kit (Miltenyi, catalog #: 130-110-188) according to the manufacture's protocol. The enriched cells were re-plated in RPMI/B27(+) + 1 μM ROCK inhibitor in 12- or 24-well plates at 500 000 cells/cm^2.

Chapter 4.

Results

4.1. Assay Optimization

4.1.1. Quantitative real time PCR (RT-qPCR)

When designing primers for the RT-qPCR panel, multiple factors that could influence the accuracy of the assay were considered. Ideally, in the panel, the various oligonucleotides (oligos) would bind all relevant transcript variants of their target gene, have no offsite binding, work at a high efficiency over a broad range of cDNA concentrations, and would run together at the same annealing temperature and PCR settings. First, the oligos were individually designed to target areas that were common amongst all transcript variants of that gene. Although most primers were designed with a preference for exon-exon borders, this was neither possible nor necessary for all the target transcripts. Processed pseudogenes are sequences that resemble known genes but do not produce functional transcripts, and lack introns.[162] These can be amplified erroneously if gDNA contamination occurs during the RT-qPCR assay.[162] As such, DNase treatment, which is routinely performed before running the assay, is more important than this aspect of the oligonucleotide design.

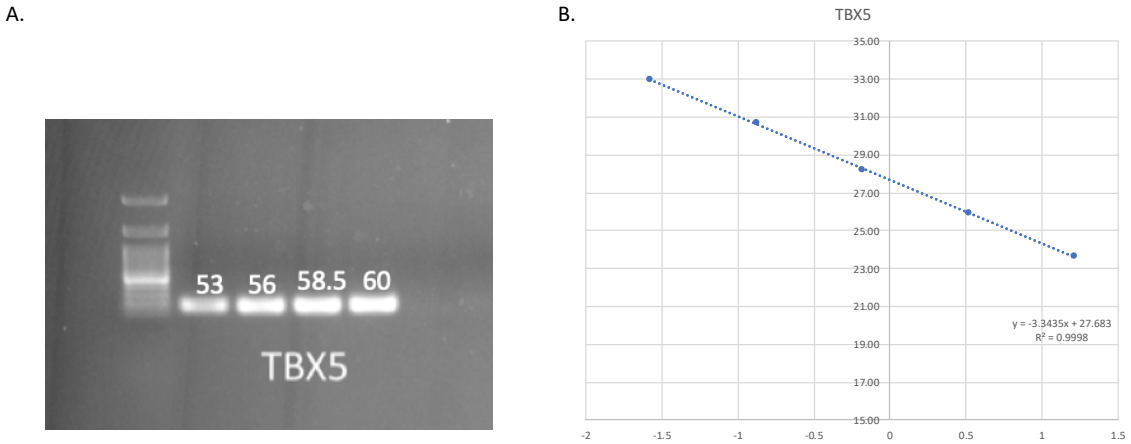

Figure 10. Optimization of TBX5 Oligo for RT-qPCR.
A: Temperature gradient optimization to determine ideal annealing temperature. B: cDNA concentration gradient to determine primer efficiency.

Once the oligos were designed, a temperature gradient test was run to determine the temperature at which the oligo would have the highest efficiency (Figure 10A).

All primers were then run through a concentration gradient test in which cDNA was diluted by 10, 5, or 2-fold. Final efficiencies between 90% and 105% with an R^2 >0.98 were considered to be acceptable (Figure 10B).[163]

Off-targets were determined in three ways (Figure 11). The first was a visual confirmation on an SDS-PAGE gel after temperature optimization (Figure 11A). Multiple bands would be indicative of off-site target amplification. The second method was through visualization of the melt curve (Figure 11B). Peaks at multiple different temperatures would indicate offsite targets, which in the case of TBX5 were not present.

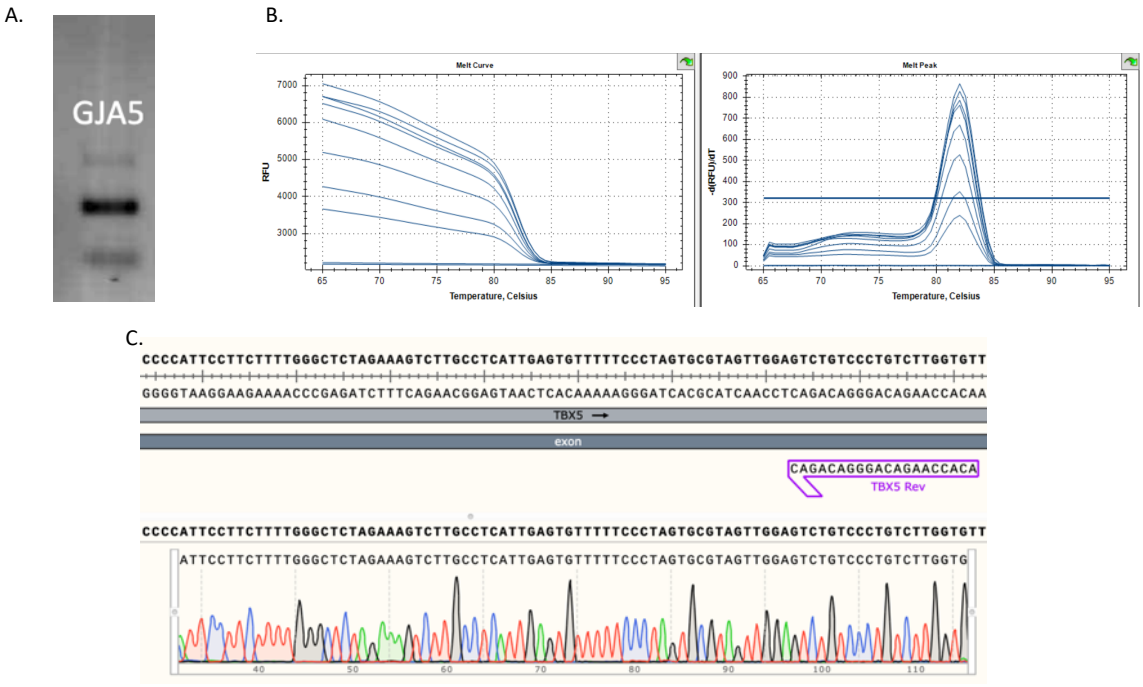

Figure 11. Determining offsites in RT-qPCR.
A: Temperature optimization of GJA5 gene where offsite amplicon targets are visible. B: RT-qPCR melt curves for TBX5 where there are no offsites visible. C: Sequencing results for the TBX5 amplicon.

Lastly, the resulting amplicons were sequenced (Figure 11C). If the oligo resulted in off-target amplification at any of these three checkpoints it was not used. In the end, a set of primers that targeted atrial, nodal, and developmental genes was optimized. In combination with the markers optimized by Dr. Sanam Shafaattalab, this list of markers provided a strong transcript-based analysis of CM phenotype.

Table 1. List of RT-qPCR primers

Subtype	Gene	Protein	Primer sequence 5'→3'
Atrial	*NPPA*	Atrial Natriuretic peptide	ACAGGATTGGAGCCCAGAG
			GGAGCCTCTTGCAGTCTGTC
Atrial	*KCNA5*	Potassium voltage-gated channel, shaker-related subfamily, member 5, $K_v1.5$	CGAGGATGAGGGCTTCATTA
			CTGAACTCAGGCAGGGTCTC
Atrial	*KCNJ3*	Potassium inwardly-rectifying channel, subfamily J, member 3, $K_{ir}3.1$	CTGCTCAAAGGATGACTTGT
			CATGGAACTGGGAGTAATCA
Atrial	*KCNN2*	Small conductance calcium-activated potassium channel 2, SK2	TAAGCCAGACCATCAGGCAG
			GGGACCGCTCAGCATTGTAA
Atrial	*PITX2*	Paired-like homeodomain transcription factor 2	GCTTGCGAGCAAGGGAGTGTA
			CATTGCATCCACCAGAGAAACTA
Atrial	*CACNA1 D*	Calcium channel, voltage-dependent, L type, alpha 1D subunit	GATGCGATAGGATGGGAATG
			CCACTAAGGACACCAAGAAC
Unknown	*KCNN3*	Small conductance calcium-activated potassium channel 3, SK3	CCTGTATGAGTCAGCCTTTC
			AGCTCTAGGGACTTCTAACC
Nodal	*TBX3*	T-box transcription factor TBX3 protein	CTTGTGATGTTTTCAGAGCC
			TTCTCTCTAAAAGCAAGCGT
Nodal	*HCN4*	Potassium/sodium hyperpolarization-activated cyclic nucleotide-gated channel 4	GGAGTACCCCATGATGCGAA
			CTTCTTGCCAATGCGGTCCA
Atrial	*GJA5*	Gap junction alpha-5 protein, connexin 40	AATCTTCCTGACCACCCTGCATG
			CAGCCACAGCCAGCATAAAGAC
Atrial	*NR2F2*	Chicken ovalbumin upstream promoter transcription factor 2	TCACCCGCCAAACTAAAGGA
			CTCTGCACCGCAAAACCATA
Atrial	*SLN*	Sarcolipin	GCTCAAGTTGGAGACAGCGAG
			GGCTTCTCCTCACCTCCTGAAG
Nodal	*SHOX2*	Short stature homeobox 2	TAAAGGTGTTCTCATAGGGGC
			CCTGAACCTGCTGAAATGGC
Developmental: ANP activator	*TBX5*	T-box transcription factor 5 TBX5 protein	TACCACCACACCCATCAAC
			ACACCAAGACAGGGACAGAC
Developmental: SA node specification	*TBX18*	T-box transcription factor 18 TBX18 protein	ACTGTCTTCACAACCGTCAC
			CTTCCAAACCCATTCTGTTGC
Developmental: ANP repressor	*TBX20*	T-box transcription factor 20 TBX20 protein	CGAGGGTCAGCCTTTACAAC
			GTTGCTATGGATGCTGTGCTG
Developmental	*GATA2*	GATA binding protein 2	GACTACAGCAGCGGACTCTT
			CTTCTGAACAGGAACGAGCC
Developmental	*GATA4*	GATA binding protein 4	CCCCAATCTGTAGATATGTTTG
			TGCCGTTCATCTTGTGGTAG
Developmental	*GATA6*	GATA binding protein 6	GGGCTCTACATAGGCGTCAG
			AAGCAGACACGAGTGGAGTG
Cardiac	*TNNT2**	Cardiac Troponin T	TTCACCAAAGATCTGCTCCT
			TACTGGTGTGGAGTGGGTG
Cardiac	*NKX2.5**	Homeobox protein Nkx-2.5	CTCCCAACATGACCCTGAGT
			GACGGCGAGATAGCAAAGG
Ventricular	*IRX4**	Iroquois-class homeodomain protein IRX-4	TTCCGTTCTGAAGCGTGGTC
			TGAAGCAGGCAATTATTGGTGT
Ventricular	*MYL2**	Myosin light chain ventricular isoform	ACAGGGATGGCTTCATTGAC
			CCGCTCCCTTAAGTTTCTCC
Atrial and some Ventricular	*MYL7**	Myosin light chain atrial isoform	GGCAAAGGGGTGGTGAAC
			TTCTCGTCTCCATGGGTGAT
Housekeeping	*GAPDH*	Glyceraldehyde 3-phosphate dehydrogenase	CATGTTCCAATATGATTCCAC
			AGTCTTCTGGGTGGCAGTGAT
Housekeeping	*ACTB*	β-actin	ATTGCCGACAGGATGCAGAA
			GGGCCGGACTCGTCATACTC

4.1.2. Flow cytometry assay

The overall goal was to create an assay in which there would be minimal cell loss during preparation, meaning that a lower number of cells would be required to complete that assay.

The first step was to optimize a cell lifting and fixing procedure. Lifted cells however would not spin down in the centrifuge resulting in immense cell loss. Large clumps were visibly floating in the centrifuge tubes. I predicted that by increasing lifting time and filtering the remaining large clumps, that I would be able to alleviate this issue. A 70 µm filter was useful in removing large clumps and helped with forming a visible pellet after centrifugation. Following this, cell lifting, fixing, and permeabilization procedures were optimized. Firstly, lifted cells were fixed with 2% or 4% paraformaldehyde solution for 10 or 20 mins. Only cells fixed in 4% paraformaldehyde for 20 mins would form a pellet when centrifuged. To find the ideal lifting and permeabilization procedure, cells were incubated in 0.25% trypsin for 2, 4, or 6 mins. Following lifting and fixing, the cells were permeabilized using either 0.1% Triton X or a saponin based solution.

Incubating cells for 6 minutes in 0.25% trypsin and permeabilizing them using saponin resulted in the highest viability (Figure 12). TrypLE™ (Thermo catalog#: 12604013) was also tested, but trypsin still showed a better overall viability.

Once there was a working protocol, I progressed to optimizing antibodies. Ideally, the panel of markers that would indicate cardiac, atrial, and ventricular expression. First, an unconjugated antibody for the cardiac marker cTnT was optimized (Figure 13). After testing multiple different concentrations with the secondary antibody at 1:500, a primary antibody concentration of 1:2000 gave a good separation of peaks with no offsite binding.

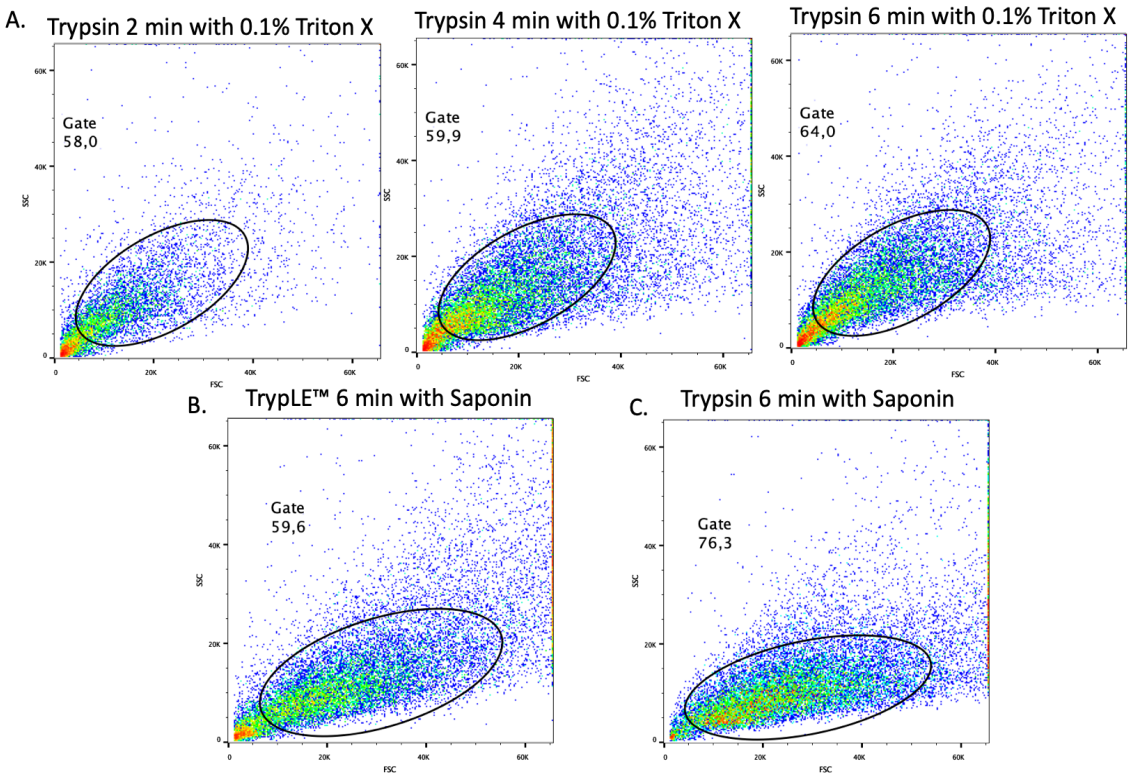

Figure 12. Optimization of flow protocol.
A: Various 0.25% Trypsin incubation times along with 0.1% Triton X permeabilization. B: 6-minute incubation with TrypLE™ along with saponin permeabilization. C: 6-minute incubation with 0.25% trypsin and saponin permeabilization. Forward scatter is on the x-axis and side scatter is on the y-axis

Next, antibodies for the ventricular marker MLC-2V were tested. I tested antibodies from three different companies: a conjugated antibody from Miltenyi Biotec (catalog #: 130-106-184), an unconjugated mouse antibody from BD (catalog #: 565497), and an unconjugated rabbit antibody from Abcam (catalog #: ab79935). The Miltenyi antibody had no fluorescence even at very high concentrations (Supplemental Figure 2.). The BD antibody despite multiple titrations had expression levels that were higher than the troponin T levels (Supplemental Figure 3.), indicating offsite binding. Because both the cTnT and MLC- 2V antibodies were both mouse antibodies, it was not possible to separate the peaks via co-stain. The Abcam antibody, however, was rabbit conjugated allowing for a co-stain. After multiple titrations of both primary and secondary antibodies, the primary antibody at 1:1000 and the secondary at 1:4000 resulted in a good separation as well as minimized offsite binding.

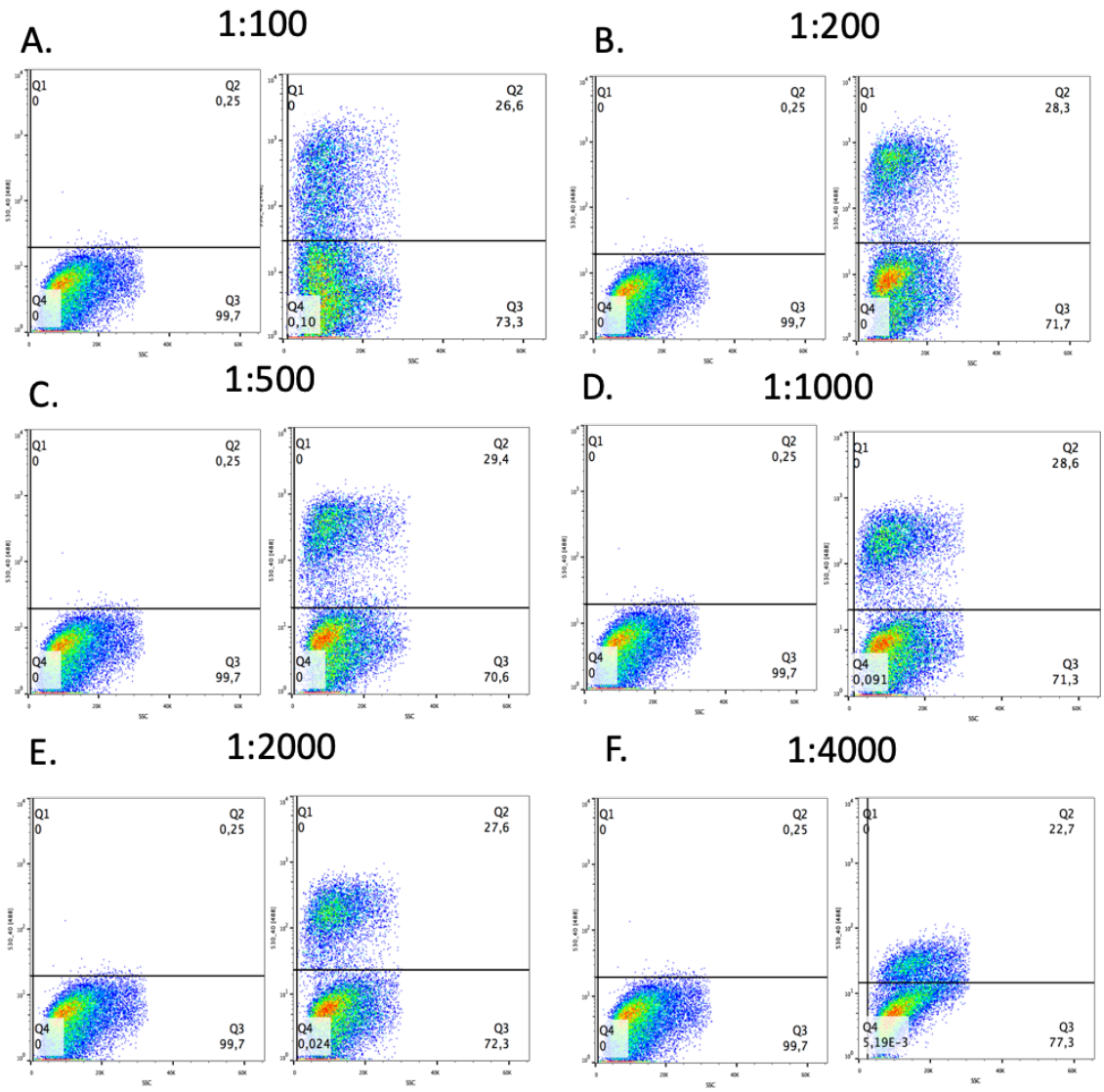

Figure 13. Titration of troponin T antibody
A: 1:100. B: 1:200. C: 1:500. D: 1:1000. E: 1:2000. F: 1:4000. The concentration of the secondary antibody was 1:500. Forward scatter is on the x-axis and side scatter is on the y-axis

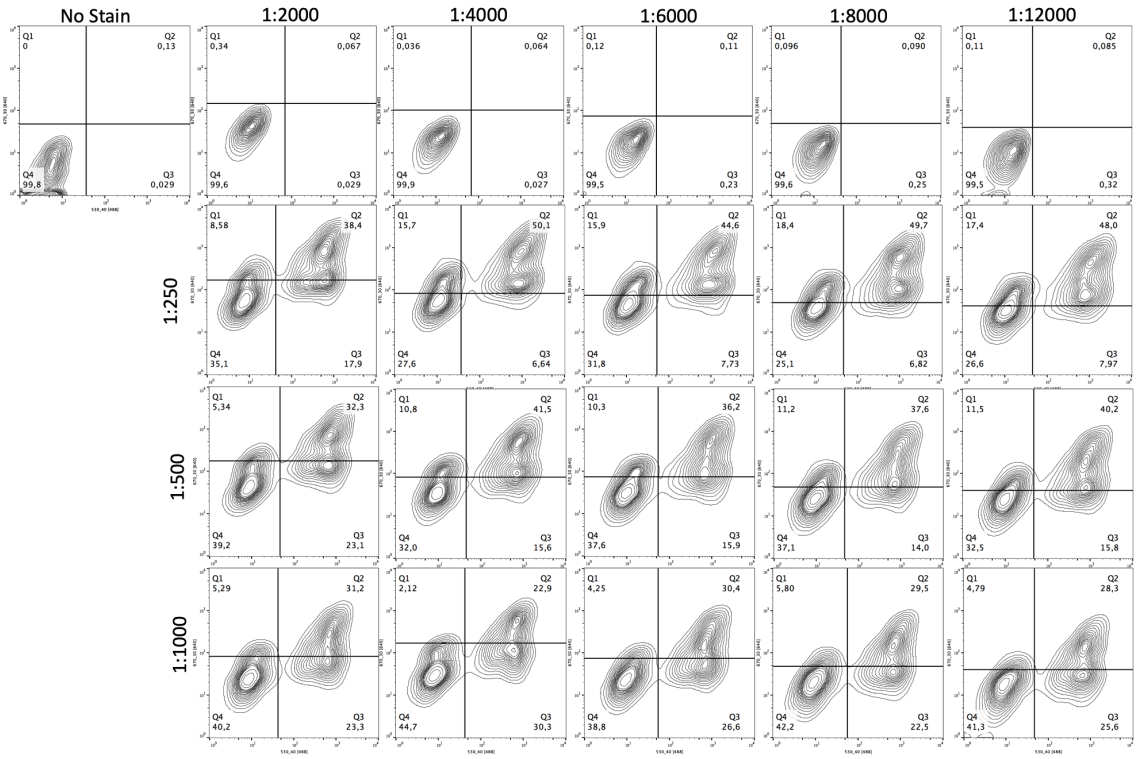

Figure 14. Titration of primary and secondary antibodies to optimize myosin light chain 2V antibody

Ratios across the top represent secondary antibody concentration and those across the side represent primary antibody concentration. Cells were co-stained with troponin T (x-axis) and MLC-2V (Y-axis). These data are shown as contour plots to better visualize the different populations.

Lastly, an antibody that would indicate atrial expression was tested. This included MLC-2A antibodies from two different companies: one from Miltenyi (catalog #: 130-106-191) and one from BD (catalog #: 565496). Both were found to be unsuitable for the same reasons as their MLC-2V variants (Supplemental Figure 2. And 3.). Following this, an antibody targeting the atrial specific potassium channel $K_v1.5$ (catalog #: sc-377110) was tested. Even after multiple titrations, this antibody was unable to distinguish expression between atrial and the ventricular control cells (Figure 15).

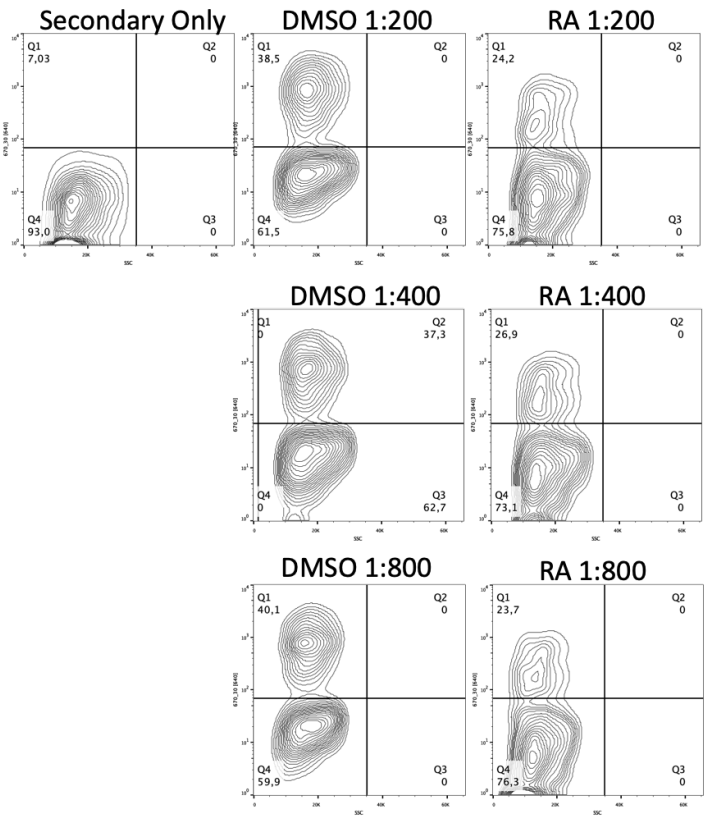

Figure 15. Titration of Kv1.5 antibody. Secondary at 1:500.
Primary antibody was titrated at 1:200, 1:400, and 1:800 for both RA and DMSO control cells. Forward scatter is on the X-axis and antibody fluorescence on the Y-axis.

Although we were not able to find a reliable positive marker for atrial expression, the combination of the cardiac and ventricular marker, functional testing with OM, and transcript analysis with the RT-qPCR panel were deemed sufficient in determining cell phenotype.

4.1.3. Magnetic-activated cell sorting

Next, a method for enriching cardiac populations using Magnetic-activated cell sorting (MACs™) was optimized. We found a sharp increase in proportion of differentiated cells expression cTnT, from 73 ± 4% to 94 ± 3%. (Figure 16). There was no significant difference in the proportion of MLC-2V expressing cells in the $cTnT^+$ populations, their expression was 59 ± 2% before and 59 ± 3% after enrichment. These data show that MACs is a viable method of enriching cardiac populations, especially if a high proportion of cardiac cells are required despite poor differentiation efficiencies.

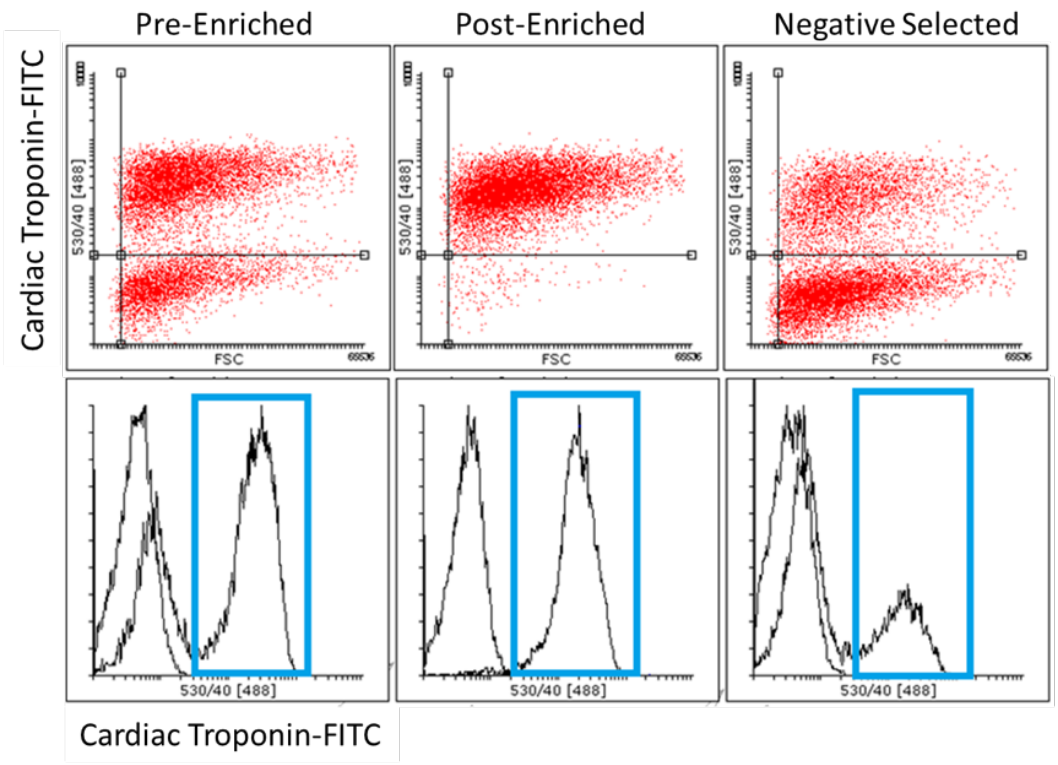

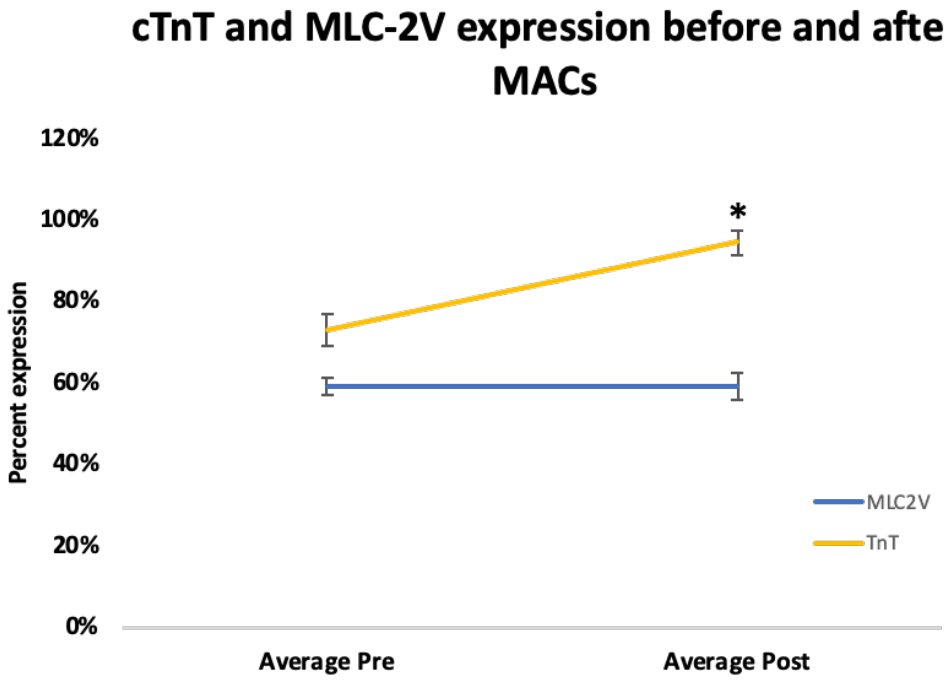

Figure 16. Enriching cardiac populations using magnetic-activated cell sorting. Before sorting, cTnT and MLC-2V expression was 73 ± 4% and 59 ± 2% respectively. Post enrichments cTnT increased substantially to 94 ± 3% whereas the proportion of MLC-2V in the cTnT population stayed at 59 ± 3%. n=3. *p<0.05 relative to the "pre" condition. Error bars represent the standard error of the mean. Data were collected by both Marvin Gunawan and I. The histograms were produced by Marvin Gunawan.

4.2. CD235A expression

Since we were not able to control the activin A/BMP ratio in our differentiation procedure, it was important to characterize the amount of ventricular-potentiated mesoderm (i.e. does not respond to retinol). CD235A expression was observed through day – 7 where cells were lifted from the wells before media addition. Expression peaked at 70 ± 5% at day 4 and continued to decrease to 60 ± 4% on day 5, 32 ± 2% on day 6, and 25 ± 2% on day 7, n=3.

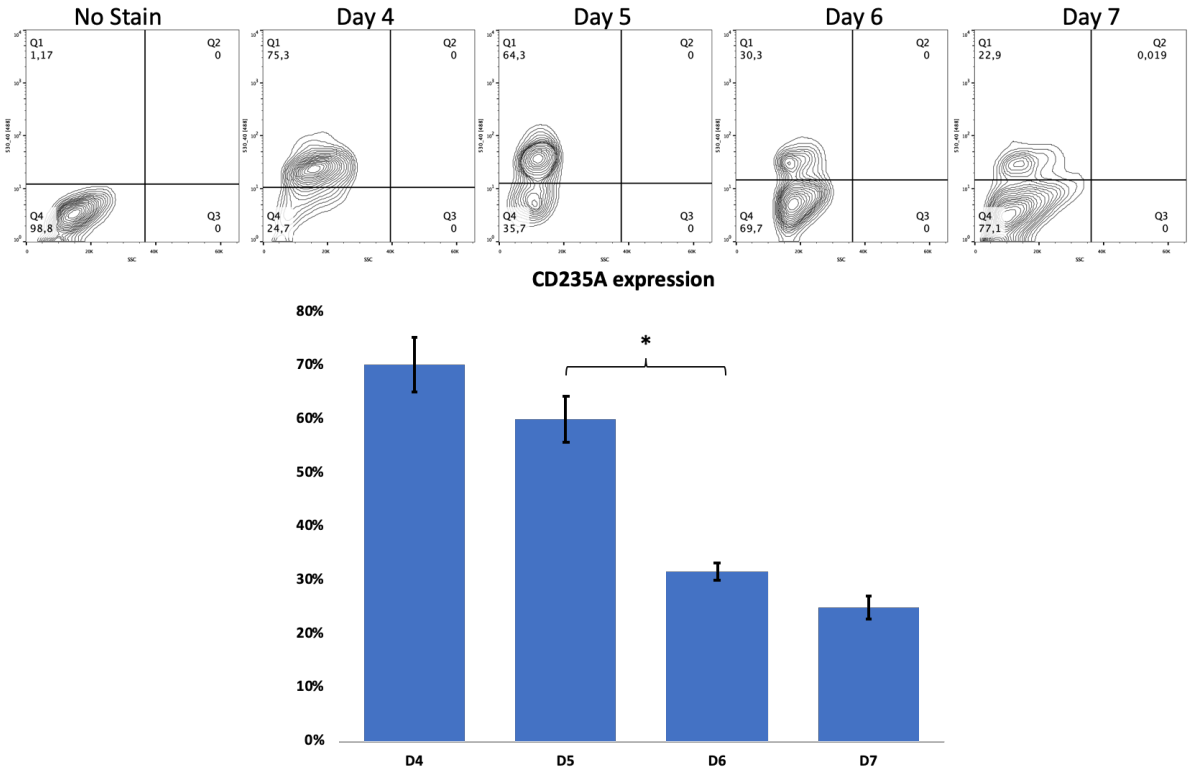

Figure 17. CD235A expression from day 4 to day 7.
Expression peaked at D4 at 70%, then 60% at day 5 then dropped to 32% and 25% on days 6 and 7 respectively. n=3. *p<.05. Error bars represent the standard error of the mean.

These data show that during a typical Lian protocol differentiation, cells are preferentially primed to become hiPSC-vCMs (due to their inability to convert retinol to retinoic acid). The addition of RA, however, circumvents this pathway and will still likely result in the production of hiPSC-aCMs.

4.3. Optimization and creation of an atrial differentiation protocol

4.3.1. Retinoic acid addition on days 3, 5, and 7

I hypothesized that RA addition between days 3 and 7 would influence the fate of the hiPSCs. Observing previous publications where atrial cardiomyocytes always had an increased rate and knowing that *SHOX2* expression is also regulated by RA, I predicted that an increase in beating frequency alone would alone be sufficient in determining whether cells were receptive to RA itself, even if significant changes in overall transcript expression did not occur.[164] Therefore, an increase in rate would determine a possible window of addition. As such, 1 μM of RA was added on either day 3, day 5, or day 7 of differentiation (Figure 18). At day 20, the beating frequency of the hiPSC-CMs was monitored. When RA was added on either day 3 or day 5 there was a marked increase in beating rate. For the vehicle (DMSO) control, the average beating frequency was 50 ± 3 bpm. For RA addition at day 3, the frequency was markedly increased to 125 ± 17 bpm and for day 5 addition the rate increased to 151 ± 17 bpm. For day 7 additions however, the rate was similar to the DMSO control at 55 ±3 bpm. Next, troponin expression was analyzed to see if the addition of 1 μM RA had an influence on differentiation efficiency. There was no significant difference in cTnT expression between the different additions compared to the vehicle control (Figure 18). Next, for the days that showed an increased rate, various markers were analyzed via RT-qPCR (Figure 20). Analyses were completed on the cardiac markers: *TNNT2* and *NKX2.5,* atrial markers: *NPPA, KCNA5*, and *CACNA1D,* the nodal marker: *SHOX2*, and lastly the ventricular markers: *MYL2* and *IRX4*. Cardiac expression was similar across all conditions and in line with the flow cytometric analyses. Out the atrial markers, only *NPPA* at day 5 RA showed a significant increase in expression. Out of the ventricular markers, none showed a significant reduction in expression for the RA conditions. As expected, *SHOX2* was markedly increased in the day 3 and day 5 RA condition but was not increased in day 7 addition (data not shown). Looking at these data, I predicted that a number of RA additions over time would more strongly drive the differentiation towards an atrial lineage. Additionally, if there was some temporal variability in RA receptiveness between individual cells, a longer window of addition would be beneficial. As such, I tested 3 windows of additions where RA was

added successively (daily additions every 24H). These windows were: days 3-5, days 3-6, and days 4-6 post initiation.

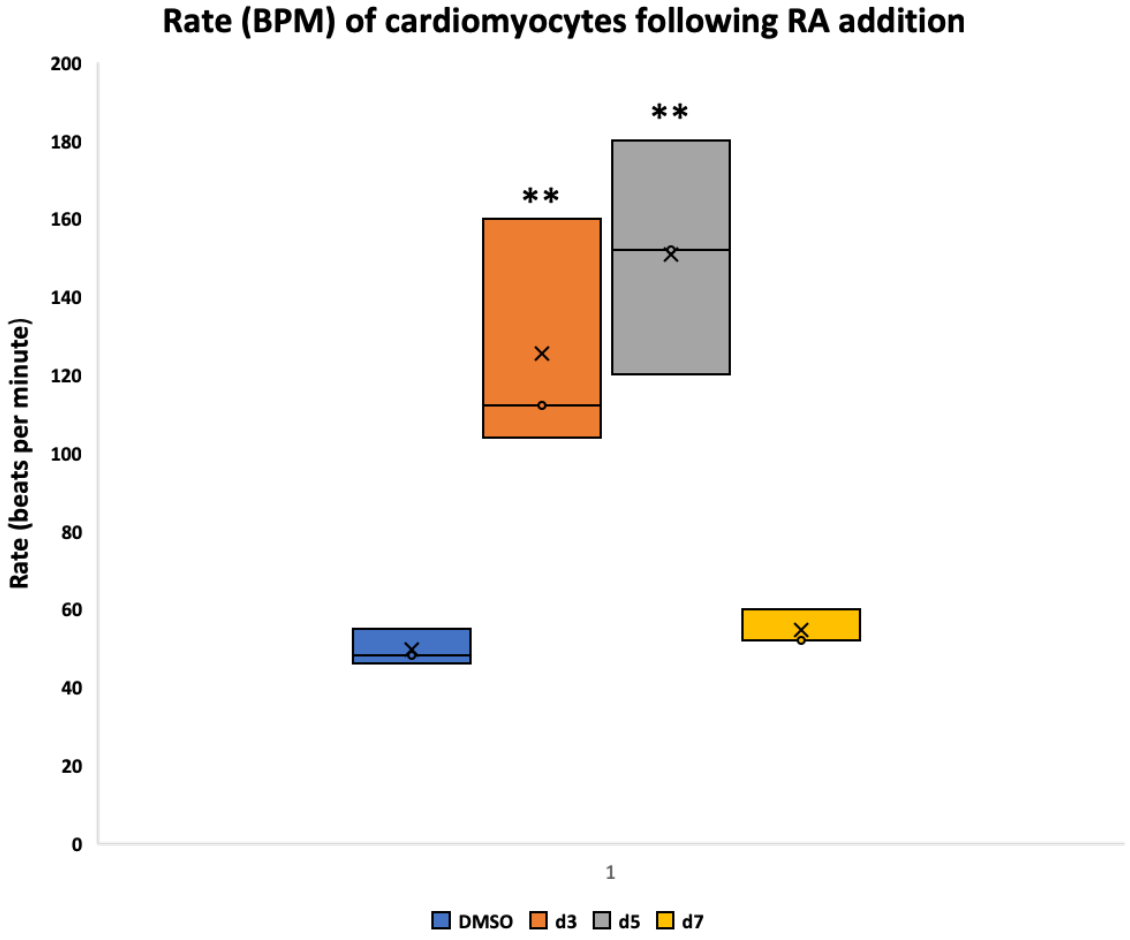

Figure 18. Beating frequency at Day 20 after 1 μM RA addition over various days.

The vehicle control (DMSO) had an average frequency of 50 ± 3 bpm. Day 3 had an average rate of 125 bpm ± 17 bpm. Day 5 had an average frequency of 151 ± 17 bpm. Day 7 had a frequency of 55 ± 3 bpm. n=3. **p<0.01 relative to the DMSO control. “x” represents the mean. Error bars represents the standard error of the mean.

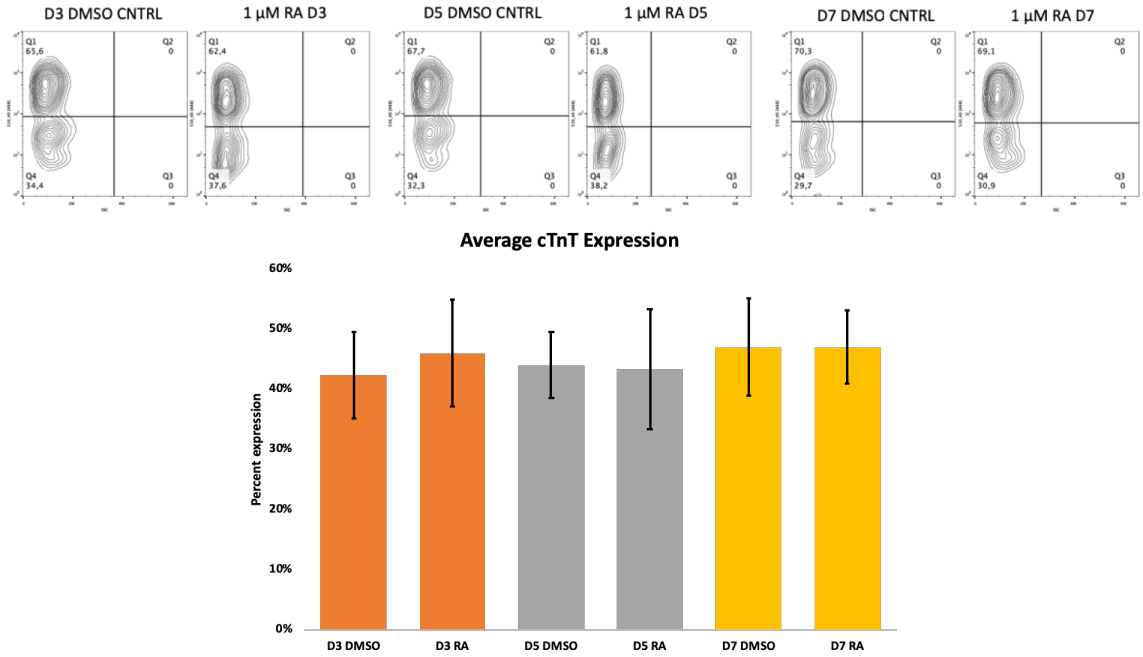

Figure 19. cTnT expression over various one-day additions of RA.
Difference in cTnT expression compared to the vehicle control when 1 µM RA was added over 1 day. n=3. Error bars represent the standard error of the mean. On the histogram, the X-axis represents the forward scatter and Y-axis represents fluorescence

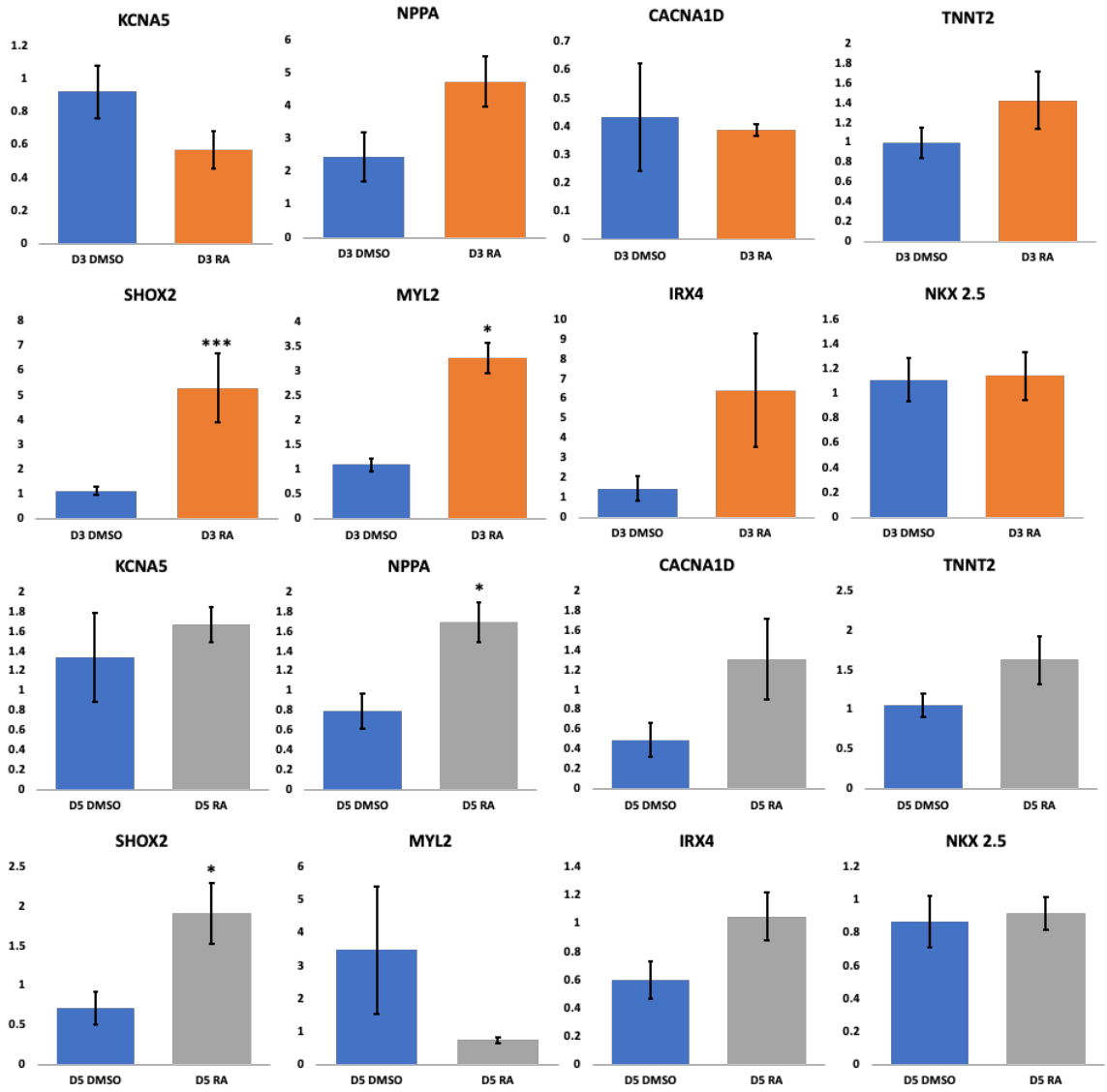

Figure 20. RT-qPCR expression profile of cells differentiated by a discrete addition of 1 μM RA compared to their respective vehicle controls.
n=3. *p < 0.05 ***p < 0.001 relative to the DMSO control. Y-axis represents the fold change in expression. Error bars represent the standard error of the mean.

4.3.2. Titrating retinoic acid additions over various time windows

The first step was to titrate different concentrations of retinoic acid over the various windows. For days 4-6, 0.75 μM RA resulted in no significant change in cTnT expression at 60 ± 3% compared to the no treatment and DMSO control which had a cTnT expression of 61 ± 3% and 63 ± 2%, respectively (Figure 21). Over days 3-5 and days 3-6 0.75 μM was also determined to be the best concentration (Supplemental Figure 4 and 5.).

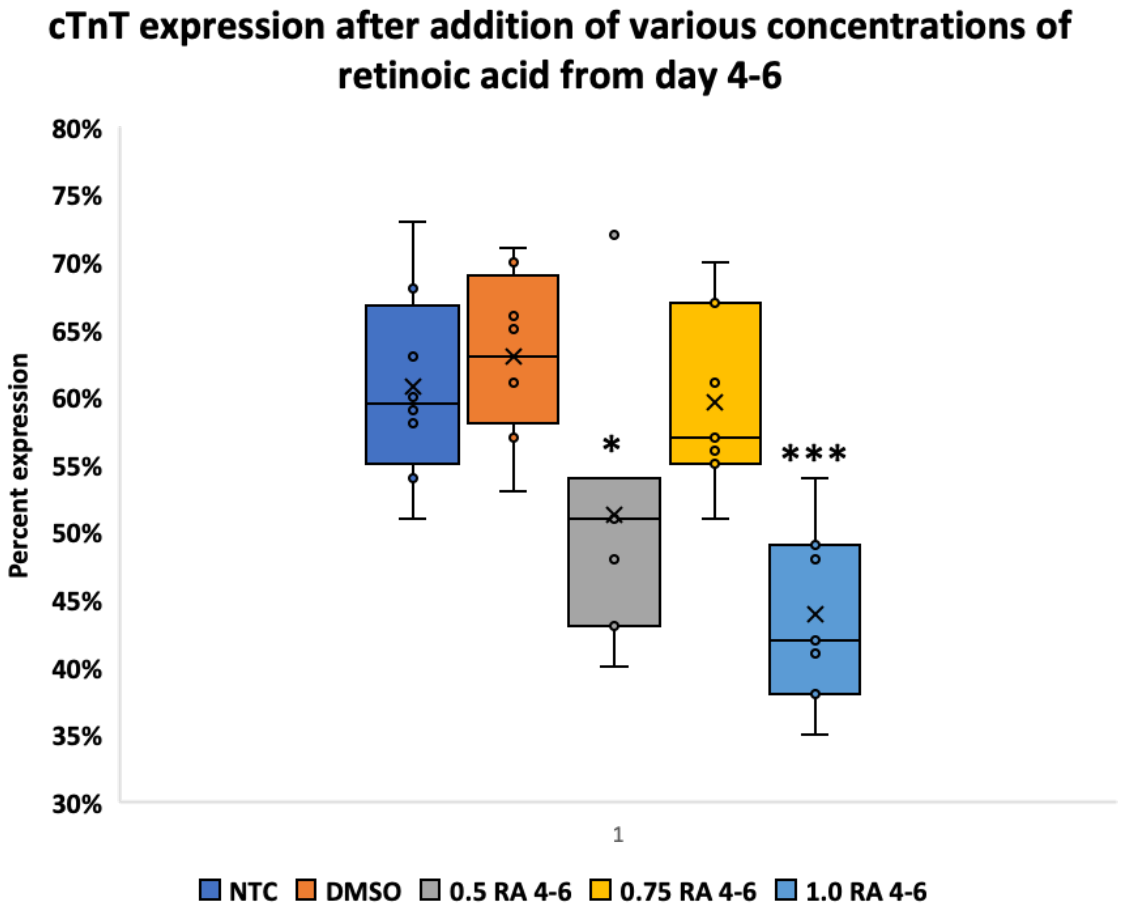

Figure 21. Retinoic acid titration from day 4-6.
There was no significant difference in cTnT expression between the no treatment control (61 ± 3%) and the DMSO vehicle control (63 ± 2%). 0.5 μM RA and 1.0 μM RA saw a significant decrease in cTnT expression, (51 ± 4%) and (44 ± 3%) respectively. 0.75 μM RA did not see a significant change in cTnT expression (60 ± 3%). n=6, for NTC and DMSO n=7. *p<0.05 ***p<0.001 relative to the DMSO control. "x" represents the mean.

At day 20, all of the various conditions were found to have an increased beating frequency compared to their respective controls (Figure 22). The no treatment and DMSO control had an average rate of 49 ± 2 bpm and 50 ± 1 bpm. For additions from day 3-6, 4-6, and 3-5, the average rates were 103 ± 3 bpm and 96 ± 7 bpm respectively. Next, the cells were analyzed using flow cytometry to again observe cTnT expression. There was no difference in expression between all of the conditions (Figure 23). When looking at the change in MLC-2V expression there were some changes in expression depending on the condition (Figure 23). Addition of RA from day 3-5 showed no significant decrease in expression, compared to its DMSO control p = 0.09. For RA additions from day 3-6 and from day 4-6 there was a significant decrease in the expression of MLC-2V.

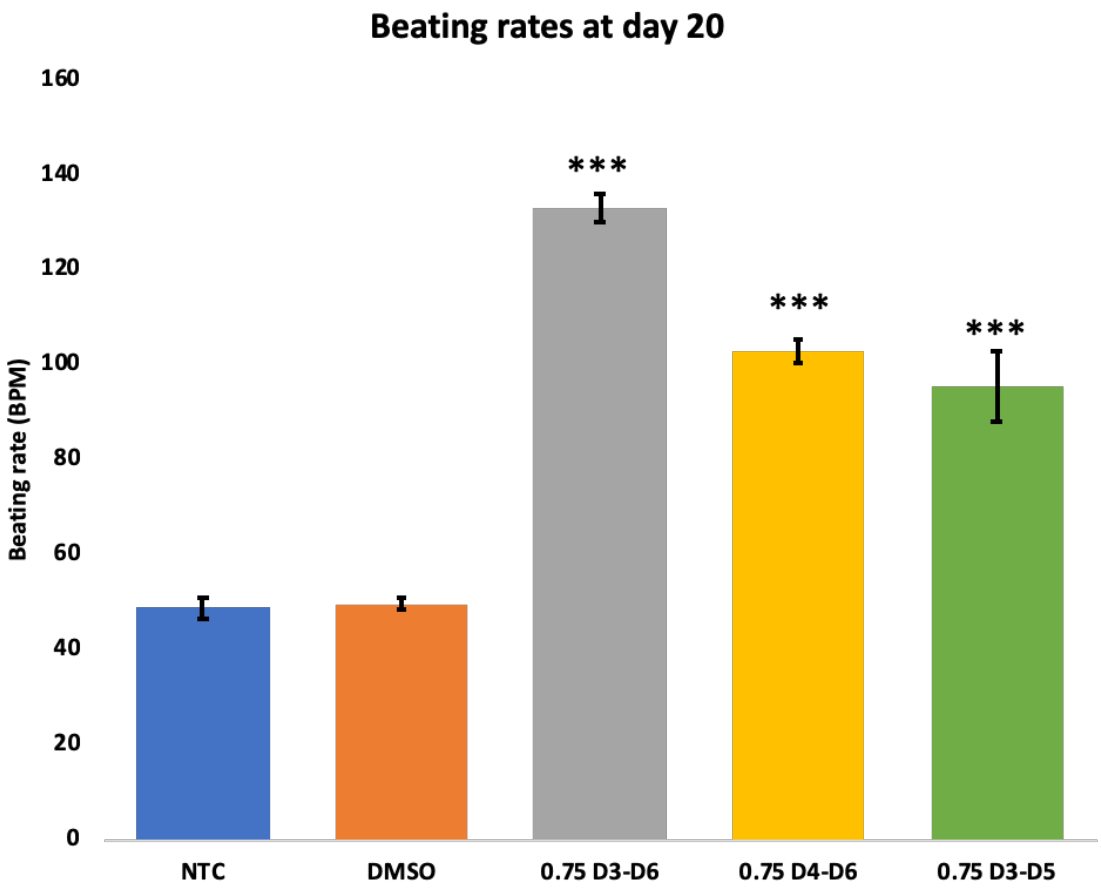

Figure 22. Beating rates at day 20 after adding 0.75 μM RA over days various windows.

The no treatment control and DMSO vehicle control had no significant difference in beating rates 49 ± 2 bpm and 50 ± 1 bpm respectively. Whereas the 0.75 μM RA D3-D6, D4-D6 and D3-D5 had significantly higher beating rates of 133 ± 3 bpm, 103 ± 3 bpm, and 96 ± 7 bpm respectively. n=7. ***p<0.001 relative to the DMSO control. Error bars represent the standard error of the mean.

For the day 3-6 addition the expression dropped from 50 ± 2% to 3 ± 2%. For the day 4-6 additions it dropped from 53 ± 1% to 8 ± 1%. The RT-qPCR analysis confirmed these findings. As expected, additions from day 3 - 5 showed no significant change in expression compared to their controls (Supplemental Figure 6.) with the exception of *SHOX2*. Next, a number of genes for the day 3 - 6 and 4 - 6 additions were analyzed. These included the atrial markers: *KCNA5*, *CACNA1D*, *NPPA*, and *KCNJ3*; ventricular markers: *IRX4 and MYL2*, as well as pan cardiac markers: *TNNT2* and *NKX 2.5 respectively*. And lastly, the nodal marker, *SHOX2*. Of all of the atrial markers, only RA additions from day 4 - 6 showed any significant increase in expression (Figure 24). There were decreases in MYL2 expression in both conditions, supporting the data from the flow

cytometry assay. Day 3 -6 saw a greater decrease relative to the control than day 4-6 additions did however only day 4 – ere 6 additions saw a significant decrease in *IRX4*. There was no significant difference in the expression of the pan-cardiac markers between all conditions.

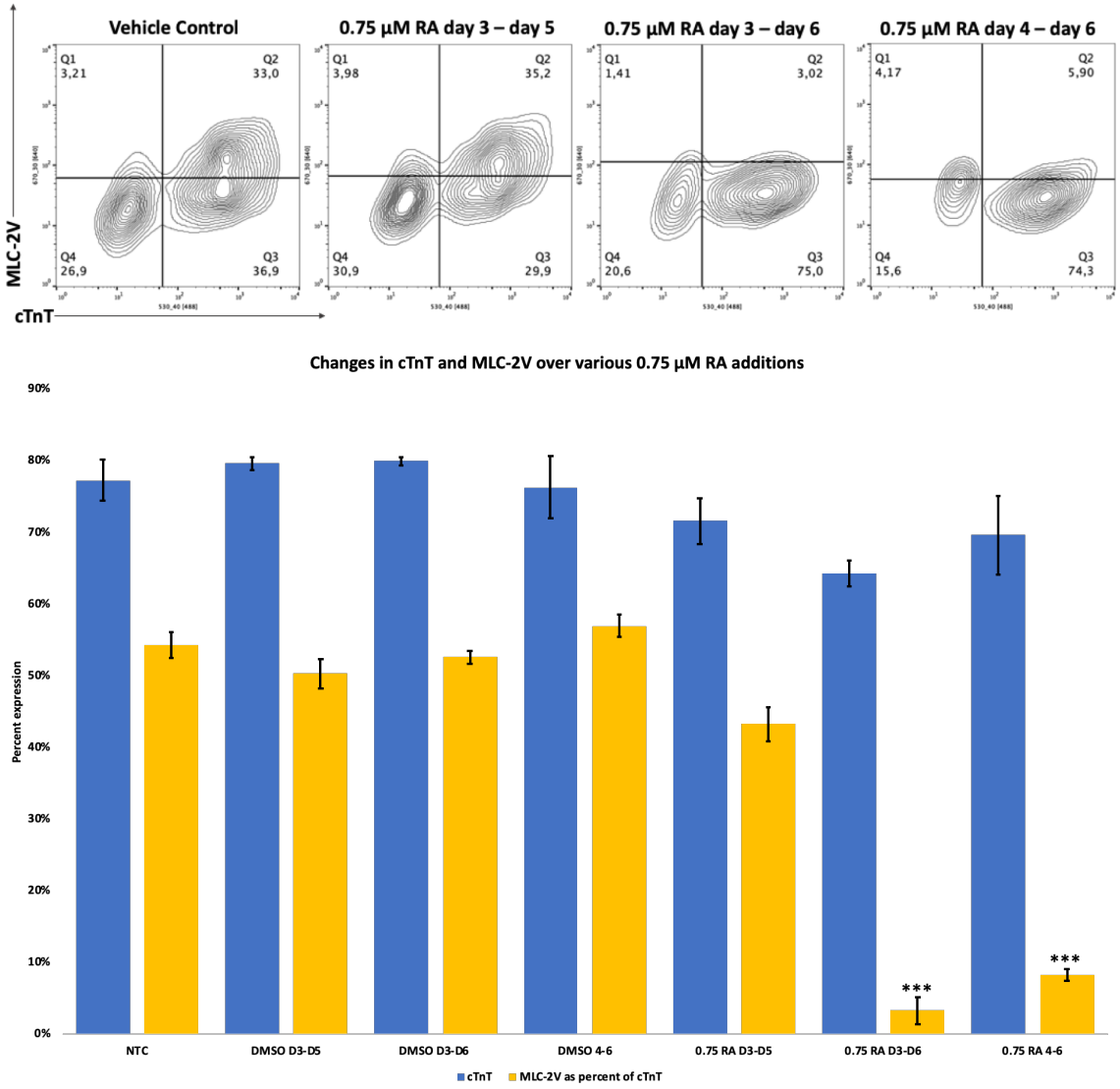

Figure 23. Flow cytometric analysis of cTnT and MLC-2V expression of various windows of 0.75 µM RA over various windows.

The no treatment control, DMSO D3-D5, DMSO D3-D6, and DMSO D4-6 had a cTnT/MLC-2V expression of 77 ± 3%/54 ± 2%, 80 ± 1%/50 ± 2%, 80 ± 1%/ 53 ± 1%, 76 ± 4%/57 ± 2%. 0.75 µM RA from days 3-5, 3-6, and 4-6 had cTnT/MLC-2V expression of 72 ± 3%/25 ± 3%, 64 ± 2%/3 ± 2%, and 70 ± 6%/8 ± 1%. n=3. ***p<0.001 relative to the respective controls. error bars represent the standard error of the mean.

These results led me to decide on the addition of 0.75 μM RA from day 4 - 6 as the final atrial differentiation protocol. Five additional markers were analyzed to confirm these results (Figure 25): *SLN, GJA5, TBX5, and MYL7,* as well as the nodo-atrial marker *HCN4*. All markers except for *MYL7* showed a significant increase in expression compared to the control. *MYL7* also did not show a significant increase in the other RA windows that were tested.

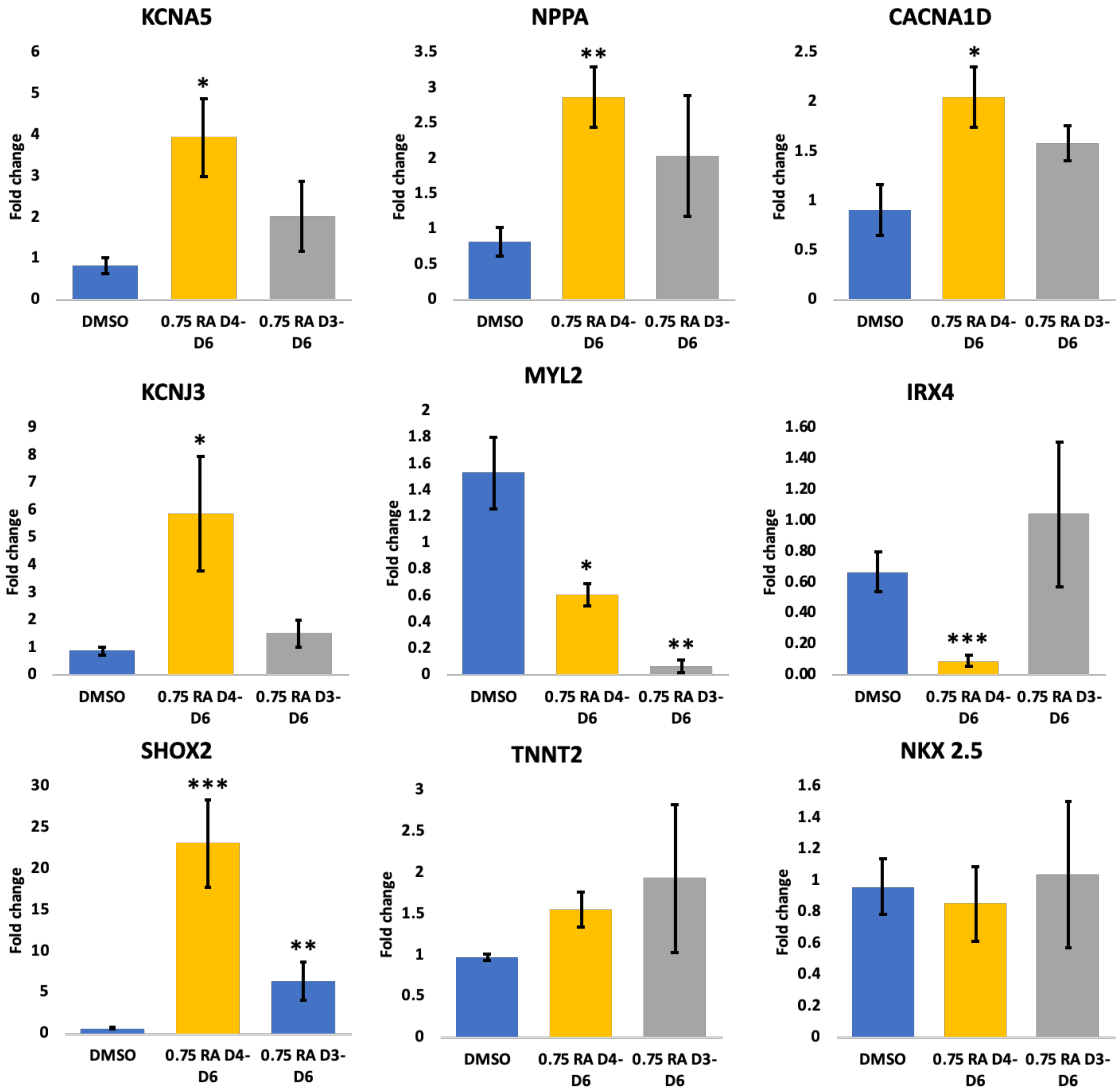

Figure 24. RT-qPCR expression of cells with 0.75 μM RA added from day 3-6 or day 4-6.

Overall, RA additions from day 4-6 showed the most atrial-like phenotype. Markers had an n = 7 except for TNNT2, CACNA1D, and MYL2 which had an n = 3. *p<0.05, **p<0.01, ***p<0.001 relative to the DMSO control. Error bars represent the standard error of the mean.

Next, the beating rates of both the hiPSC-aCMS and vCMs were analyzed over the course of differentiation (Figure 26). The aCMs began to beat at day 10 (rate of 69 ± 2 bpm). The ventricular CMs began to beat two days later on day 12 (43 ± 1 bpm). At day 12, the aCMs increased in rate to 76 ± 2 bpm and maintained a higher rate. At day 20, the final observation date, aCMs had an average beating frequency of 120 ± 5 bpm, whereas the ventricular CMs had a beating frequency nearly half of that at 63 ± 5 bpm.

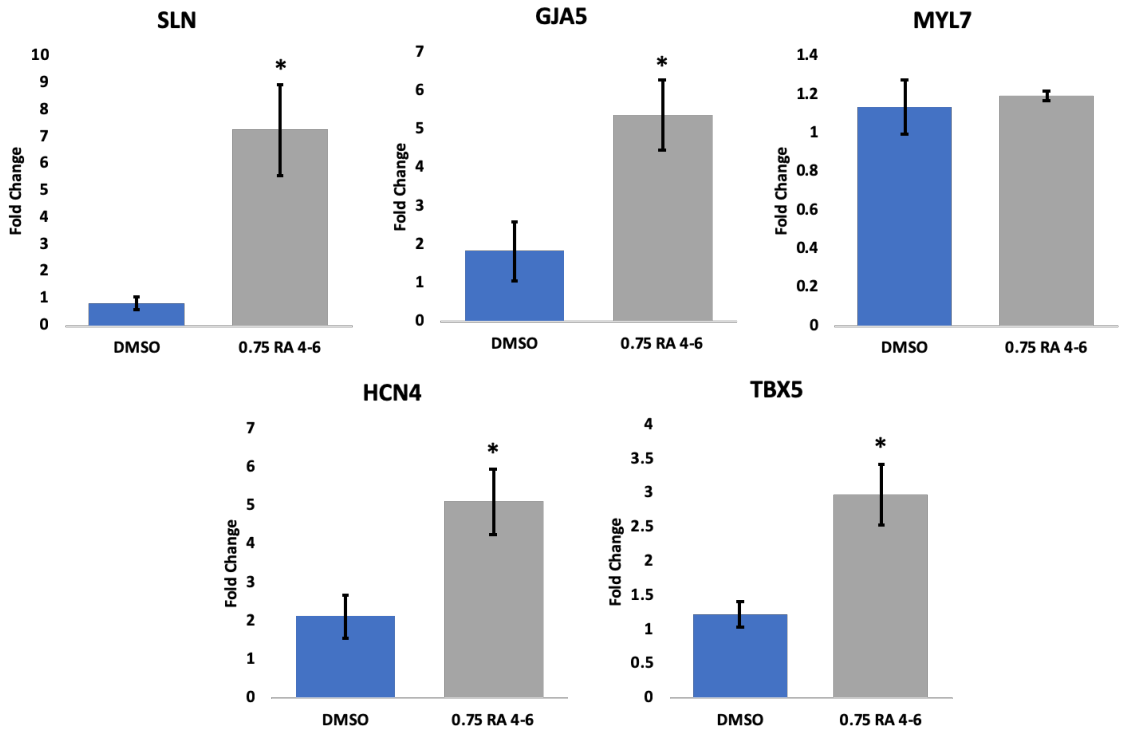

Figure 25. RT-qPCR expression of cells with the atrial differentiation protocol. From cells with 0.75 μM RA added from day 4-6. All of the markers shown above, with the exception of MYL7, had a significant increase in expression in the "atrial" protocol compared to the control. *p<0.05 relative to the control. Error bars represent the standard error of the mean. n = 3

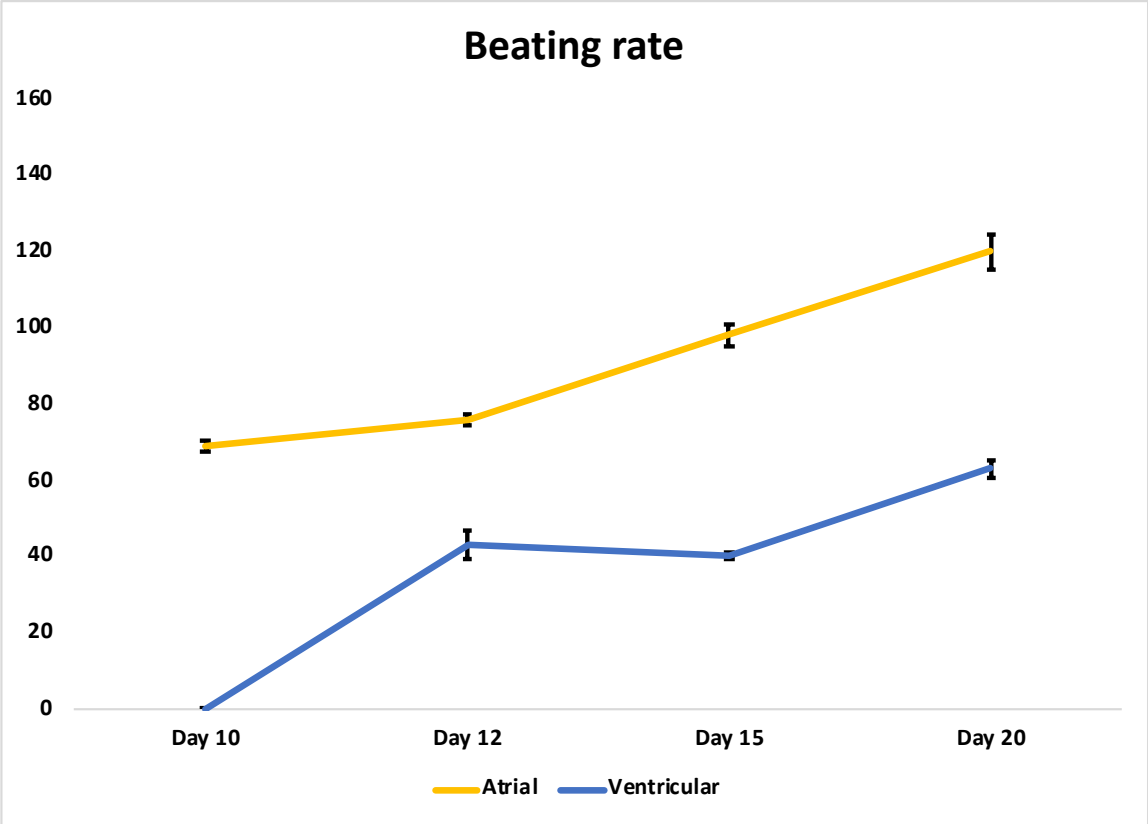

Figure 26. Observed frequency of beating from days 10,12, 15, and 20 in atrial and ventricular CMs.

At day 10, the atrial CMs had a beating frequency of 69 ± 2 bpm. The ventricular CMs did not begin to beat until day 12, at a rate of 43 ± 4 bpm. By this time the atrial CMs were beating at 76 ± 2 bpm. At day 15, the atrial and ventricular CMs were beating at 98 ± 3 bpm and 40 ± 1 bpm respectively. At day 20, the atrial and ventricular CMs beat at 120 ± 5 bpm and 63 ± 2 bpm. n = 3

After flow and RT-qPCR confirmation, cells were characterized functionally using optical mapping (Figure 27). From monolayers paced at 60 bpm, the action potential duration in the hiPSC-aCMs was markedly shorter than the hiPSC-vCMs. Additionally, the atrial action potential did not have a pronounced plateau phase as seen in the vCMs.

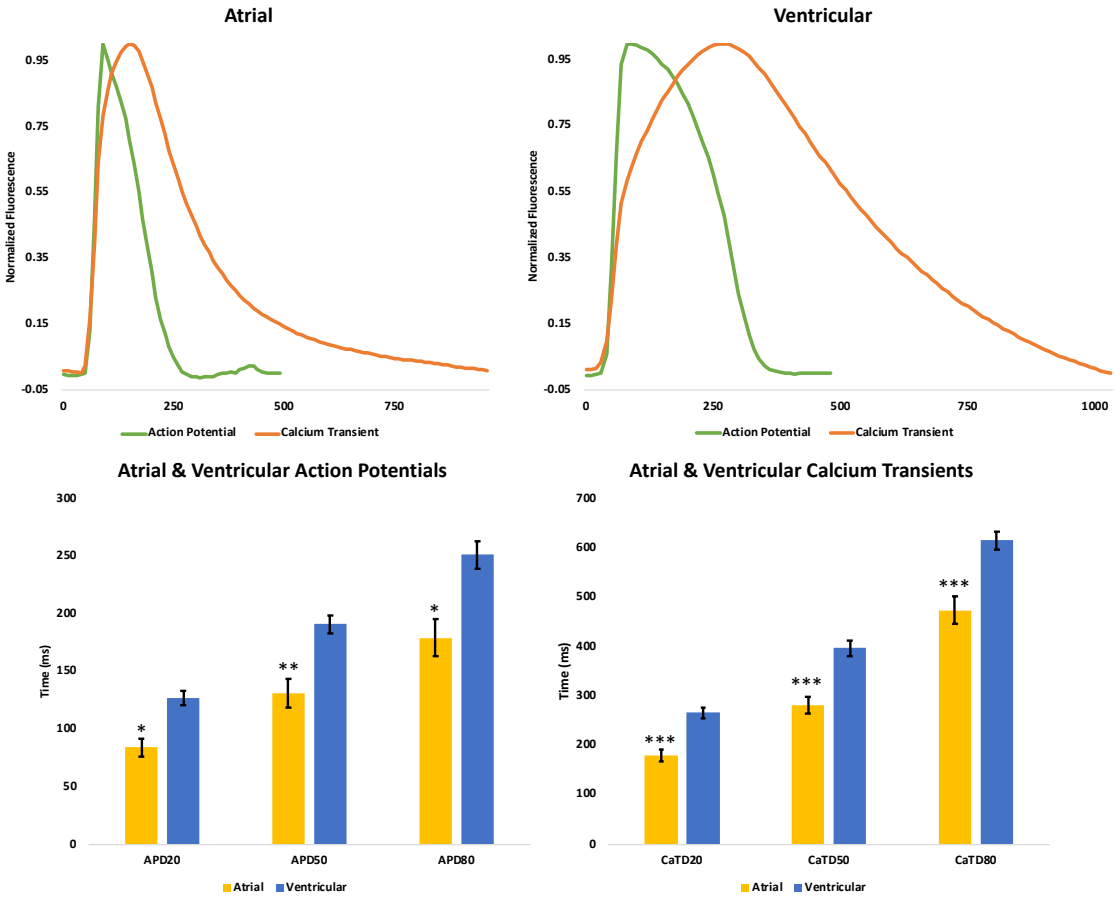

Figure 27. Action potential and calcium transient characteristics of atrial and ventricular CMs.

The average APD 20 of the atrial and ventricular CMs was 84 ± 8 ms and 127 ± 6 ms respectively. APD 50 was 131 ± 12 ms and 191 ± 8 ms. APD 80 was 179 ± 16 ms and 251 ± 12 ms. The calcium transients in the atrial CMs were both faster to rise and faster to decay compared to the ventricular CMs. The CaT 20 in the atrial and ventricular CMs was 180 ± 12 ms and 266 ± 12 ms respectively. The CaT 50 was 282 ± 18 ms and 397 ± 16 ms. The CaT 80 was 474 ± 27 ms and 615 ± 18 ms. n = 6. *p<0.05, **p<0.01, **p<0.001 relative to ventricular CMs. Error bars represent the standard error of the mean.

Next, the cells were characterized by their response to the clinically approved intravenous atrial cardioversion drug, vernakalant (Figure 28). hiPSC-aCMs showed a substantial percent change in APD. The APD 20, 50 and 80 increased by 84 ± 6%, 70 ± 5%, and 77 ± 4%. hiPSC-vCMs however showed little change in APD. The APD 20, 50 and 80 changed by -7 ± 3%, -2 ± 2%, and 3 ± 3% compared to the control.

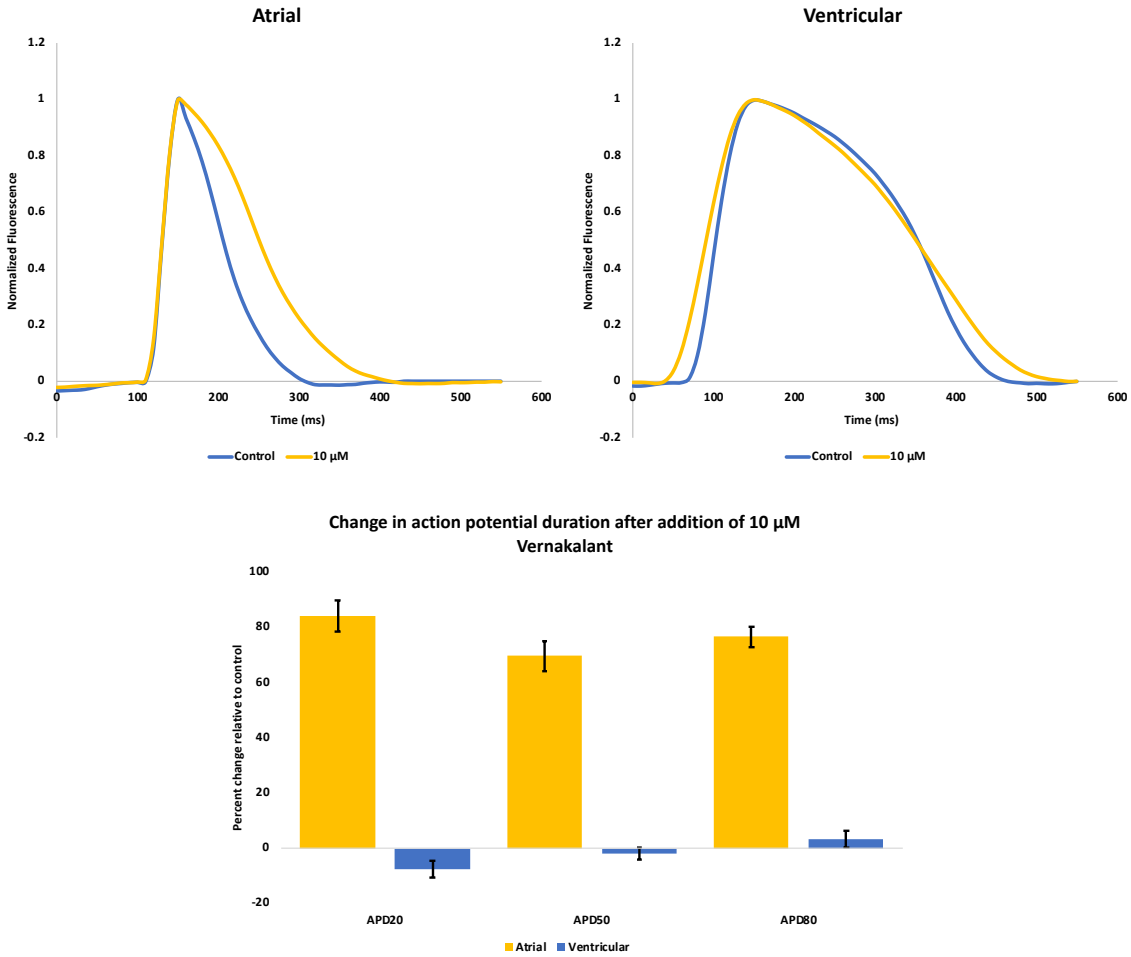

Figure 28. Characterization change in APD after the addition of vernakalant to atrial and ventricular CMs.

In atrial CMs, the APD20, 50 and 80 increased by 84 ± 6%, 70 ± 5 %, and 77 ± 4% respectively. The ventricular CMs saw a percent change of -7 ± 3%, -2 ± 2%, and 3 ± 3%. n = 3. Error bars represent the standard error of the mean.

Taken together, the combination of transcript analysis, protein analysis, basic functional analysis presents the argument that the addition of RA at 0.75 µM from days 4-6 produce a predominately atrial population. In addition, these cells show an atrial selective response to Vernakalant.

4.4. CRISPR-Cas9 genome edited KCNN3 Knockout

In this phase, I went on to design *SK3 channel* knockout strategy using CRISPR-Cas9 genome editing technology. First, the expression of both the *KCNN2* and *KCNN3*, the genes expressing SK2 and SK3, in our hiPSC-aCMs and vCMs was analyzed (Figure 29). The *KCNN2* gene exhibited no significant differences in expression between the atrial and vCMs. The *KCNN3* gene however, showed a preferential increase in expression in the aCMs.

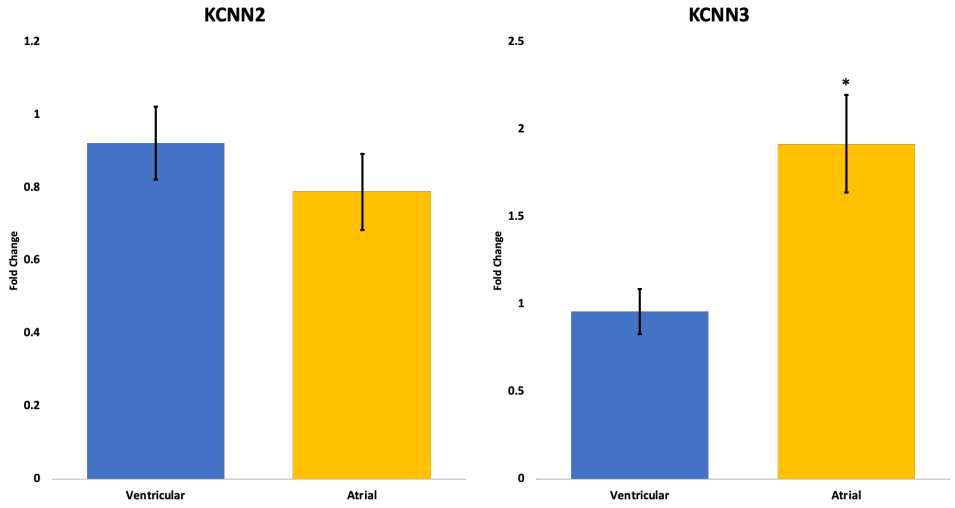

Figure 29. Transcript analysis of KCNN2 and KCNN3 in atrial vs ventricular CMs.

KCNN2 showed no significant difference in expression between atrial and ventricular CMs. *KCNN3* did show a significant increase in atrial cardiomyocytes compared to the ventricular CMs. n = 3. *p<0.05. Error bars represent the standard error of the mean

Following confirmation, a sgRNA, an ssODN template, and primers for amplification to prepare for sequencing were designed (Table 2).

Table 2. KCNN3 KO design

Primer	Primer sequence 5'→3' (Fwd/Rev)
KCNN3 nested primer "IN"	GCTCATGCAGCCTGTCTAAA
	CTGGTGTTTCCTCACTTTGGC
KCNN3 nested primer "OUT"	TCTCAGGCAAAGCTCGGAAG
	CAGACCCAGTTCACCACTCC
sgRNA forward	/5Phos/caccgAGATTAACCATGTTTCCCGA
sgRNA reverse	/5Phos/aaacTCGGGAAACATGGTTAATCTc
ssODN template	CCACAAAAATGAACCTAAGAAAATGAACCTGATAGCA GCCTACTTTATTTATTCTTCCTTAGATCAAGAATGCTGC AGCCAATGTTCTTCGGGAAACATGATTAATCTATAAAC ACACAAAGCTGCT

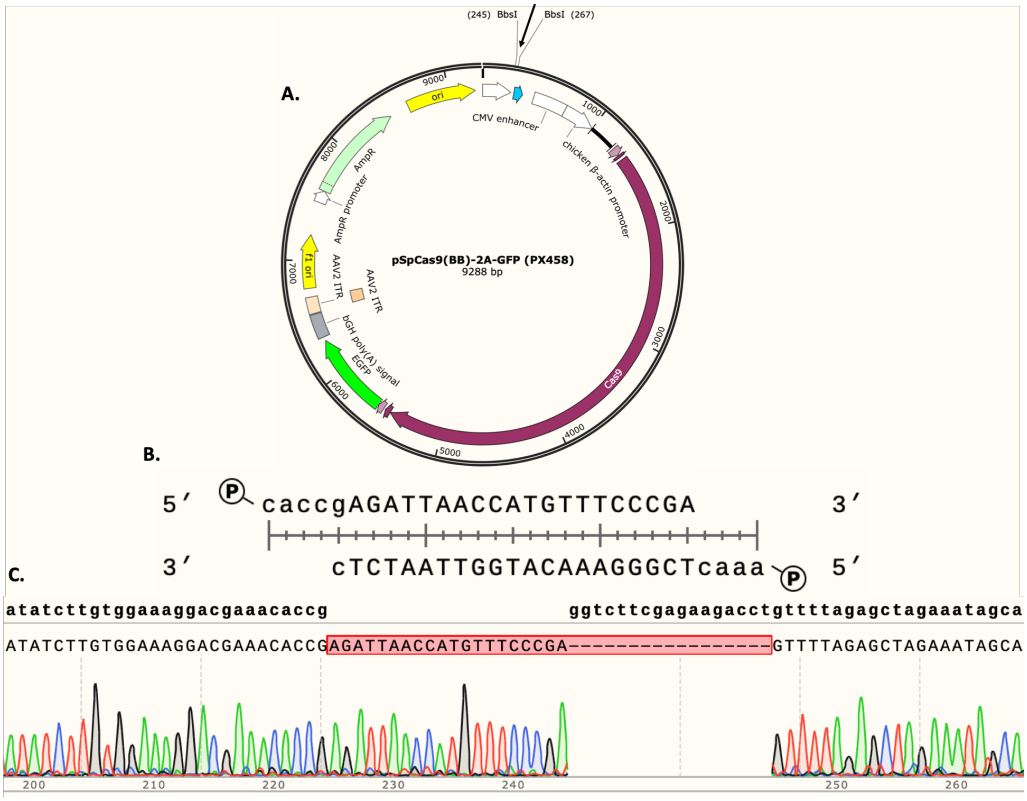

Figure 30. Schematic and sequencing results of successful sgRNA insertion into plasmid.

A. Schematic of the plasmid. Arrow represents the insertion sites with the cut sites also stated. B. schematic of the hybridization of the sgRNA before insertions. C. Sequencing results showing successful insertion of the sgRNA into the plasmid.

The sgRNA insert was successfully hybridized and inserted into the plasmid (Figure 30), as confirmed by Sanger sequencing. After transfection, cell sorting, colony selection and sequencing of hiPSCs, the early stop codon was successfully inserted into the target of interest (Figure 31). The first was a homozygous insertion, in this case both

alleles had the mutation. The second, was likely a heterozygous mutation. Both the STOP codon and silent mutation were successful in one allele. However, because the identity of the second and third codons were not clear, the mutation could not be confirmed with a high certainty. Unfortunately, because the cells became contaminated, they could not be re-sequenced, nor could they be differentiated for analysis by OM.

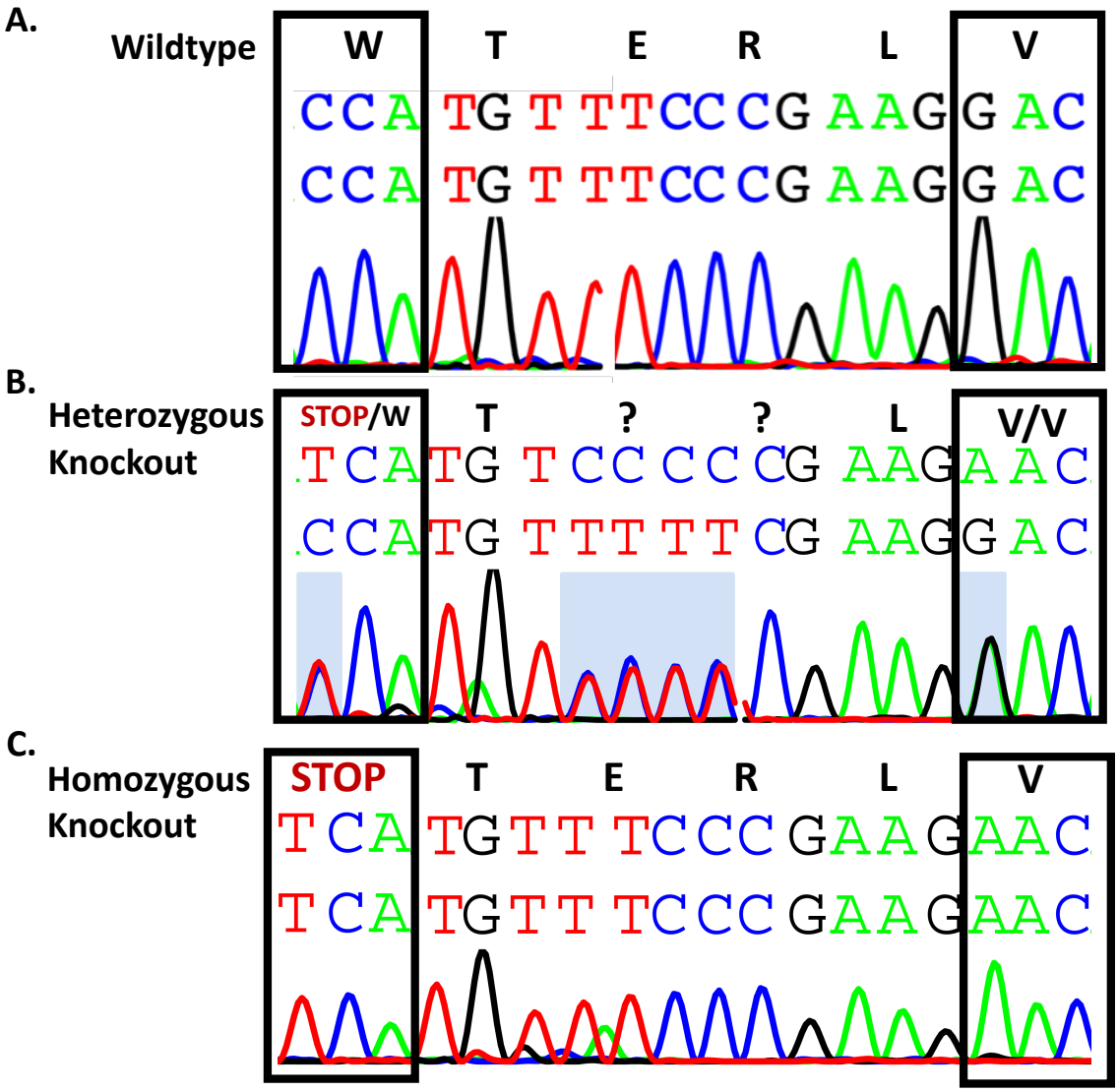

Figure 31. Sequencing results showing the various genome editing outcomes. A. Wildtype sequencing of the antisense strand. The rectangles show the codon of interest as well as the PAM site. B. A likely heterozygous knockout with the inserted stop codon and silent PAM mutation. C. A homozygous insertion of the stop codon and silent PAM mutation. Line breaks are a result of merging sequencing data from different rows.

Chapter 5.

Discussion

5.1. Atrial Differentiation

My results show that the addition of RA from days 4 – 6 at a concentration of 0.75 μM was able to direct cells to an atrial fate at a transcript, protein, and functional level while preserving the cardiac efficacy of differentiation of hiPSC-CMs.

With the number of different protocols available, there can be some variation in the days of RA addition. As such, my comparisons will be in reference to the day of WNT inhibition. I will not be comparing our protocol with Lee et al.[55] Although all mesoderm can be driven to become atrial, the modification increasing RALDH2 expression in their protocol resulted a fundamentally different protocol.

In our protocol, RA was added 1-day post WNT inhibition with a total exposure of 4 days. These data support the findings of Cyganek et al.[87] who completed the most thorough analyses. They also added RA 1 day after WNT inhibition with a total exposure time of 4 days. Devalla et al.[58] did not use a WNT inhibitor in their differentiation protocol so a direct comparison is more difficult. RA was added one day after the first media change (the media change occurring 3 days after initiation) with a total exposure of 4 days. It is possible there is a time delay in activating the correct signalling pathways after WNT inhibition and adding retinoic acid at the same time may activate alternate pathways as cells have not yet reached the cardiac mesoderm stage. For example, after WNT signalling is inhibited there may be a temporal delay in which subsequent pathways are activated, although further experiments are required to confirm these assertions. Zhang et al.[165] used a protocol of a total RA exposure of 4 days but added the same day as WNT inhibition (via DKK1). This WNT inhibitor may have a different time-course of inhibition than that used in our protocol. As an outlier, Argenziano et al.[166] were able to produce atrial cells with RA exposure time of 6 days, and was added 3 days after WNT inhibition.

In our assays, 1 μM RA resulted in a decrease in cardiac differentiation efficiency. This is in contrast to the other protocols, in which 1 μM was found to be the optimal concentration. Although Devalla et al.[58] observed a 10% drop in NKX 2.5 expression and

Zhang et al.[165] observed a 14% drop in cTnT expression, other groups did not see any significant changes, likely due to decreased cardiac toxicity.

The most visually striking feature in the hiPSC-aCMs is the increase in beating frequency. These data are consistent with previous literature.[58,86,87,166,167] Although the absolute frequencies themselves vary, the relative beating frequencies are always higher in hiPSC-aCMs than the hiPSC-vCMS. Not only do our aCMs beat faster they also begin to beat earlier. These data confirm work done by Hiroi et al.[22] in 2001 in P19CL9 cells, which found that populations that were transfected with pCDNA3–TBX5 plasmids began to beat two days earlier than the wildtype line. Our hiPSC-aCMs also begin beating two days earlier, at day 10, than vCMs which begin to beat at day 12.

In our assays, *MYL7* was found to be a poor marker of the atrial phenotype. There was no significant increase in expression with the addition of RA in any of the various addition windows. This included day 3 - 6 additions, as well as day 4 - 6 RA additions (Supplemental Figure 7). These data are corroborated by our attempts at optimizing an MLC-2A antibody, in which we were unable to discern subtype populations. Lee & Protze et al.[85] who analyzed cells at day 20 did not find any difference in *MYL7* expression. Argenziano et al.[166] who analyzed cells at Day 20-30, did not observe *MYL7* or MLC-2A, instead they observed an increase in Kv1.5 expression using immunocytochemistry (ICC) and flow cytometry. We were not able to confirm these findings. Devalla et al.[58] also lifted cells at day 27-31, but did not investigate *MYL7*/MLC-2A expression. Zhang et al.[165] and Cyganek et al.[87] did, however, observe a difference in MLC-2A and *MYL7* expression. Analyses in these studies were carried out at the earliest, day 60, suggesting *MYL7*/MLC-2A expression may require additional maturation. Working with human models, Piccini et al.[168] tested *MYL7* expression in adult atria compared to adult ventricles, using next generation sequencing, and found no significant difference between them.

SHOX2 was shown to have an increased expression in any RA addition window within the set day 3 – 6 boundaries. As mentioned above, RA activates *SHOX2* through TBX5. As such, an increase in the *SHOX2* transcript is unavoidable when differentiating hPSCs to aCMs with RA. An increase in *SHOX2* was not associated with a substantial change in atrial phenotype, however in our experiments, it was associated with an increase in beating rate. Consequently, an increase in beating rate may be an indicator of an effect associated with RA. These data suggest that an increase in rate could be an

indicator of cells being receptive to RA. Because previous studies found that HPSC-ACMs were found to have an increased rate, we used it as an exclusion criterion in determining the RA addition windows. A more in-depth analysis, however, is required to confirm these hypotheses.

Functionally, the hiPSC-aCMs displayed a shorter action potential duration as well as an abbreviated plateau phase. RT-qPCR data support this observation, with *KCNA5*, the gene expressing $K_v1.5$, being expressed at significantly higher levels in hPSC-aCMs compared to hPSC-vCMs. The values themselves, however, were not the same as the published literature.[58,86,87,166,167] These differences may be the result of differing techniques. One of the main advantages of optical mapping is that data is acquired from hPSC-CM sheets which behave as a functional syncytium; whereas with patch clamping, single cells are isolated by chemical digestion which can change their behavior. Additionally, recordings are completed in a single cell format where native behaviour is less likely to be observed. In optical mapping, the final APD and calcium measurements are taken as an average of the whole sheet. This means that although cells are predominantly of one type, other cardiac cell types exist and can shift voltage and calcium dynamics. This can be overcome by drawing regions of interest to isolate certain populations.

In our study, the calcium transient was both faster to rise and faster to decay in hiPSC-aCMs compared to hiPSC-vCMs. Cyganek et al.[87] observed similar relationships in their hPSC-CMs.

Vernakalant is a pyrrolidine based, mixed channel antiarrhythmic drug. Vernakalant targets early and late sodium currents as well as I_{to}, I_{kr}, I_{kach}, and I_{kur}.[169] Due to its preferential targeting of I_{kur} and I_{kach}, it is considered to be atrial-selective. Because of these atrial selective properties, vernakalant is approved for by the US Food and Drug Administration (FDA) for IV cardioversion of AF.[170]

Our study found that vernakalant induced a significant lengthening of the APD_{20}, APD_{50}, and APD_{80} in the hiPSC-aCMs whereas in the vCMs, there were minimal changes. These results were consistent with Devalla et al.[58] who found a prolongation of APD_{20}, APD_{50}, and APD_{90} with the addition of vernakalant. They also found a significant decrease in the action potential upstroke (dV/dt), which has been shown to be an important target

for vernakalant.[171] Because the acquisition rates in our optical mapping rigs are 100 fps, we were unable to accurately observe the upstroke (dv/dt) of the action potential. Additionally, because these measurements are fluorescence based, we are unable to determine the absolute resting membrane potential as well as action potential amplitude.

At a transcript level, hiPSC-aCMs expressed a profile indicative of atrial phenotype. At a protein level, hiPSC-aCM differentiation did not alter the cardiac efficiency but resulted in decreased MLC-2V expression. Functionally, our hiPSC-aCMs have an action potential morphology, calcium transient, and drug response that is similar to native atrial cardiomyocytes and other hPSC-aCMs.

5.2. KCNN3

RT-qPCR results, for the first time, showed that the *KCNN3* gene is preferentially expressed in hPSC-aCMs. As mentioned in the background section, SK3 was not shown to be preferentially expressed in murine or rabbit atria, and no expression data comparing SK3 in the atria vs the ventricles in human models are available. These expression results show that KCNN3 may directly influence atrial repolarization. KCNN2 however, did not show preferential expression in hiPSC aCMs, contradicting data published by Xe et al.[154]

SK2 and SK3 expression data in fetal as well as adult hearts have not yet been published, and further experimentation is required to determine whether these data indicate normal physiological expression.

I was able to successfully insert an early stop codon (CCA→TCA) into exon 7 of the KCNN3 gene in hiPSCs enabling the creation of a confirmed homozygous mutation and a potential heterozygous mutation.

The National Center for Biotechnology Information (NCBI) lists three different splice variants of SK3. Isoform A is the reference splice variant. Isoform B contains an alternate exon 1 resulting in a truncated N-terminal. Lastly, isoform C contains an extra coding region resulting in an alternate exon 4 and a 3' shift of the following exons. Exon 3 is the largest common exon amongst all splice variants, coding for transmembrane segments S3-S5. Although this may be an attractive target as a cut site, as the largest exon it would be more valuable as a target for a qRT-PCR expression assay. Therefore, based on the genomic sequence, I chose exon 7 as a target.

The heterozygous knockout sequence contains some ambiguous base pairs. The peaks in this sequencing data were separated using the poly peak parser tool.[172] Poly peak parser was unable to determine the wildtype strand from these peaks. This implies that the sequencing data was not clean and further confirmation sequencing was required. Due to cell contamination however, the heterozygous knockout could not be confirmed.

Despite no longer having the cell line, I was able to confirm that my design and approach resulted in a successful mutation and simply needs to be repeated rather than re-optimized.

5.3. Limitations and future directions

5.3.1. RT-qPCR

As a technique, RT-qPCR has allowed researchers to measure gene expression in a more accurate manner.[173–175] RT-qPCR uses fluorescent dyes such as SYBR Green or EvaGreen® that preferentially intercalate double stranded DNA. The thermo-cycler is fitted to detect these changes in fluorescence. Therefore, we are able to visualize DNA amplification in “real time” and assign quantifiable endpoint values. The combination of reverse transcription PCR with RT-qPCR allows researchers to determine the expression levels of select transcripts relative to each other. This RT-qPCR technique is a mainstay in molecular research. The advantages of RT-qPCR are that the instruments are precise, specific and sensitive, detecting very small differences in expression levels; and compared to previous assays, RT-qPCR is faster.[176,177] RT-qPCR also a number of drawbacks. RT-qPCR can depend heavily on the user and can vary from person-to-person. As such, the results can be inaccurate, and variable. The MIQE guidelines were introduced in 2009 in an attempt to standardize run and analysis procedures.[178] These include requirements for RNA extraction, reverse transcriptions, and RT-qPCR validation.

Despite standardization, RT-qPCR still has its limitations. The multiple amplification steps, differences in amplification efficiency, and variability in RNA quality can result in inaccurate results. Users manually perform RNA extractions, reverse transcriptase PCR, and load 96-well plates manually using single channel pipette making the procedure laborious. As such, RT-qPCR does not have the throughput to measure large numbers of transcripts. Additionally, because fluorescence, rather than DNA count

is measured, copy number measurements must be extrapolated using a DNA standard. More typically, expression data are presented in a “fold change” manner where expression is quantified relative to a control. Although, RT-qPCR was invaluable in determining the ideal atrial differentiation procedure, a fully quantitative higher throughput system would be essential to analyze transcription pathways during development as well as confirming overall phenotype.

nCounter® by NanoString technologies is one of those tools. The nCounter® system is a molecular counter that quantifies transcripts by counting barcoded reporters. This system uses a series of capture probes that will bind target RNA as well as hybridize to barcoded biotinylated reporter probes.[179] The hybridized probes then bind to a streptavidin-coated cartridge and are immobilized. After a series of washing steps, to remove unhybridized probes, the coded transcripts are counted. The nCounter® is a high-throughput system that can analyze over 800 different targets in one run. Because this system is directly counting transcripts rather than relying on amplification (which can introduce bias) it is also more accurate, sensitive and specific than RT-qPCR.[179,180] . Additionally, nCounter® is able to count and quantify hard to amplify transcripts that RT-qPCR would not.[179,180] Also, because probe design is completed by the company, optimization time is significantly decreased, as is assay run time. The nCounter® system would provide valuable data on the phenotype of these hiPSC-derived aCMs.

5.3.2. Atrial protein markers

Another limitation of my study was that I was unable to optimize an atrial marker for flow cytometry. I tested out multiple different antibodies and two separate targets. Successful flow cytometry assays rely on appropriate antibodies. As such, adding an antibody to the assay requires extensive trial and error as well as procedure optimization before it can be used. Additionally, the target features also affect success for the assays. Ideally, protein targets are highly expressed, and the epitopes of interest are exposed. Therefore, contractile proteins are ideal and preferred over transmembrane proteins. Therefore, the first atrial target I attempted to optimize for flow cytometry was MLC-2A. As my RT-qPCR results demonstrated, *MYL7* (the gene expressing MLC-2A) transcript expression is not differentially expressed between hiPSC-aCMs and hiPSC-vCMs; indicating a possible reason for the failure of the flow assay.

Other atrial-specific targets I considered were: ANP, $K_{ir}3.1$, SLN, and MHC-α. ANP would not be suitable for flow cytometry as it is a peptide hormone that does not remain fixed in place. $K_{ir}3.1$, like $K_v1.5$ is a transmembrane protein. Sarcolipin (SLN) is a short 31 amino acid sarcoplasmic reticulum imbedded protein with 7 amino acids exposed cytosolically, and would likely not be successful.[181] Another possible atrial marker, MHC-α seems like an ideal candidate.[182] This protein is expressed in fetal and adult atria with minimal expression levels in the ventricles. Additionally, as a contractile protein, they are cytosolic and heavily expressed. Unfortunately, MHC-α (NP_002462) shares a 93% sequence homology with MHC-ß (NP_000248) the ventricular myosin heavy chain isoform.[182183,184] In contrast, atrial light chain MLC-2A (NP_067046) and ventricular light chain (NP_000423) have only a 53% sequence homology. This high sequence homology makes antibody selection difficult. The only monoclonal α-MHC antibodies available target: RELEEISERLEEA, KLEQQVDDLEGSLEQ, and LTQESIMDLENDKLQ epitopes. These sequences are not unique to MHC-α but are in fact shared with MHC-ß, which would likely result in inaccurate findings. Previous publications have also not used α-MHC as protein expression marker.

There are other assays available as well. The first is a western blot. In this technique, cells are lysed before the addition of antibodies. We are, therefore, better able to detect transmembrane proteins. This technique has its set of drawbacks as well. It requires extensive optimization of experiment conditions (buffers, run conditions etc.) and testing of multiple antibodies. If the antibodies are unverified or if there is offsite binding, the results can be inaccurate. Additionally, incidental phosphorylation of proteins can promote the formation of multiple bands on the membrane. Finally, the results of a western blot are not quantitative and can only determine in which direction the expression of the protein has changed rather than the total amount of protein.

Another possible assay is the Atrial Natriuretic Peptide (ANP) Competitive ELISA (enzyme-linked immunosorbent assay). ELISA is a well-established antibody-based fluorescence technique. ELISA is not limited to detecting structural proteins and channels, but is also able to detect peptides, in this case ANP. Additionally, it is procedurally less extensive and because it is available as a kit, the technique requires minimal optimization. This assay would be useful for quantifying an exclusively atrial marker.

Overall, these previous techniques produce low throughput results. Expanding the library of proteins to test would require marker-to-marker optimization, which would be impractical. Stable isotope labeling by amino acids in cell culture (SILAC) is a fairly novel technique using mass spectrometry.[185] Cells are labelled in culture with heavy isotope labeled (typically13C- or 15N-labeled) amino acids or, fed with normal media. These cells are then lysed and analyzed using a mass spectrometer. This technique would be able to comprehensively determine the proteome of hiPSC-aCMs and compare them to hiPSC-vCMs.

5.3.3. Testing of KCNN3 KO and RS13376333 intronic mutation

Upon re-insertion of the stop codon into the hiPSCs. We will be using our atrial differentiation protocol to create hiPSC-aCMs that contain the knockout without the knockout. Next, we will be using RT-qPCR to determine if there has been a functional knockout. Following confirmation, the mutant and wildtype hiPSC-aCMS will be analyzed using optical mapping. We will be able to characterize the contributions that SK3 makes to the action potential duration as well as potential alterations in calcium handling. These tests will for the first time determine SK3 function in human PSC derived aCMs. Furthermore, it will facilitate hypothesis generation when testing the RS13376333 intronic mutation.

5.4. Conclusions

Overall, I was able to create a differentiation protocol with retinoic acid that produced hiPSC-CMs with a distinct atrial phenotype verified by flow cytometry, RT-qPCR, as well as optical mapping. The atrial protocol did not affect differentiation efficiency, measured by cTnT protein expression, and *TNNT2* and *NKX 2.5* transcript expression. Functionally, the cardiomyocytes showed an atrial-like action potential morphology, as well as an atrial specific drug response.

I successfully used CRISPR-Cas9 genome editing technology to insert an early stop codon within exon 7 of the *KCNN3* gene. Unfortunately, the cells did not survive for differentiation and subsequent testing. I hope to continue this project in the future to eventually determine the role that *KCNN3* plays in atrial cardiomyocyte function.

References

1. Kelly RG, Buckingham ME, Moorman AF. Heart fields and cardiac morphogenesis. *Cold Spring Harb Perspect Med*. 2014;4(10). doi:10.1101/cshperspect.a015750

2. Moore KL, Persaud TV. *The Developming Human*. 8th ed. Saunders

3. MOORMAN AFM, CHRISTOFFELS VM. Cardiac Chamber Formation: Development, Genes, and Evolution. *Physiol Rev*. 2015;83(4):1223-1267. doi:10.1152/physrev.00006.2003

4. Conti RC. *The Netter Collection of Medical Illustrations*. 2nd ed. Saunders; 2014.

5. Kelly RG. *The Second Heart Field*. Vol 100. Elsevier Inc.; 2012. doi:10.1016/B978-0-12-387786-4.00002-6

6. Kwon C, Arnold J, Hsiao EC, Taketo MM, Conklin BR, Srivastava D. Canonical Wnt signaling is a positive regulator of mammalian cardiac progenitors. *PNAS*. 2017;104(26):10894-10899. doi:10.1109/ICCCI.2017.8117716

7. Christoffels VM, Habets PEMH, Franco D, et al. Chamber formation and morphogenesis in the developing mammalian heart. *Dev Biol*. 2000;223(2):266-278. doi:10.1006/dbio.2000.9753

8. Costello I, Pimeisl IM, Dräger S, Bikoff EK, Robertson EJ, Arnold SJ. The T-box transcription factor Eomesodermin acts upstream of Mesp1 to specify cardiac mesoderm during mouse gastrulation. *Nat Cell Biol*. 2011;13(9):1084-1092. doi:10.1038/ncb2304

9. David R, Jarsch VB, Schwarz F, et al. Induction of MesP1 by Brachyury(T) generates the common multipotent cardiovascular stem cell. *Cardiovasc Res*. 2011;92(1):115-122. doi:10.1093/cvr/cvr158

10. Saga Y, Hata N, Kobayashi S. MesP1: a novel basic helix-loop-helix protein expressed in the nascent mesodermal cells during mouse gastrulation. *Development*. 1996;122:2769-2778. http://dev.biologists.org/content/122/9/2769.short.

11. Saga Y, Kitajima S, Miyagawa-Tomita S. Mesp1 expression is the earliest sign of cardiovascular development. *Trends Cardiovasc Med*. 2000;10(8):345-352. doi:10.1016/S1050-1738(01)00069-X

12. Saga Y, Miyagawa-Tomita S, Takagi A, Kitajima S, Miyazaki J i, Inoue T. MesP1 is expressed in the heart precursor cells and required for the formation of a single heart tube. *Development*. 1999;126(15):3437-3447. http://www.ncbi.nlm.nih.gov/pubmed/10393122.

13. David R, Brenner C, Stieber J, et al. MesP1 drives vertebrate cardiovascular differentiation through Dkk-1-mediated blockade of Wnt-signalling. *Nat Cell Biol*. 2008;10(3):338-345. doi:10.1038/ncb1696

14. Lian X, Zhang J, Azarin SM, et al. Directed cardiomyocyte differentiation from human pluripotent stem cells by modulating Wnt/β-catenin signaling under fully defined conditions. *Nat Protoc*. 2013;8(1):162-175. doi:10.1038/nprot.2012.150

15. Liberatore CM, Searcy-Schrick RD, Yutzey KE. Ventricular expression of tbx5 inhibits normal heart chamber development. *Dev Biol*. 2000;223(1):169-180. doi:10.1006/dbio.2000.9748

16. Tian Y, Yuan L, Goss AM, et al. Characterization and In Vivo Pharmacological Rescue of a Wnt2-Gata6 Pathway Required for Cardiac Inflow Tract Development. *Dev Cell*. 2010;18(2):275-287. doi:10.1016/j.devcel.2010.01.008

17. Kelly RG, Brown NA, Buckingham ME. The Arterial Pole of the Mouse Heart Forms from Fgf10-Expressing Cells in Pharyngeal Mesoderm. *Dev Cell*. 2001;1:435-440. papers2://publication/uuid/961D992B-2807-45B2-B504-06B53259052B.

18. Lindsley RC, Gill JG, Murphy TL, et al. Mesp1 coordinately regulates cardiovascular fate restriction and epithelial-mesenchymal transition in differentiating ESCs. *Cell Stem Cell*. 2008;3(1):55-68. doi:10.1016/j.stem.2008.04.004

19. Shirai M, Osugi T, Koga H, et al. The Polycomb-group gene Rae28 sustains Nkx2.5/Csx expression and is essential for cardiac morphogenesis. *J Clin Invest*. 2002;110(2):177-184. doi:10.1172/JCI14839

20. Lints TJ, Parsons LM, Hartley L, Lyons I, Harvey RP. Nkx-2.5: a novel murine homeobox gene expressed in early heart progenitor cells and their myogenic descendants. *Development*. 1993;119:419-431. http://dev.biologists.org/content/develop/119/2/419.full.pdf. Accessed April 21, 2019.

21. Arceci RJ, King AA, Simon MC, Orkin SH, Wilson DB. Mouse GATA-4: a retinoic acid-inducible GATA-binding transcription factor expressed in endodermally derived tissues and heart. *Mol Cell Biol*. 2015;13(4):2235-2246. doi:10.1128/mcb.13.4.2235

22. Hiroi Y, Kudoh S, Monzen K, et al. Tbx5 associates with Nkx2-5 and synergistically promotes cardiomyocyte differentiation. *Nat Genet*. 2001;28(3):276-280. doi:10.1038/90123

23. Pizard A, Burgon PG, Paul DL, Bruneau BG, Seidman CE, Seidman JG. Connexin 40, a Target of Transcription Factor Tbx5, Patterns Wrist, Digits, and Sternum. *Mol Cell Biol*. 2005;25(12):5073-5083. doi:10.1128/MCB.25.12.5073-5083.2005

24. Christoffels VM, Mommersteeg MTM, Trowe MO, et al. Formation of the venous pole of the heart from an Nkx2-5-negative precursor population requires Tbx18. *Circ Res*. 2006;98(12):1555-1563. doi:10.1161/01.RES.0000227571.84189.65

25. Sepulveda JL, Belaguli N, Nigam V, et al. *GATA-4 and Nkx-2.5 Coactivate Nkx-2 DNA Binding Targets Role for Regulating Early Cardiac Gene Expression*. Vol 18.; 1998. http://mcb.asm.org/. Accessed April 21, 2019.

26. Zhou L, Liu Y, Lu L, Lu X, Dixon RAF. Cardiac Gene Activation Analysis in Mammalian Non-Myoblasic Cells by Nkx2-5, Tbx5, Gata4 and Myocd. *PLoS One*. 2012;7(10):48028. doi:10.1371/journal.pone.0048028

27. Huang W-Y, Cukerman E, Liew C-C. *Identification of a GATA Motif in the Cardiac Cz-Myosin Heavy-Chain-Encoding Gene and Isolation of a Human GATA-4 CDNA (Transcription Factor; Cis-Acting Element; Electrophoretic Mobility Shift Assay)*. Vol 155.; 1995. doi:10.1016/0378-1119(94)00893-W

28. Lescroart F, Chabab S, Lin X, et al. Early lineage restriction in temporally distinct populations of Mesp1 progenitors during mammalian heart development. *Nat Cell Biol*. 2014;16(9):829-840. doi:10.1038/ncb3024

29. Bardot E, Calderon D, Santoriello F, et al. Foxa2 identifies a cardiac progenitor population with ventricular differentiation potential. *Nat Commun*. 2017;8:1-15. doi:10.1038/ncomms14428

30. Kleiner-Bössaler A, DeLuca HF. Formation of retinoic acid from retinol in the kidney. *Arch Biochem Biophys*. 1971;142(1):371-377. doi:10.1016/0003-9861(71)90295-5

31. Clagett-Dame M, Deluca HF. The role of vitamin A in mammalian reproduction and embryonic development. *Annu Rev Nutr*. 2002;22:347-381. doi:10.1146/annurev.nutr.22.010402.102745E

32. Wilson JG, Roth CB, Warkany J. An analysis of the syndrome of malformations induced by maternal vitamin a deficiency. Effects of restoration of vitamin a at various times during gestation. *Am J Anat*. 1953;92(2):189-217. doi:10.1002/aja.1000920202

33. Kawaguchi R, Yu J, Honda J, et al. A Membrane Receptor for Retinol Binding Protein Mediates Cellular Uptake of Vitamin A. *Science (80-)*. 2007;315(5813):820-825. doi:10.1126/science.1136244

34. Parés X, Farrés J, Kedishvili N, Duester G. Medium- and short-chain dehydrogenase/reductase gene and protein families. *Cell Mol Life Sci*. 2008;65(24):3936-3949. doi:10.1007/s00018-008-8591-3

35. Duester G. Retinoic Acid Synthesis and Signaling during Early Organogenesis. *Cell*. 2008;134(6):921-931. doi:10.1016/j.cell.2008.09.002

36. Niederreither K, Dollé P. Retinoic acid in development: towards an integrated view. *Nat Rev Genet*. 2008;9(7):541-553. doi:10.1038/nrg2340

37. Niederreither K, Vermot J, Schuhbaur B, Chambon P, Dollé P. Embryonic retinoic acid synthesis is essential for heart morphogenesis in the mouse. *Development*. 2001;128:1019-1031. http://www.ncbi.nlm.nih.gov/pubmed/12117807.

38. Giguere V, Ong ES, Segui P, Evans RM. Identification of a receptor for the morphogen retinoic acid. *Nature*. 1987;330(6149):624-629. doi:10.1038/330624a0

39. Petkovich M, Brand NJ, Krust A, Chambon P. A human retinoic acid receptor which belongs to the family of nuclear receptors. *Nature*. 1987;330(6147):444-450. doi:10.1038/330444a0

40. Nolen GA. Variations in teratogenic response to hypervitaminosis A in three strains of the albino rat. *Food Cosmet Toxicol*. 1969;7(3):209-214. http://www.ncbi.nlm.nih.gov/pubmed/5804862. Accessed April 23, 2019.

41. WILSON JG, WARKANY J. Cardiac and aortic arch anomalies in the offspring of vitamin A deficient rats correlated with similar human anomalies. *Pediatrics*. 1950;5(4):708-725. http://www.ncbi.nlm.nih.gov/pubmed/15417271. Accessed April 23, 2019.

42. Cunningham TJ, Duester G. Mechanisms of retinoic acid signalling and its roles in organ and limb development. *Nat Rev Mol Cell Biol*. 2015;16(2):110-123. doi:10.1038/nrm3932

43. Yashiro K, Zhao X, Uehara M, et al. Regulation of retinoic acid distribution is required for proximodistal patterning and outgrowth of the developing mouse limb. *Dev Cell*. 2004;6(3):411-422. http://www.ncbi.nlm.nih.gov/pubmed/15030763. Accessed April 23, 2019.

44. Abu-Abed S, Dollé P, Metzger D, Beckett B, Chambon P, Petkovich M. The retinoic acid-metabolizing enzyme, CYP26A1, is essential for normal hindbrain patterning, vertebral identity, and development of posterior structures. *Genes Dev*. 2001;15(2):226-240. http://www.ncbi.nlm.nih.gov/pubmed/11157778. Accessed April 23, 2019.

45. Sakai Y, Meno C, Fujii H, et al. The retinoic acid-inactivating enzyme CYP26 is essential for establishing an uneven distribution of retinoic acid along the anterio-posterior axis within the mouse embryo. *Genes Dev*. 2001;15(2):213-225. http://www.ncbi.nlm.nih.gov/pubmed/11157777. Accessed April 23, 2019.

46. Hernandez RE, Putzke AP, Myers JP, Margaretha L, Moens CB. Cyp26 enzymes generate the retinoic acid response pattern necessary for hindbrain development. *Development*. 2007;134(1):177-187. doi:10.1242/dev.02706

47. Balmer JE, Blomhoff R. Gene expression regulation by retinoic acid. *J Lipid Res*. 2002;43. doi:10.1194/jlr.R100015-JLR200

48. Moss JB, Shapiro MD, Nayeem SM, Mccaffery P, Dra UC, Rosenthal N. Dynamic Patterns of Retinoic Acid Synthesis and Response in the Developing Mammalian Heart. *Dev Biol*. 1998;71(199):55-71.

49. Kostetskii I, Jiang Y, Kostetskaia E, Yuan S, Evans T, Zile M. Retinoid signaling required for normal heart development regulates GATA- 4 in a pathway distinct from cardiomyocyte differentiation. *Dev Biol*. 1999;206(2):206-218. doi:10.1006/dbio.1998.9139

50. Xavier-Neto J, Neville C. A retinoic acid-inducible transgenic marker of sino-atrial development in the mouse heart. *Development*. 1999;2687:2677-2687. http://dev.biologists.org/content/126/12/2677.short.

51. Xavier-Neto J, Shapiro MD, Houghton L, Rosenthal N. Sequential programs of retinoic acid synthesis in the myocardial and epicardial layers of the developing avian heart. *Dev Biol*. 2000;219(1):129-141. doi:10.1006/dbio.1999.9588

52. Rosenthal N, Xavier-Neto J. From the bottom of the heart: Anteroposterior decisions in cardiac muscle differentiation. *Curr Opin Cell Biol*. 2000;12(6):742-746. doi:10.1016/S0955-0674(00)00162-9

53. Ross SA, Mccaffery PJ, Drager UC, De Luca LM. *Retinoids in Embryonal Development*.; 2000. www.physrev.physiology.org. Accessed April 23, 2019.

54. Hochgreb T, Linhares VL, Menezes DC, et al. A caudorostral wave of RALDH2 conveys anteroposterior information to the cardiac field. *Development*. 2003;130(22):5363-5374. doi:10.1242/dev.00750

55. Lee JH, Protze SI, Laksman Z, Backx PH, Keller GM. Human Pluripotent Stem Cell-Derived Atrial and Ventricular Cardiomyocytes Develop from Distinct Mesoderm Populations. *Cell Stem Cell*. 2017;21(2):179-194.e4. doi:10.1016/j.stem.2017.07.003

56. Hoogaars WHM, Barnett P, Moorman AFM, CHRISTOFFELS VM. T-box factors determine cardiac design. *Cell Mol Life Sci*. 2007;64:646-660. doi:10.1007/s00018-007-6524-1

57. Wu S pin, Cheng CM, Lanz RB, et al. Atrial Identity Is Determined by a COUP-TFII Regulatory Network. *Dev Cell*. 2013;25(4):417-426. doi:10.1016/j.devcel.2013.04.017

58. Devalla HD, Schwach V, Ford JW, et al. Atrial-like cardiomyocytes from human pluripotent stem cells are a robust preclinical model for assessing atrial-selective pharmacology. *EMBO Mol Med*. 2015;7(4):394-410. doi:10.15252/emmm.201404757

59. Mori AD, Zhu Y, Vahora I, et al. Tbx5-dependent rheostatic control of cardiac gene expression and morphogenesis. *Dev Biol*. 2006;297(2):566-586. doi:10.1016/j.ydbio.2006.05.023

60. Wiese C, Grieskamp T, Airik R, et al. Formation of the sinus node head and differentiation of sinus node myocardium are independently regulated by Tbx18 and Tbx3. *Circ Res*. 2009;104(3):388-397. doi:10.1161/CIRCRESAHA.108.187062

61. Blaschke RJ, Hahurij ND, Kuijper S, et al. Targeted Mutation Reveals Essential Functions of the Homeodomain Transcription Factor Shox2 in Sinoatrial and Pacemaking Development. *Circulation*. 2007;115(14):1830-1838. doi:10.1161/CIRCULATIONAHA.106.637819

62. Espinoza-Lewis RA, Yu L, He F, et al. Shox2 is essential for the differentiation of cardiac pacemaker cells by repressing Nkx2-5. *Dev Biol*. 2009;327(2):376-385. doi:10.1016/j.ydbio.2008.12.028

63. Mommersteeg MTM, Hoogaars WMH, Prall OWJ, et al. Molecular pathway for the localized formation of the sinoatrial node. *Circ Res*. 2007;100(3):354-362. doi:10.1161/01.RES.0000258019.74591.b3

64. DUPAYS L, JARRYGUICHARD T, MAZURAIS D, et al. Dysregulation of connexins and inactivation of NFATc1 in the cardiovascular system of Nkx2?5 null mutants. *J Mol Cell Cardiol*. 2005;38(5):787-798. doi:10.1016/j.yjmcc.2005.02.021

65. Takahashi K, Yamanaka S. Induction of pluripotent stem cells from mouse embryonic and adult fibroblast cultures by defined factors. *Cell*. 2006;126(4):663-676. doi:10.1016/j.cell.2006.07.024

66. Yamanaka S, Takahashi K, Tanabe K, et al. Induction of pluripotent stem cells from adult human fibroblasts by defined factors. *Cell*. 2007;131(5):861-872. doi:10.1016/j.cell.2007.11.019

67. He X, Semenov M, Tamai K, Zeng X. LDL receptor-related proteins 5 and 6 in Wnt/ -catenin signaling: Arrows point the way. *Development*. 2004;131(8):1663-1677. doi:10.1242/dev.01117

68. Yost C, Torres M, Miller JR, Huang E, Kimelman D, Moon RT. The axis-inducing activity, stability, and subcellular distribution of beta-catenin is regulated in Xenopus embryos by glycogen synthase kinase 3. *Genes Dev*. 1996;10(12):1443-1454. http://www.ncbi.nlm.nih.gov/pubmed/8666229. Accessed May 9, 2019.

69. Liu C, Li Y, Semenov M, et al. Control of beta-catenin phosphorylation/degradation by a dual-kinase mechanism. *Cell*. 2002;108(6):837-847. http://www.ncbi.nlm.nih.gov/pubmed/11955436. Accessed May 9, 2019.

70. Hagen T, Di Daniel E, Culbert AA, Reith AD. Expression and Characterization of GSK-3 Mutants and Their Effect on β-Catenin Phosphorylation in Intact Cells. *J Biol Chem*. 2002;277(26):23330-23335. doi:10.1074/jbc.M201364200

71. Mummery C, Ward-van Oostwaard D, Doevendans P, et al. Differentiation of Human Embryonic Stem Cells to Cardiomyocytes. *Circulation*.

2003;107(21):2733-2740. doi:10.1161/01.CIR.0000068356.38592.68

72. Freund C, Ward-van Oostwaard D, Monshouwer-Kloots J, et al. Insulin Redirects Differentiation from Cardiogenic Mesoderm and Endoderm to Neuroectoderm in Differentiating Human Embryonic Stem Cells. *Stem Cells*. 2008;26(3):724-733. doi:10.1634/stemcells.2007-0617

73. Passier R, Oostwaard DW, Snapper J, et al. Increased Cardiomyocyte Differentiation from Human Embryonic Stem Cells in Serum-Free Cultures. *Stem Cells*. 2005;23(6):772-780. doi:10.1634/stemcells.2004-0184

74. Kattman SJ, Witty AD, Gagliardi M, et al. Stage-specific optimization of activin/nodal and BMP signaling promotes cardiac differentiation of mouse and human pluripotent stem cell lines. *Cell Stem Cell*. 2011;8(2):228-240. doi:10.1016/j.stem.2010.12.008

75. Yang L, Soonpaa MH, Adler ED, et al. Human cardiovascular progenitor cells develop from a KDR+ embryonic-stem-cell-derived population. *Nature*. 2008;453(7194):524-528. doi:10.1038/nature06894

76. Nostro MC, Cheng X, Keller GM, Gadue P. Wnt, Activin, and BMP Signaling Regulate Distinct Stages in the Developmental Pathway from Embryonic Stem Cells to Blood. *Cell Stem Cell*. 2008;2(1):60-71. doi:10.1016/j.stem.2007.10.011

77. Willems E, Spiering S, Davidovics H, et al. Small-Molecule Inhibitors of the Wnt Pathway Potently Promote Cardiomyocytes From Human Embryonic Stem Cell–Derived Mesoderm. *Circ Res*. 2011;109(4):360-364. doi:10.1161/CIRCRESAHA.111.249540

78. Wang X, Moon J, Dodge ME, et al. The development of highly potent inhibitors for porcupine. *J Med Chem*. 2013;56(6):2700-2704. doi:10.1021/jm400159c

79. Laflamme MA, Chen KY, Naumova A V, et al. Cardiomyocytes derived from human embryonic stem cells in pro-survival factors enhance function of infarcted rat hearts. *Nat Biotechnol*. 2007;25(9):1015-1024. doi:10.1038/nbt1327

80. Paige SL, Osugi T, Afanasiev OK, Pabon L, Reinecke H, Murry CE. Endogenous Wnt/β-Catenin Signaling Is Required for Cardiac Differentiation in Human Embryonic Stem Cells. Verfaillie CM, ed. *PLoS One*. 2010;5(6):e11134. doi:10.1371/journal.pone.0011134

81. Uosaki H, Fukushima H, Takeuchi A, et al. Efficient and Scalable Purification of Cardiomyocytes from Human Embryonic and Induced Pluripotent Stem Cells by VCAM1 Surface Expression. Prosper F, ed. *PLoS One*. 2011;6(8):e23657. doi:10.1371/journal.pone.0023657

82. Hudson J, Titmarsh D, Hidalgo A, Wolvetang E, Cooper-White J. Primitive Cardiac Cells from Human Embryonic Stem Cells. *Stem Cells Dev*. 2012;21(9):1513-1523. doi:10.1089/scd.2011.0254

83. Lian X, Hsiao C, Wilson G, et al. Cozzarelli Prize Winner: Robust cardiomyocyte differentiation from human pluripotent stem cells via temporal modulation of canonical Wnt signaling. *Proc Natl Acad Sci*. 2012;109(27):E1848-E1857. doi:10.1073/pnas.1200250109

84. Burridge PW, Matsa E, Shukla P, et al. Chemically defned generation of human cardiomyocytes. *Nat Methods*. 2014;11(8):855-860. doi:10.1038/nMeth.2999

85. Lee JH, Protze SI, Laksman Z, Backx PH, Keller GM. Human Pluripotent Stem Cell-Derived Atrial and Ventricular Cardiomyocytes Develop from Distinct Mesoderm Populations. *Cell Stem Cell*. 2017;21(2):179-194.e4. doi:10.1016/j.stem.2017.07.003

86. Zhang Q, Jiang J, Han P, et al. Direct differentiation of atrial and ventricular myocytes from human embryonic stem cells by alternating retinoid signals. *Cell Res*. 2011;21(4):579-587. doi:10.1038/cr.2010.163

87. Cyganek L, Tiburcy M, Sekeres K, et al. Deep phenotyping of human induced pluripotent stem cell–derived atrial and ventricular cardiomyocytes. *JCI Insight*. 2018;3(12). doi:10.1172/jci.insight.99941

88. Bootman MD, Smyrnias I, Thul R, Coombes S, Roderick HL. Atrial cardiomyocyte calcium signalling. *Biochim Biophys Acta - Mol Cell Res*. 2011;1813(5):922-934. doi:10.1016/j.bbamcr.2011.01.030

89. Gaborit N, Le Bouter S, Szuts V, et al. Regional and tissue specific transcript signatures of ion channel genes in the non-diseased human heart. *J Physiol*. 2007;582(Pt 2):675-693. doi:10.1113/jphysiol.2006.126714

90. Giles WR, Imaizumi Y. Comparison of potassium currents in rabbit atrial and ventricular cells. *J Physiol*. 1988;405(1):123-145. doi:10.1113/jphysiol.1988.sp017325

91. Grant AO. Cardiac ion channels. *Circ Arrhythmia Electrophysiol*. 2009;2(2):185-194. doi:10.1161/CIRCEP.108.789081

92. Mitcheson JS, Sanguinetti MC. Biophysical Properties and Molecular Basis of Cardiac Rapid and Slow Delayed Rectifier Potassium Channels. *Cell Physiol Biochem*. 1999;9(4-5):201-216. doi:10.1159/000016317

93. Wang Z, Fermini B, Nattel S. Rapid and slow components of delayed rectifier current in human atrial myocytes. *Cardiovasc Res*. 1994;28(10):1540-1546. http://www.ncbi.nlm.nih.gov/pubmed/8001043. Accessed May 10, 2019.

94. Grandi E, Pandit S V, Voigt N, et al. Human atrial action potential and Ca2+ model: sinus rhythm and chronic atrial fibrillation. *Circ Res*. 2011;109(9):1055-1066. doi:10.1161/CIRCRESAHA.111.253955

95. Fedida D, Wible B, Wang Z, et al. Identity of a novel delayed rectifier current from human heart with a cloned K+ channel current. *Circ Res*. 1993;73(1):210-216. http://www.ncbi.nlm.nih.gov/pubmed/8508531. Accessed May 10, 2019.

96. Ellinor PT, Lunetta KL, Glazer NL, et al. Common Variants in KCNN3 are Associated with Lone Atrial Fibrillation. *Nat Genet*. 2010;42(3):240-244. doi:10.1021/ja8019214.Optimization

97. Schumacher M a, Rivard a F, Bächinger HP, Adelman JP. Structure of the gating domain of a Ca^{2+}-activated K^+ channel complexed with Ca^{2+}/calmodulin. *Nature*. 2001;410(6832):1120-1124. doi:10.1038/35074145

98. Amos GJ, Wettwer E, Metzger F, Li Q, Himmel HM, Ravens U. Differences between outward currents of human atrial and subepicardial ventricular myocytes. *J Physiol*. 1996;491(1):31-50. doi:10.1113/jphysiol.1996.sp021194

99. Ravens U. Atrial-selective K+ channel blockers – potential antiarrhythmic drugs in atrial fibrillation? *Can J Physiol Pharmacol*. 2017;(1):1-19.

100. Bers DM. Cardiac excitation-contraction coupling. *Nature*. 2002;415(6868):198-205. doi:10.1038/415198a

101. Asghari P, Scriven DRL, Hoskins J, Fameli N, van Breemen C, Moore EDW. The structure and functioning of the couplon in the mammalian cardiomyocyte. *Protoplasma*. 2012;249(SUPPL. 1):31-38. doi:10.1007/s00709-011-0347-5

102. Lu ZQ, Sinha A, Sharma P, Kislinger T, Gramolini AO. Proteomic analysis of human fetal atria and ventricle. *J Proteome Res*. 2014;13(12):5869-5878. doi:10.1021/pr5007685

103. Lin BL, Song T, Sadayappan S. Myofilaments: Movers and Rulers of the Sarcomere. In: *Comprehensive Physiology*. Hoboken, NJ, USA: John Wiley & Sons, Inc.; 2017:675-692. doi:10.1002/cphy.c160026

104. Igarashi T, Finet JE, Takeuchi A, et al. Connexin Gene Transfer Preserves Conduction Velocity and Prevents Atrial Fibrillation. *Circulation*. 2012;125(2):216-225. doi:10.1161/CIRCULATIONAHA.111.053272

105. Gollob MH, Jones DL, Krahn AD, et al. Somatic Mutations in the Connexin 40 Gene (GJA5) in Atrial Fibrillation. *N Engl J Med*. 2006;354(25):2677-2688. doi:10.1056/NEJMoa052800

106. Frankel G, Kamrul R, Kosar L, Jensen B. Rate versus rhythm control in atrial fibrillation. *Can Fam Physician*. 2013;59(2):161-168. doi:10.1345/aph.1D396

107. Veenhuyzen GD, Simpson CS, Abdollah H. Atrial fibrillation. *Cmaj*. 2004;171(7):755-760. doi:10.1016/S0140-6736(11)61514-6

108. Lévy S. Classification system of atrial fibrillation. *Curr Opin Cardiol*. 2000;15(1):54-57.

109. Camm AJ, Kirchhof P, Lip GYH, et al. Guidelines for the management of atrial fibrillation. *Eur Heart J*. 2010;31(19):2369-2429. doi:10.1093/eurheartj/ehq278

110. Ott A, Breteler MMB, de Bruyne MC, van Harskamp F, Grobbee DE, Hofman A. Atrial Fibrillation and Dementia in a Population-Based Study: The Rotterdam Study. *Stroke*. 1997;28(2):316-321. doi:10.1161/01.STR.28.2.316

111. Krahn AD, Manfreda J, Tate RB, Mathewson FAL, Cuddy TE. The natural history of atrial fibrillation: Incidence, risk factors, and prognosis in the manitoba follow-up study. *Am J Med*. 1995;98(5):476-484. doi:10.1016/S0002-9343(99)80348-9

112. Piccini JP, Fauchier L. Rhythm control in atrial fibrillation. *Lancet*. 2016;388(10046):829-840. doi:10.1016/S0140-6736(16)31277-6

113. Lloyd-Jones DM. Lifetime Risk for Development of Atrial Fibrillation: The Framingham Heart Study. *Circulation*. 2004;110(9):1042-1046. doi:10.1161/01.CIR.0000140263.20897.42

114. Dzeshka MS, Lip GYH, Snezhitskiy V, Shantsila E. Cardiac Fibrosis in Patients With Atrial Fibrillation. *J Am Coll Cardiol*. 2015;66(8):943-959. doi:10.1016/j.jacc.2015.06.1313

115. Wakili R, Voigt N, Kääb S, Dobrev D, Nattel S. Recent advances in the molecular pathophysiology of atrial fibrillation. *J Clin Invest*. 2011;121(8):2955-2968. doi:10.1172/JCI46315

116. Pandit S V., Berenfeld O, Anumonwo JMB, et al. Ionic determinants of functional reentry in a 2-D model of human atrial cells during simulated chronic atrial fibrillation. *Biophys J*. 2005;88(6):3806-3821. doi:10.1529/biophysj.105.060459

117. Qi XY, Yeh Y-H, Xiao L, et al. Cellular Signaling Underlying Atrial Tachycardia Remodeling of L-type Calcium Current. *Circ Res*. 2008;103(8):845-854. doi:10.1161/CIRCRESAHA.108.175463

118. Heijman J, Voigt N, Wehrens XHT, Dobrev D. Calcium dysregulation in atrial fibrillation: The role of CaMKII. *Front Pharmacol*. 2014;5 MAR. doi:10.3389/fphar.2014.00030

119. Ellinor PT, Lunetta KL, Glazer NL, et al. Common variants in KCNN3 are associated with lone atrial fibrillation. *Nat Genet*. 2010;42(3):240-244. doi:10.1038/ng.537

120. Kim MH, Johnston SS, Chu B-C, Dalal MR, Schulman KL. Estimation of Total Incremental Health Care Costs in Patients With Atrial Fibrillation in the United States. *Circ Cardiovasc Qual Outcomes*. 2011;4(3):313-320.

doi:10.1161/CIRCOUTCOMES.110.958165

121. O'Reilly DJ, Hopkins RB, Healey JS, et al. The Burden of Atrial Fibrillation on the Hospital Sector in Canada. *Can J Cardiol*. 2013;29(2):229-235. doi:10.1016/j.cjca.2012.03.023

122. Magnani JW, Rienstra M, Lin H, et al. Atrial fibrillation: Current knowledge and future directions in epidemiology and genomics. *Circulation*. 2011;124(18):1982-1993. doi:10.1161/CIRCULATIONAHA.111.039677.Atrial

123. Stewart S, Murphy N, McGuire A, JJV M. Cost of an emerging epidemic: an economic analysis of atrial fibrillation in the UK. *Heart*. 2004;90(3):286-292. doi:10.1136/hrt.2002.008748

124. Miyasaka Y. Secular Trends in Incidence of Atrial Fibrillation in Olmsted County, Minnesota, 1980 to 2000, and Implications on the Projections for Future Prevalence. *Circulation*. 2006;114(2):119-125. doi:10.1161/CIRCULATIONAHA.105.595140

125. Boyden PA. Electromhvsiolouic Basis of Cardiac Arrhythmias. *Am J Cardiol*. 1996;78(964A):4-11.

126. Dobrev D, Nattel S. New antiarrhythmic drugs for treatment of atrial fibrillation. *Lancet (London, England)*. 2010;375(9721):1212-1223. doi:10.1016/S0140-6736(10)60096-7

127. Yeh Y-H, Wakili R, Qi X-Y, et al. Calcium-Handling Abnormalities Underlying Atrial Arrhythmogenesis and Contractile Dysfunction in Dogs With Congestive Heart Failure. *Circ Arrhythmia Electrophysiol*. 2008;1(2):93-102. doi:10.1161/CIRCEP.107.754788

128. Haissaguerre M, Jais P, Shah DC, et al. Spontaneous Initiation of Atrial Fibrillation by Ectopic Beats Originating in the Pulmonary Veins. *N Engl J Med*. 1998;339(10):659-666. doi:10.1056/NEJM199809033391003

129. Pertsov a M, Davidenko JM, Salomonsz R, Baxter WT, Jalife J. Spiral waves of excitation underlie reentrant activity in isolated cardiac muscle. *Circ Res*. 1993;72(3):631-650. doi:10.1161/01.RES.72.3.631

130. Allessie M a, Bonke FI, Schopman FJ. Circus movement in rabbit atrial muscle as a mechanism of tachycardia. III. The "leading circle" concept: a new model of circus movement in cardiac tissue without the involvement of an anatomical obstacle. *Circ Res*. 1977;41(1):9-18. doi:10.1161/01.RES.41.1.9

131. Christophersen IE, Ellinor PT. Genetics of atrial fibrillation: from families to genomes. *J Hum Genet*. 2015;(April):1-10. doi:10.1038/jhg.2015.44

132. Lip GYH, Fauchier L, Freedman SB, et al. Atrial fibrillation. *Nat Rev Dis Prim*.

2016;2:16016. doi:10.1038/nrdp.2016.16

133. Arentz T, Haegeli L, Sanders P, et al. High-density mapping of spontaneous pulmonary vein activity initiating atrial fibrillation in humans. *J Cardiovasc Electrophysiol*. 2007;18(1):31-38. doi:10.1111/j.1540-8167.2006.00682.x

134. Ghaye B, Szapiro D, Dacher J-N, et al. Percutaneous Ablation for Atrial Fibrillation: The Role of Cross-sectional Imaging. *RadioGraphics*. 2003;23(suppl_1):S19-S33. doi:10.1148/rg.23si035513

135. Cappato R, Calkins H, Chen SA, et al. Updated worldwide survey on the methods, efficacy, and safety of catheter ablation for human atrial fibrillation. *Circ Arrhythmia Electrophysiol*. 2010;3(1):32-38. doi:10.1161/CIRCEP.109.859116

136. Schreiber D, Rostock T, Fröhlich M, et al. Five-year follow-up after catheter ablation of persistent atrial fibrillation using the stepwise approach and prognostic factors for success. *Circ Arrhythmia Electrophysiol*. 2015;8(2):308-317. doi:10.1161/CIRCEP.114.001672

137. DiMasi JA, Grabowski HG, Hansen RW. Innovation in the pharmaceutical industry: New estimates of R&D costs. *J Health Econ*. 2016;47:20-33. doi:10.1016/j.jhealeco.2016.01.012

138. Denning C, Anderson D. Cardiomyocytes from human embryonic stem cells as predictors of cardiotoxicity. *Drug Discov Today Ther Strateg*. 2008;5(4):223-232. doi:10.1016/j.ddstr.2008.08.002

139. Redfern WS, Carlsson L, Davis AS, et al. Relationships between preclinical cardiac electrophysiology, clinical QT interval prolongation and torsade de pointes for a broad range of drugs: evidence for a provisional safety margin in drug development. *Cardiovasc Res*. 2003;58(1):32-45. doi:10.1016/s0008-6363(02)00846-5

140. Camm AJ, Yapp YG. *Essentials of Atrial Fibrillation*. London: Springer Healthcare; 2014.

141. Darbar D, Herron KJ, Ballew JD, et al. Familial atrial fibrillation is a genetically heterogeneous disorder. *J Am Coll Cardiol*. 2003;41(12):2185-2192. doi:10.1016/S0735-1097(03)00465-0

142. Ellinor PT, Yoerger DM, Ruskin JN, MacRae CA. Familial aggregation in lone atrial fibrillation. *Hum Genet*. 2005;118(2):179-184. doi:10.1007/s00439-005-0034-8

143. Fox CS, Parise H, D'Agostino RB, et al. Parental atrial fibrillation as a risk factor for atrial fibrillation in offspring. *JAMA*. 2004;291(23):2851-2855. doi:10.1001/jama.291.23.2851

144. Arnar DO, Thorvaldsson S, Manolio T a., et al. Familial aggregation of atrial fibrillation in Iceland. *Eur Heart J*. 2006;27:708-712. doi:10.1093/eurheartj/ehi727

145. Christophersen IE, Rienstra M, Roselli C, et al. Large-scale analyses of common and rare variants identify 12 new loci associated with atrial fibrillation. *Nat Genet*. 2017;49(6):946-952. doi:10.1038/ng.3843

146. Nielsen JB, Fritsche LG, Zhou W, et al. Genome-wide Study of Atrial Fibrillation Identifies Seven Risk Loci and Highlights Biological Pathways and Regulatory Elements Involved in Cardiac Development. *Am J Hum Genet*. 2017;102:103-115. doi:10.1016/j.ajhg.2017.12.003

147. Nadadur RD, Broman MT, Boukens B, et al. *Pitx2* modulates a *Tbx5* -dependent gene regulatory network to maintain atrial rhythm. *Sci Transl Med*. 2016;8(354):354ra115-354ra115. doi:10.1126/scitranslmed.aaf4891

148. Zhang X-D, Timofeyev V, Li N, et al. Critical roles of a small conductance Ca^{2+}-activated K^+ channel (SK3) in the repolarization process of atrial myocytes. *Cardiovasc Res*. 2014;101(2):317-325. doi:10.1093/cvr/cvt262

149. Köhler AM, Hirschberg B, Bond CT, et al. Small-Conductance , Calcium-Activated Potassium Channels from Mammalian Brain. *Science (80-)*. 1996;273(5282):1709-1714.

150. Bond CT, Maylie J, Adelman JP. Small-conductance calcium-activated potassium channels. *Ann N Y Acad Sci*. 1999;868:370-378. doi:10.1111/j.1749-6632.1999.tb11298.x

151. Luján R, Maylie J, Adelman JP. New sites of action for GIRK and SK channels. *Nat Rev Neurosci*. 2009;10:475-480. doi:10.1038/nrn2668

152. Xia XM, Fakler B, Rivard a, et al. Mechanism of calcium gating in small-conductance calcium-activated potassium channels. *Nature*. 1998;395(6701):503-507. doi:10.1038/26758

153. Tuteja D, Rafizadeh S, Timofeyev V, et al. Cardiac small conductance Ca^{2+}-activated K^+ channel subunits form heteromultimers via the coiled-coil domains in the C termini of the channels. *Circ Res*. 2010;107:851-859. doi:10.1161/CIRCRESAHA.109.215269

154. Xu Y, Tuteja D, Zhang Z, et al. Molecular identification and functional roles of a Ca^{2+}-activated K^+ channel in human and mouse hearts. *J Biol Chem*. 2003;278(49):49085-49094. doi:10.1074/jbc.M307508200

155. Skibsbye L, Poulet C, Diness JG, et al. Small-conductance calcium-activated potassium (SK) channels contribute to action potential repolarization in human atria. *Cardiovasc Res*. 2014;103(1):156-167. doi:10.1093/cvr/cvu121

156. Tuteja D, Xu D, Timofeyev V, et al. Differential expression of small-conductance Ca^{2+}-activated K^+ channels SK1, SK2, and SK3 in mouse atrial and ventricular myocytes. *Am J Physiol Heart Circ Physiol*. 2005;289(6):H2714-23. doi:10.1152/ajpheart.00534.2005

157. Ozgen N, Dun W, Sosunov EA, et al. Early electrical remodeling in rabbit pulmonary vein results from trafficking of intracellular SK2 channels to membrane sites. *Cardiovasc Res*. 2007;75(4):758-769. doi:10.1016/j.cardiores.2007.05.008

158. Miller MJ, Rauer H, Tomita H, et al. Nuclear Localization and Dominant-negative Suppression by a Mutant SKCa3 N-terminal Channel Fragment Identified in a Patient with Schizophrenia. *J Biol Chem*. 2001;276(30):27753-27756. doi:10.1074/jbc.C100221200

159. Chang Y-F, Imam JS, Wilkinson MF. The Nonsense-Mediated Decay RNA Surveillance Pathway. *Annu Rev Biochem*. 2007;76(1):51-74. doi:10.1146/annurev.biochem.76.050106.093909

160. Popp MW, Maquat LE. Leveraging rules of nonsense-mediated mRNA decay for genome engineering and personalized medicine. *Cell*. 2016;165(6):1319-1332. doi:10.1016/j.cell.2016.05.053

161. Richardson CD, Ray GJ, DeWitt MA, Curie GL, Corn JE. Enhancing homology-directed genome editing by catalytically active and inactive CRISPR-Cas9 using asymmetric donor DNA. *Nat Biotechnol*. 2016;34(3). doi:10.1038/nbt.3481

162. Chandrasekaran Chitra, Betran Esther. Origins of New Genes and Pseudogenes. *Nat Educ*. 2008;1(2):181.

163. Taylor S, Wakem M, Dijkman G, Alsarraj M, Nguyen M. *A Practical Approach to RT-QPCR — Publishing Data That Conform to the MIQE Guidelines*.; 2015. doi:10.1016/j.saa.2003.10.029

164. Christoffels VM, Smits GJ, Kispert A, Moorman AFM. Development of the pacemaker tissues of the heart. *Circ Res*. 2010;106(2):240-254. doi:10.1161/CIRCRESAHA.109.205419

165. Zhang Q, Jiang J, Han P, et al. Direct differentiation of atrial and ventricular myocytes from human embryonic stem cells by alternating retinoid signals. *Cell Res*. 2011;21(4):579-587. doi:10.1038/cr.2010.163

166. Argenziano M, Lambers E, Hong L, et al. Electrophysiologic Characterization of Calcium Handling in Human Induced Pluripotent Stem Cell-Derived Atrial Cardiomyocytes. *Stem Cell Reports*. 2018;10(6):1867-1878. doi:10.1016/j.stemcr.2018.04.005

167. Pei F, Jiang J, Bai S, et al. Chemical-defined and albumin-free generation of human atrial and ventricular myocytes from human pluripotent stem cells. *Stem Cell Res*. 2017;19:94-103. doi:10.1016/j.scr.2017.01.006

168. Piccini I, Rao J, Seebohm G, Greber B. Human pluripotent stem cell-derived cardiomyocytes: Genome-wide expression profiling of long-term in vitro maturation in comparison to human heart tissue. *Genomics Data*. 2015;4:69-72. doi:10.1016/j.gdata.2015.03.008

169. Fedida D, Orth PMR, Chen JYC, et al. The Mechanism of Atrial Antiarrhythmic Action of RSD1235. :1227-1238. doi:10.1111/j.1540-8167.2005.50028.x

170. Savelieva I, Graydon R, Camm AJ. Pharmacological cardioversion of atrial fibrillation with vernakalant: Evidence in support of the ESC Guidelines. *Europace*. 2014;16(2):162-173. doi:10.1093/europace/eut274

171. Wettwer E, Christ T, Endig S, et al. The new antiarrhythmic drug vernakalant: Ex vivo study of human atrial tissue from sinus rhythm and chronic atrial fibrillation. *Cardiovasc Res*. 2013;98(1):145-154. doi:10.1093/cvr/cvt006

172. Hill JT, Demarest BL, Bisgrove BW, Su YC, Smith M, Yost HJ. Poly peak parser: Method and software for identification of unknown indels using sanger sequencing of polymerase chain reaction products. *Dev Dyn*. 2014;243(12):1632-1636. doi:10.1002/dvdy.24183

173. Higuchi R, Dollinger G, Walsh PS, Griffith R. Simultaneous amplification and detection of specific DNA sequences. *Biotechnology (N Y)*. 1992;10(4):413-417. http://www.ncbi.nlm.nih.gov/pubmed/1368485. Accessed April 29, 2019.

174. Higuchi R, Fockler C, Dollinger G, Watson R. Kinetic PCR analysis: real-time monitoring of DNA amplification reactions. *Biotechnology (N Y)*. 1993;11(9):1026-1030. http://www.ncbi.nlm.nih.gov/pubmed/7764001. Accessed April 29, 2019.

175. Wittwer CT, Herrmann MG, Moss AA, Rasmussen RP. Continuous Fluorescence Monitoring of Rapid Cycle DNA Amplification. *Biotechniques*. 1997;22(1):130-138. doi:10.2144/97221bi01

176. Bustin SA, Mueller R. Real-time reverse transcription PCR (qRT-PCR) and its potential use in clinical diagnosis. *Clin Sci*. 2005;109(4):365-379. doi:10.1042/CS20050086

177. van den Berg RJ, Vaessen N, Endtz HP, Schulin T, van der Vorm ER, Kuijper EJ. Evaluation of real-time PCR and conventional diagnostic methods for the detection of Clostridium difficile-associated diarrhoea in a prospective multicentre study. *J Med Microbiol*. 2007;56(1):36-42. doi:10.1099/jmm.0.46680-0

178. Bustin SA, Benes V, Garson JA, et al. The MIQE Guidelines: Minimum Information for Publication of Quantitative Real-Time. *Clin Chem*. 2009;55(4). doi:10.1373/clinchem.2008.112797

179. Geiss GK, Bumgarner RE, Birditt B, et al. Direct multiplexed measurement of gene expression with color-coded probe pairs. *Nat Biotechnol*. 2008;26(3):317-325. doi:10.1038/nbt1385

180. Veldman-Jones MH, Brant R, Rooney C, et al. Evaluating Robustness and Sensitivity of the NanoString Technologies nCounter Platform to Enable Multiplexed Gene Expression Analysis of Clinical Samples. *Cancer Res*. 2015;75(13):2587-2593. doi:10.1158/0008-5472.CAN-15-0262

181. Odermatt A, Taschner PEM, Scherer SW, et al. Characterization of the Gene Encoding Human Sarcolipin (SLN), a Proteolipid Associated with SERCA1: Absence of Structural Mutations in Five Patients with Brody Disease. *Genomics*. 1997;45(3):541-553. doi:10.1006/geno.1997.4967

182. Reiser PJ, Portman MA, Ning X-H, Moravec CS. Human cardiac myosin heavy chain isoforms in fetal and failing adult atria and ventricles. *Am J Physiol Circ Physiol*. 2001;280(4):H1814-H1820. doi:10.1152/ajpheart.2001.280.4.H1814

183. Altschul SF, Wootton JC, Gertz EM, et al. Protein database searches using compositionally adjusted substitution matrices. *FEBS J*. 2005;272(20):5101-5109. doi:10.1111/j.1742-4658.2005.04945.x

184. Altschul SF, Madden TL, Schäffer AA, et al. Gapped BLAST and PSI-BLAST: a new generation of protein database search programs. *Nucleic Acids Res*. 1997;25(17):3389-3402. http://www.ncbi.nlm.nih.gov/pubmed/9254694. Accessed April 29, 2019.

185. Ong S-E, Blagoev B, Kratchmarova I, et al. Stable Isotope Labeling by Amino Acids in Cell Culture, SILAC, as a Simple and Accurate Approach to Expression Proteomics*. *Mol Cell Proteomics*. 2002;1:376-386. doi:10.1074/mcp.M200025-MCP200

Appendix.

Supplemental Figures

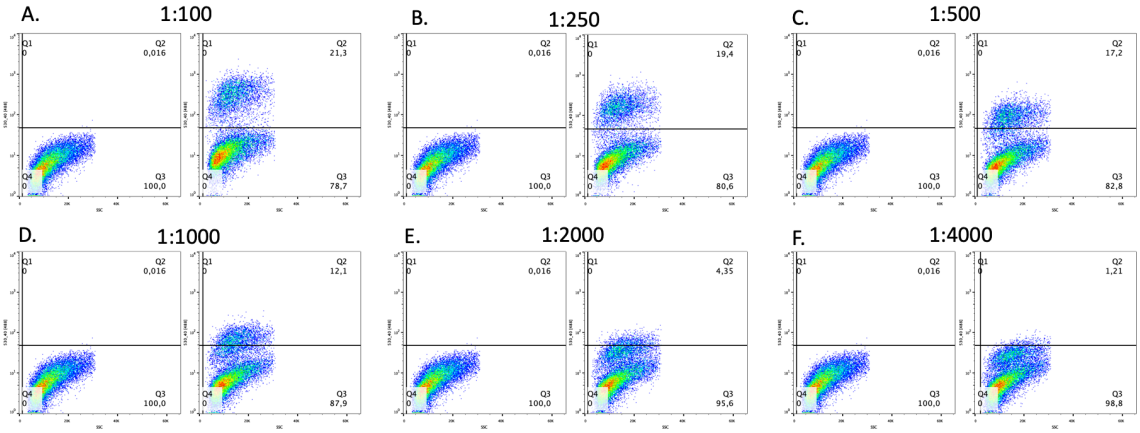

Supplemental Figure 1. Titration of FITC conjugated troponin T antibody.
A: 1:100. B: 1:250. C: 1:500. D: 1:1000. E: 1:2000. F: 1:4000

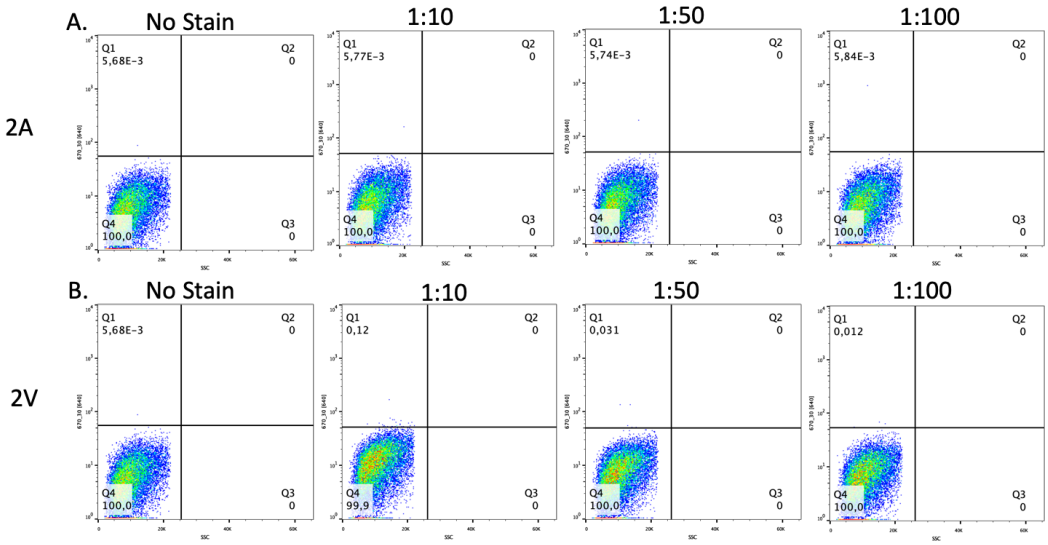

Supplemental Figure 2. Titration of conjugated Miltenyi antibodies.
A. 1:10 to 1:100 titration of PE conjugated myosin light chain 2A antibody. B: 1:10 to 1:100 titration of APC conjugated myosin light chain 2V antibody

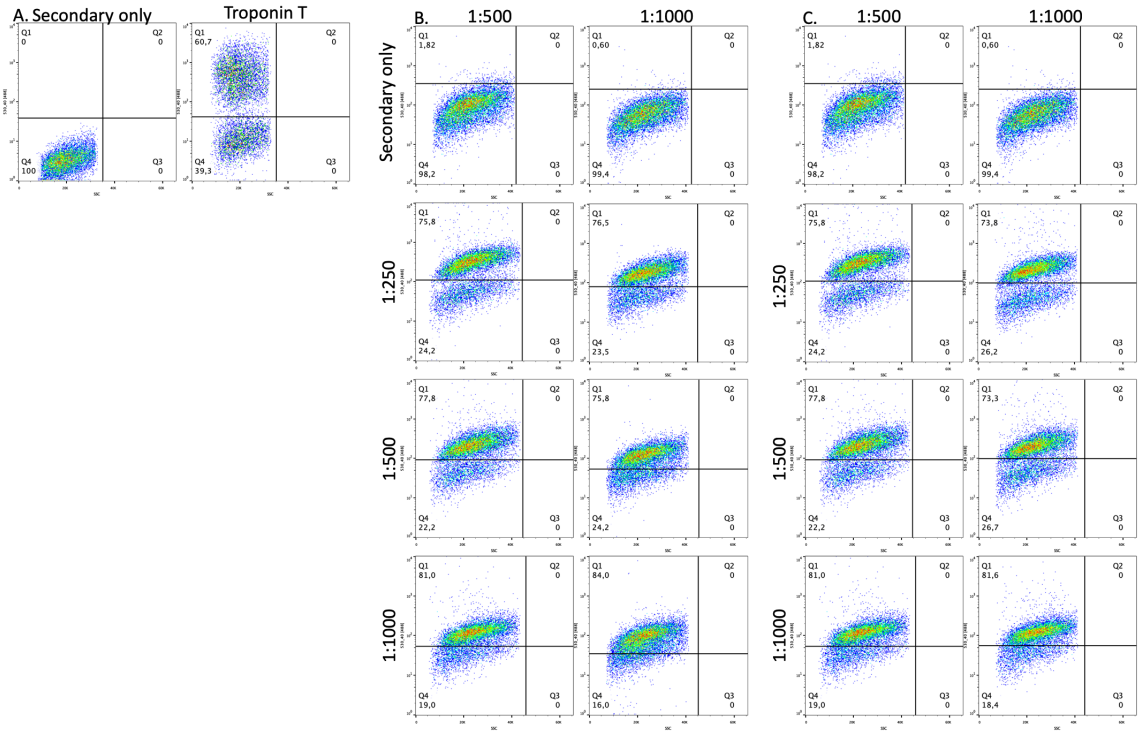

Supplemental Figure 3. Titration of unconjugated antibodies from BD.
This group of cells showed adequate Troponin T expression (A). B: Myosin light chain 2V and C: Myosin light chain 2A were tested at two different concentrations (X-axis) and three different secondary antibody concentrations (Y-axis).

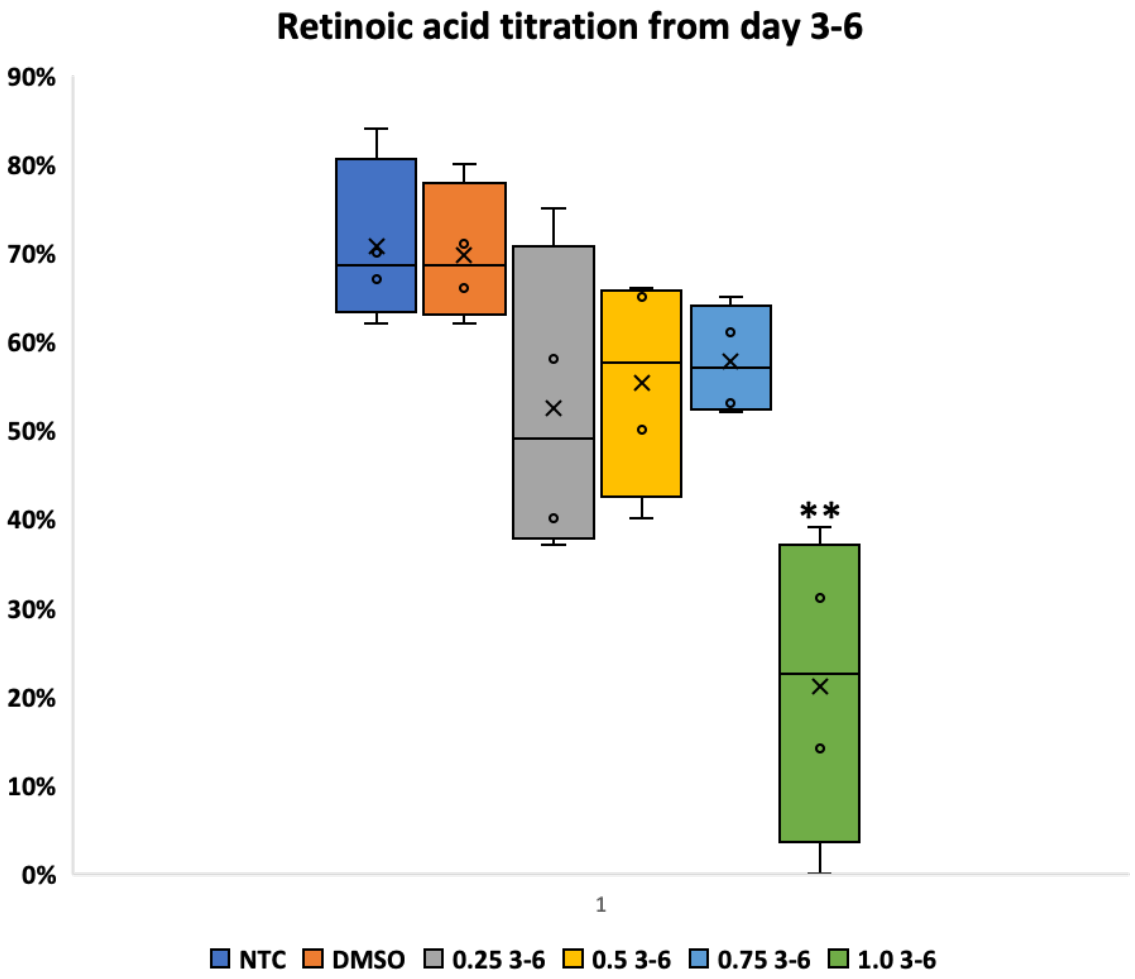

Supplemental Figure 4. Assessment of cTnT expression at day 20 after RA titration from day 3-6.

None of the concentrations had a significant decrease in cTnT except for 1 μM RA which had an average cTnT expression of 28 ± 7%. n=4. **p<0.01. "x" represents the mean

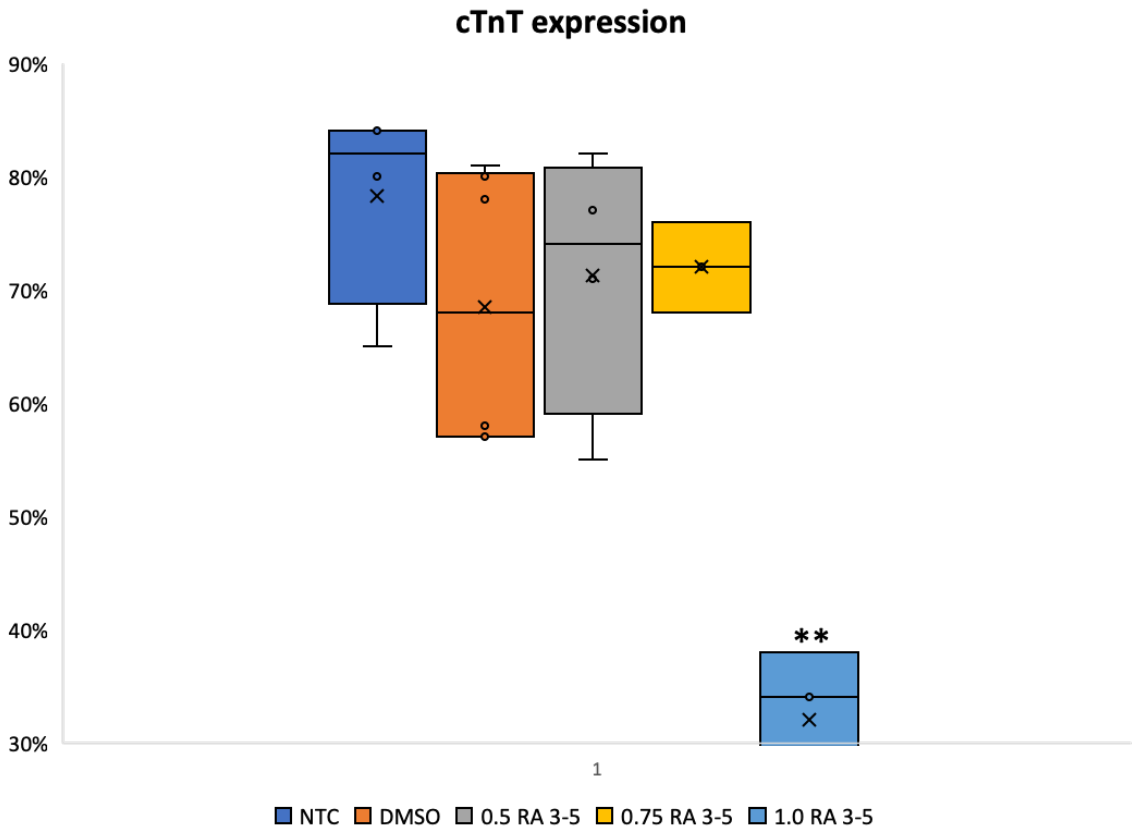

Supplemental Figure 5. cTnT expression at day 20 after titrating RA from days 3 to 5.

There was no significant difference in cTnT expression between the No template control (78 ±5%) and the vehicle DMSO control (69 ± 5%). 0.5 μM RA and 0.75 μM RA had similar cTnT expression as well, 64 ± 6% and 72 ± 2% respectively. 1.0 μM RA however had a sharp drop in cTnT expression, 32 ± 4%. n=4. **p<0.01. “x” represents the mean.

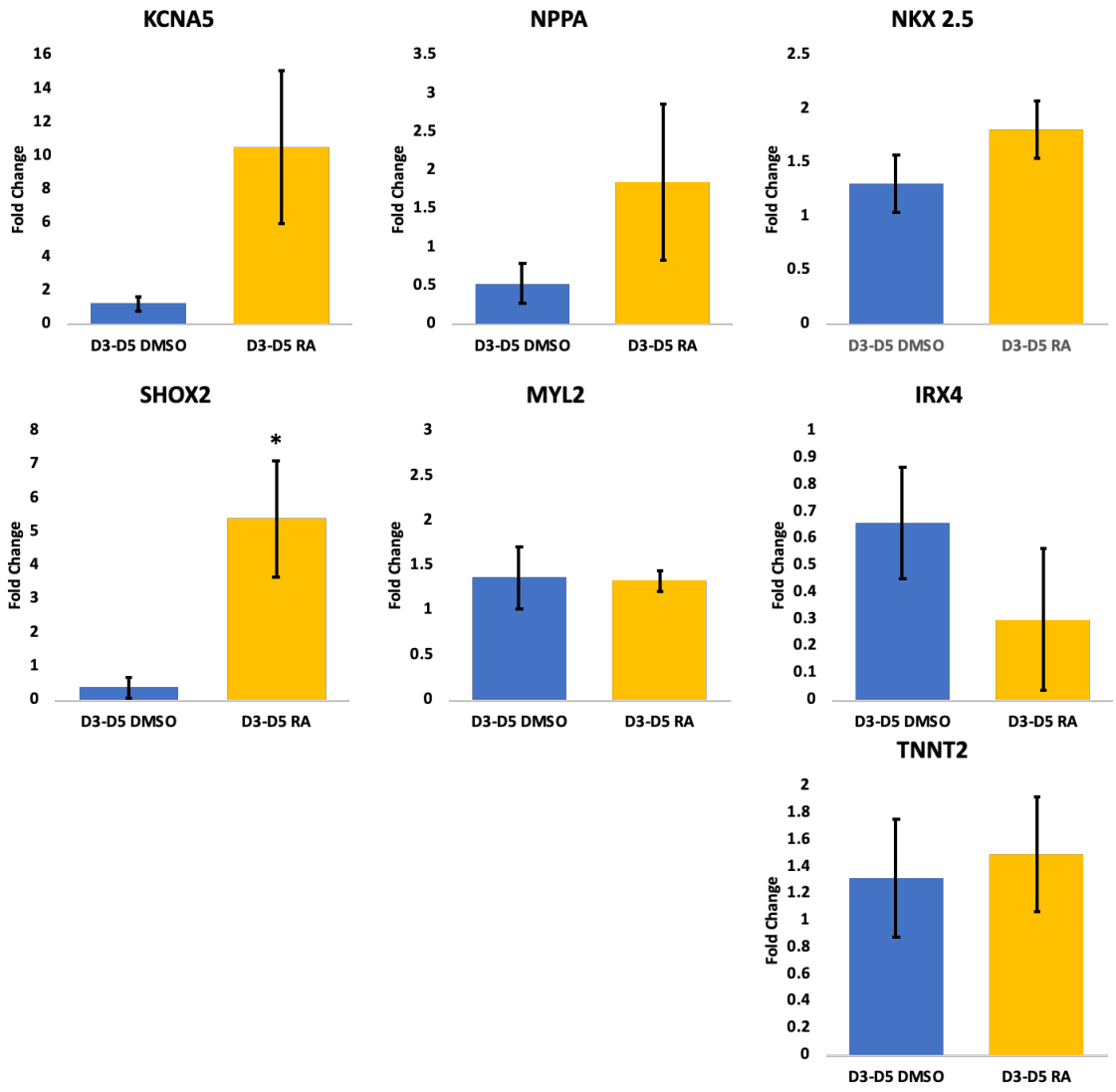

Supplemental Figure 6. RT-qPCR expression profile of cells differentiated with 0.75 μM RA from day 3-5.

There was no significant increase in expression of the atrial markers NPPA and KCNA5. MYL2 showed a similar level of expression in both conditions. There was no significant difference in the expression of cardiac markers NKX2.5 and TNNT2. SHOX2 still showed a significant increase in expression compared to the control. n=3. *p<0.05.

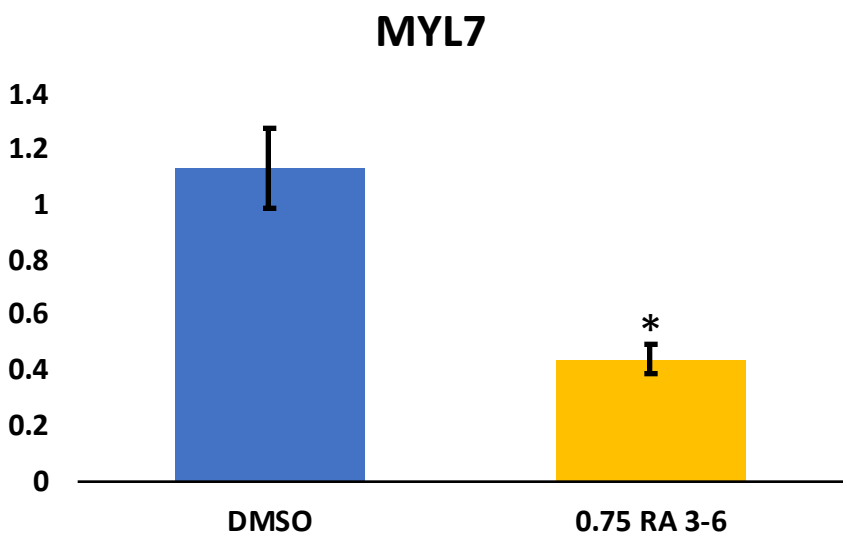

Supplemental Figure 7. Relative expression of MYL7 between cardiomyocytes with RA

RA was added at a concentration of 0.75 μM RA over days 3 – 6 compared to the vehicle DMSO control. n = 3. *p<0.05